


1-1-2016

Role Of Secretory Granule Heterogeneity In Calcium-Triggered Exocytosis

Tejeshwar Rao
Wayne State University,

Follow this and additional works at: https://digitalcommons.wayne.edu/oa_dissertations

 Part of the [Biology Commons](#), [Neurosciences Commons](#), and the [Physiology Commons](#)

Recommended Citation

Rao, Tejeshwar, "Role Of Secretory Granule Heterogeneity In Calcium-Triggered Exocytosis" (2016). *Wayne State University Dissertations*. 1579.

https://digitalcommons.wayne.edu/oa_dissertations/1579

This Open Access Dissertation is brought to you for free and open access by DigitalCommons@WayneState. It has been accepted for inclusion in Wayne State University Dissertations by an authorized administrator of DigitalCommons@WayneState.

**ROLE OF SECRETORY GRANULE HETEROGENEITY IN
CALCIUM-TRIGGERED EXOCYTOSIS**

by

TEJESHWAR RAO

DISSERTATION

Submitted to the Graduate School

of Wayne State University,

Detroit, Michigan

in partial fulfillment of the requirements

for the degree of

DOCTOR OF PHILOSOPHY

2016

MAJOR: BIOLOGICAL SCIENCES

Approved By:

Advisor

Date

DEDICATION

To caffeine and sugar, my companions through many a long nights of experimentation, analysis and writing. To my family, who know not what I do but are proud nonetheless. And to Mitra for always being a strong support.

ACKNOWLEDGEMENTS

I wish to extend my heartfelt gratitude to all who have contributed to my research and training at Wayne State University. I particularly need to thank the department of Biological Sciences for their continued support in numerous ways over the years. I would also like to thank the students, staff and faculty of the PhD program in Biological Sciences, at Wayne State University.

Special thanks must go to my official advisor, Arun Anantharam, who could not have provided me with a better mentorship. His criticisms were always constructive, his experimental advice logically sound, and he pushed me to become a better communicator and presenter of my data. Importantly, he never said no to an experiment, even if it seemed anti-dogmatic or risky at the time. Also, I will add that his colorful personality and ever willingness to crack a joke, have not gone unappreciated over the years.

Furthermore, for their helpful suggestions and general guidance over the past few years, I want to thank the members of my thesis advisory committee, Edward Stuenkel, David Njus, and Karen Beningo. Their continued support and advice during and outside committee meetings has been of tremendous help and value.

I also want to thank both the past and present members of the Anantharam Lab, for being such wonderful colleagues. I would specially like to thank Mike Schmidtke, Peter Dahl and Andrew Peleman with whom I have spent the maximum amount of time in the laboratory. From the simplest technical

assistance, to reading through manuscripts, and critiquing my presentations, they have helped me immensely. Others include: Alexandria Ranski, Lisa Spencer, Paul Sellers, Matt Hutchinson, Rachel Jarrard, Madhurima Das, and Dan Passmore, with whom I have had the honor of working with while pursuing my PhD. I would also like to acknowledge the help of the undergraduate students who have been part of the Anantharam lab, specifically Jessica, Sandhya, Lauren, and Briana. Other students in the biology department, including Zuzer Dhoondia, Shashwat Mishra, Nikita Deshpande, and countless others, have collectively provided me with a unique research experience second to none, and I cannot express how grateful I am for it.

I would also like to thank the Graduate School for the financial support in the form of Graduate Teaching Assistantships and the Thomas C. Rumble Fellowship. I would also like to thank the department for the Graduate Enhancement Research funding and Travel Awards.

I would like to thank my friend Ojas Natarajan for always being there for me and forcing me to apply to the graduate program at Wayne State University. I also would like to thank my friend Pravin Sail back home in India for always being there for my family and me. I would like to thank my girlfriend, Mitra for her love and support. She has been both understanding and forgiving throughout my PhD research and continues to be my pillar of strength. Lastly, I would not have made it this far without the unflinching love and support from my parents, Prema and Chandrashekar Rao. They have always been present when needed and

supported me through all of my decisions. It was my Mom who instilled in me her “never-say-die” attitude. I would also like to thank my sisters, Sarveshwari and Rajeshwari Rao for always lightening my mood, and showing immense love, care, and belief in my abilities. Finally, I thank my brother-in law, Sunil Bharadwaj for always showing enthusiasm about my research and motivating me in my career. All of you mean the world to me.

TABLE OF CONTENTS

Dedication.....	ii
Acknowledgements.....	iii
List of Figures	viii
CHAPTER 1 – INTRODUCTION OF EXOCYTOSIS.....	1
CHAPTER 2 – CHROMAFFIN CELLS: AN IDEAL FOR THE STUDY OF EXOCYTOSIS	16
CHAPTER 3 - DISTINCT FUSION PROPERTIES OF SYNAPTOTAGMIN-1 AND SYNAPTOTAGMIN-7 BEARING DENSE CORE GRANULES	
Abstract	24
Introduction.....	25
Materials and Methods	28
Results.....	34
Discussion	58
Acknowledgements.....	66
CHAPTER 4 - CHROMAFFIN CELL SYNAPTOTAGMIN ISOFORMS FORM FUNCTIONALLY AND SPATIALLY SEPARABLE GRANULE POOLS	
Abstract	67
Introduction.....	68
Materials and Methods	71
Results.....	84
Discussion	115
CHAPTER 5 – SUMMARY AND SIGNIFICANCE.....	125

References	128
Abstract.....	167
Autobiographical Statement.....	171

LIST OF FIGURES

Figure 2.1: Structure and location of adrenal chromaffin cells (ACCs) residing within the adrenal medulla	18
Figure 3.1: Confocal imaging of Syt isoform expression on NPY-containing granules	35
Figure S3.1: Confocal imaging of overexpressed Syt isoforms and NPY Cerulean	37
Figure 3.2: TIRF imaging of Syt isoforms to visualize surface distribution following depolarization.....	39
Figure S3.2: Confocal imaging of Syt isoforms both within cells and on membrane following depolarization.....	40
Figure 3.3: Syt-7 fluorescence persists at sites of fusion for tens of seconds	43
Figure 3.4: Fusion of Syt-7 granules sometimes results in cavicapture	45
Figure 3.5: Syt-1 diffusion.....	47
Figure 3.6: Changes in membrane curvature following Syt fusion	49
Figure S3.3: Percentage endocytosis for Syt isoforms and changes in membrane curvature for VMAT-2 following fusion	51
Figure 3.7: Syt-1 granules release luminal contents more quickly than Syt-7 granules	53
Figure 3.8: A granule membrane protein is released slowly from Syt-7 granules upon fusion	54
Figure 3.9: Syt-1 and Syt-7 are differentially activated by depolarization.....	57
Figure 3.10: Model for Syt isoform mediated exocytosis in chromaffin cells	59
Figure S4.1: Confocal imaging of endogenous Syt isoform distribution within chromaffin cells.....	85
Figure 4.1: Distribution of Syt isoforms with respect to a rendered cell surface..	87

Figure 4.2: Characterization of docked and newcomer granules following membrane depolarization	90
Figure 4.3: Differential time course for activation of Syt isoforms	93
Figure 4.4: Lateral mobility of Syt isoform bearing chromaffin granules.....	95
Figure 4.5: Effect of repeated stimulation on Syt fusion competency.....	98
Figure 4.6: Determination of $[Ca^{2+}]_i$ in chromaffin cells using TIRF microscopy and the effects of cytosolic Ca^{2+} on Syt fusion.....	100
Figure S4.2: Patch-clamped chromaffin cells depolarized with elevated KCl....	101
Figure S4.3: Effect of different Ca^{2+} channel blockers (alone or in combination) on Ca^{2+} entry and Syt isoform fusion in chromaffin cells following membrane depolarization	103
Figure 4.7: Effect of different Ca^{2+} channel blockers (alone or in combination) on Syt isoform fusion in chromaffin cells following membrane depolarization.....	104
Figure S4.4: Fusion of NPY GFP granules following differential stimulation.....	105
Figure S4.5: Confocal imaging of Syt isoform distribution on NPY-containing granules	107
Figure 4.8: NPY pH release kinetics from granules overexpressing Syt-1 or Syt-7 mCherry	109
Figure 4.9: Super-resolution imaging of chromaffin cells transfected with Syt isoforms to determine membrane distribution following depolarization	112
Figure S4.6: Distribution of Syt isoforms on the plasma membrane and their in vitro disassembly kinetics from liposomes	114

CHAPTER 1 - INTRODUCTION TO EXOCYTOSIS

Exocytosis is the process by which intracellular vesicles (granules) move to the cell surface and fuse with the plasma membrane to release their contents. It is a vital mechanism regulating many critical cellular functions. First, exocytosis provides a means by which additional membrane can be added to the plasma membrane as the vesicle fuses with it (Breckenridge and Almers, 1987). Exocytosis can therefore restore or increase the plasma membrane, which is essential for cell repair and growth. Second, exocytosis is the process by which cells release hormones or neurotransmitters for intercellular signaling (Kelly, 1985). The two main functions of the nervous system are to process and relay information, and these are achieved primarily when neurotransmitter filled vesicles undergo exocytosis in a Ca^{2+} -dependent manner. This in turn then prompts further neuronal activity (Kelly, 1993; Albright *et al.*, 2000). Hormonal secretion has also been implicated in crucial physiological functions, including insulin secretion from pancreatic β -cells, where dysfunction results in diabetes mellitus (Turner *et al.*, 1995). Finally, exocytosis is pivotal in transferring many different membrane proteins to the plasma membrane. Vesicles turn inside out upon fusion with the plasma membrane. Thus, many membrane proteins, such as receptors exposed to the interior surface of the vesicle, are displayed on the cell surface following fusion. Postsynaptic receptors involved in long term modulation of learning and memory are expressed by this method (Lledo *et al.*, 1998).

1.1 A Brief History of Exocytosis Research

The era of modern cell biology blossomed in the middle of 19th century following application of electron microscopy to biology (Farquhar and Palade, 1998). Cells were found to contain an abundance of protein-containing vesicles. By 1970, George Palade and colleagues discovered a pathway for protein transfer between different cellular compartments, from which the field of “membrane trafficking” first developed (Palade, 1975; Sabatini, 1999). Parallel research in the field of neuroscience by Sir Bernard Katz and colleagues uncovered the concept of quantal release of neurotransmitters and suggested that they are packaged within discrete vesicles and released in a Ca^{2+} -dependent manner (Katz, 1971). Their work revealed the general pathway for exocytosis. Following synthesis in the endoplasmic reticulum (ER), secretory proteins are passed through the Golgi apparatus. Packaged vesicles budding from the trans-Golgi network (TGN) are finally exocytosed at the plasma membrane when triggered by a stimulus. However, the mechanisms by which these processes are regulated were still unknown. In the last two decades, the research of Randy Schekman, James Rothman, and many others has greatly advanced our understanding regarding the molecular mechanisms involved in membrane trafficking (Rothman, 2002; Schekman, 2002). The “SNARE hypothesis” is the most important concept developed during this time which suggests that each vesicle has a distinct v-SNARE protein (‘v’ for vesicle) that recognizes a t-SNARE protein (‘t’ for target) on the target membrane, and this

interaction is critical to achieve membrane fusion (Sollner *et al.*, 1993). More recent research has suggested this association to be a more general mechanism for fusion, and the SNARE proteins have been implicated to participate in many other facets of membrane trafficking other than fusion (Hong, 2005; Jahn and Scheller, 2006).

Exocytosis can be classified into two broad categories, constitutive or regulated, based on whether the secretion requires an initial stimulus (Burgess and Kelly, 1987). Constitutive exocytosis is found in all types of eukaryotic cells, and is primarily involved in the secretion of proteins and lipids to maintain the plasma membrane integrity. On the contrary, regulated exocytosis occurs in specialized secretory cells, such as neurons, chromaffin cells of the adrenal medulla, pancreatic β -cells, kidney duct cells, etc. These cells release content in response to certain physiological stimuli that result in an increase in intracellular Ca^{2+} which then acts as a trigger for exocytosis (Katz and Miledi, 1965; Neher *et al.*, 1987). As mentioned earlier, the SNARE hypothesis provides a molecular model explaining the steps leading to fusion, but does not shed light on how Ca^{2+} (trigger) might be involved in regulating fusion itself. Since the early 1990s, the work of Thomas Südhof and others have proposed the involvement of another vesicle membrane protein, synaptotagmin, which serves as a sensor for Ca^{2+} during exocytosis (Perin *et al.*, 1990; Chapman, 2002). Thus synaptotagmin, in combination with the other SNARE proteins, provide a more general model explaining the process of Ca^{2+} -triggered exocytosis.

1.2 Regulated Exocytosis

Our current knowledge of regulated exocytosis mostly stems from the study of neuronal synapses and other cell types such as adrenal chromaffin cells (ACC) (Burgoyne and Morgan, 2003). Other endocrine cells, like pancreatic β -cells, have also been used to study regulated exocytosis due to their physiological significance. Based on these studies, regulated exocytosis is generally believed to occur via two different types of secretory vesicles: small synaptic vesicles (SSVs) and large dense core granules (LDCGs). SSVs are the storage compartments for neurotransmitters, and have been well characterized in neurons. These vesicles are thought to originate from recycled endosomes, and are relatively small, with a diameter of less than 60 nm (Calakos and Scheller, 1996). SSV exocytosis is triggered by Ca^{2+} influx through voltage-gated Ca^{2+} channels following stimulation of the axon terminal with an action potential. On the contrary, LDCGs are more abundant in chromaffin and pancreatic β -cells with a diameter ranging between 200-400 nm. The granules show an electron-dense core due to condensed proteins and peptides present within them.

Neurons and neuroendocrine cells contain both types of vesicles and show similarities in the basic molecular mechanism underlying exocytosis of these vesicles, despite differences in their physiological significance (Morgan and Burgoyne, 1997; Martin, 2003). Both vesicles utilize SNARE proteins to mediate membrane fusion, and employ Ca^{2+} as a major signal to trigger exocytosis. Thus, understanding exocytosis for one vesicle type will provide insights into the

mechanisms employed in the other type. The research presented here will focus on Ca^{2+} -triggered LDCG release from adrenal chromaffin cells (ACCs).

1.3 Characterization of granule pools

On average, bovine ACCs contain between 17,000 - 22,000 LDCGs (Vitale *et al.*, 1995; Plattner *et al.*, 1997). These granules are classified into distinct pools based on their kinetic, morphological, and regulatory properties (Garcia *et al.*, 2006). The majority of granules are found in what has been termed the “reserve pool”, where they may remain for an extended period of time. A second pool, known as the “readily releasable pool”, contains LDCGs that can be rapidly mobilized for release within seconds. Finally, an intermediate pool, the “slowly releasable pool”, has also been described where granules reside in a docked but unprimed state (Steyer *et al.*, 1997; Trifaro *et al.*, 1997; Voets *et al.*, 1999a). LDCGs situated within these releasable pools are docked at the plasma membrane and may be in a primed (readily releasable pool) or unprimed stage (slowly releasable pool). That is, the granules are either fully fusion competent or require more priming steps involving ATP to enter that stage. Furthermore, LDCGs from each of the three pools can be selectively mobilized depending upon differential levels of stimulation and the secretagogue involved (Duncan *et al.*, 2003; Fulop *et al.*, 2005; Haynes *et al.*, 2007; Doreian *et al.*, 2009).

1.4 Molecular Mechanism of Regulated Exocytosis

In the last two decades, with the advancement of modern molecular technology, hundreds of proteins have been discovered and suggested to

participate in regulated exocytosis (Südhof, 2004; Brunger, 2005). A key concept in understanding exocytosis is the SNARE (soluble Nethylmaleimide-sensitive factor attachment protein receptor) hypothesis, which is the first working molecular model to explain the docking and fusion steps in vesicle cycling. The SNARE hypothesis suggests that vesicle exocytosis is mediated by three SNARE proteins: synaptobrevin (also called vesicle-associated membrane protein (VAMP)), syntaxin, and SNAP-25 (synaptosomal associated protein of 25 kDa). Synaptobrevin resides on the vesicle membrane (v-SNARE), whereas syntaxin and SNAP-25 are found on the plasma membrane (t-SNAREs) (Rothman, 1994; Jahn and Südhof, 1999; Chen *et al.*, 2001). The interaction of these three proteins permits the docking of granules at the plasma membrane, and zippering of their helices drives membrane fusion (Sollner *et al.*, 1993; Rothman, 1994; Chen *et al.*, 2001). The model alone cannot account for all the aspects of regulated exocytosis but it certainly serves as a great starting point for understanding how the process works and has inspired numerous studies in the field of membrane trafficking leading to our current understanding of exocytosis. Here, I will use the SNARE hypothesis concept to describe the molecular mechanism regulating exocytosis with specific focus on ACCs.

1.5 Stages of exocytosis in chromaffin cell LDCGs

Docking: Docking as a process has been defined in many different ways. One of which is on the basis of proximity of the fusing vesicle with respect to the plasma membrane when observed using an electron microscope. Electron micrographs

of mouse embryonic ACCs reveal that about 30% of LDCGs localize to within 50 nm of the plasma membrane and are regarded as being in a docked state. Of the major molecules involved in exocytosis, Munc18-1 and the syntaxins play a crucial role in docking. In Munc18-1 knockout mice, less than 5% of LDCGs are able to dock at the plasma membrane (Voets *et al.*, 2001c; Gulyas-Kovacs *et al.*, 2007). Being a soluble protein, Munc18-1 is thought to regulate docking of LDCGs by binding to the proteins on the granules and/or plasma membrane. Syntaxins are able to interact with Munc18-1 (Hata *et al.*, 1993; Pevsner *et al.*, 1994). There are many isoforms of syntaxin, and at least five (syntaxin1A, 1B, 2, 3 and 4) localize to the plasma membrane. The expression level of syntaxin1 is reduced by about half in Munc18-1-deficient neurons and ACCs (Voets *et al.*, 2001c; Gulyas-Kovacs *et al.*, 2007). Furthermore, viral infection of ACCs with botulinum neurotoxin C1, which cleaves syntaxin1A, 1B, 2 and 3, is shown to significantly reduce docking of LDCGs (Wit *et al.*, 2006). Other SNARE proteins, including SNAP-25 and synaptobrevin, do not seem to be involved in the docking of LDCGs. Although secretion is strongly suppressed in SNAP-25 deficient ACCs, the docking of the LDCGs is not affected (Sorensen *et al.*, 2003b). Therefore, it is the interaction of Munc18-1 and syntaxin (and not the SNARE protein complex as a whole) that is crucial for docking of granules (Gulyas-Kovacs *et al.*, 2007).

Rab3, a small monomeric Ras-like GTPase associated with granules has also been implicated in the process of docking (Schlüter *et al.*, 2002).

Overexpression of Rabs in PC12 cells, derivatives of ACCs, increased the total number of granules docked at the plasma membrane (Martelli *et al.*, 2000). Many other proteins that interact with SNARE proteins, such as rabphilin that interacts with SNAP-25, Mint (Munc-18-interacting) and Slpa2/granulophilin that interact with Munc18, and RIM (Rab3 interacting molecule) that interacts with Rab, seem to play an important role in vesicle docking but this remains to be fully determined (Schoch *et al.*, 2002; Schütz *et al.*, 2005; Tsuboi and Fukuda, 2006; Tsuboi *et al.*, 2007).

Priming: Following docking of the LDCGs, they must be primed to undergo fast Ca^{2+} -triggered exocytosis. Priming involves both ATP-dependent and -independent steps (Holz *et al.*, 1989; Xu *et al.*, 1998). Three cytosolic proteins have been identified to assume a prominent role in the ATP-dependent priming steps of exocytosis. These proteins include phosphatidylinositol transfer protein (PITP), type I phosphatidylinositol 4-phosphate-5-kinase (PIP5KI) and NSF (Malhotra *et al.*, 1988; Hay and Martin, 1993; Hay *et al.*, 1995). The recruitment of phosphoinositide by PITP followed by the phosphorylation of phosphoinositide by PIP5KI is thought to constitute a major component of ATP-dependent priming. Previous studies in PC12 cells have shown that PITP and PIP5KI are essential for priming to occur (Hay and Martin, 1993; Hay *et al.*, 1995). Essentially, PIP5KI requires ATP to phosphorylate phosphatidylinositol 4-phosphate (PIP) and generate phosphatidylinositol 4, 5-bisphosphate (PIP₂). PIP₂ then binds to synaptotagmin (Syt) and Ca^{2+} -dependent activator protein for secretion 1

(CAPS1), two major proteins implicated in the final steps of Ca^{2+} -triggered exocytosis. In support of this view, the level of PIP2 has been shown to control the size of the readily releasable granule pool (Milosevic *et al.*, 2005). Therefore, the generation and regulation of PIP2 by P1TIP and PIP5KI seems to be crucial in ATP-dependent priming.

The ATPase protein, N-ethylmaleimide-sensitive factor (NSF), is also known to serve a crucial role in ATP-dependent priming (Malhotra *et al.*, 1988; Kuner *et al.*, 2008). This is supported by studies in PC12 cells where overexpressing NSF increases granule priming leading to secretion (Banerjee *et al.*, 1996). Importantly, NSF also disassembles the cis-SNARE complex (formed following fusion) into the trans-complex wherein the SNARE proteins are no longer on the same membrane so that another round of exocytosis can proceed (Weber *et al.*, 2000).

At least two protein groups, Munc13 and CAPS1, are thought to serve a crucial role in ATP-independent priming. Although the expression level of Munc13-1 is low in ACCs and knockout mice show no signs of secretion defects, overexpression of Munc13-1 leads to an increase in LDCG secretion (Ashery *et al.*, 2000; Stevens *et al.*, 2005). Furthermore, Munc13-1 point mutants that do not bind syntaxin1 also fail to prime LDCGs (Stevens *et al.*, 2005). Therefore, the binding of Munc13-1 to syntaxin1 may contribute to priming in ACCs. In addition to its role in docking, Munc18-1 and Munc13-1 act together on the SNARE complex to promote priming (Gulyas-Kovacs *et al.*, 2007).

In PC12 cells, the cytosolic protein Ca^{2+} -dependent activator protein for secretion 1 (CAPS1), acts at a rate-limiting priming step (Fujita *et al.*, 2007; Sugita, 2008). Specifically, CAPS1 contains a Pleckstrin homology (PH) domain that binds to PIP2 in a Ca^{2+} -dependent manner. This interaction with PIP2 seems to regulate the number of LDCGs that undergo exocytosis (Grishanin *et al.*, 2002; Grishanin *et al.*, 2004). In mouse ACCs, however, the priming function of CAPS1 is not so clear. CAPS1-deficient embryonic ACCs show evidence that CAPS1 may play a role in loading catecholamines into LDCGs without necessarily being involved in the actual exocytosis process (Speidel *et al.*, 2005). However, embryonic (but not adult) ACCs also express CAPS2, a close isoform of CAPS1, making it difficult to isolate the role of CAPS1 in these cells. Furthermore, CAPS1 knockout mice die immediately after birth, making it difficult to analyze the function of this protein in adult ACCs (Speidel *et al.*, 2003). A CAPS1 knockdown line of PC12 cells, which also do not express CAPS2, has recently been employed to circumvent this issue (Fujita *et al.*, 2007). That study found CAPS1 to be critical in the priming and refilling of the releasable pools of LDCGs, but not for granule loading. Therefore CAPS1 not only plays a critical role in priming of docked granules, but also in the actual fusion process associated with Ca^{2+} -dependent, regulated exocytosis (Fujita *et al.*, 2007).

Triggering: The trigger for LDCG exocytosis is well known to be an influx of Ca^{2+} into the cell through voltage-gated Ca^{2+} channels during membrane depolarization. This implies the presence of a Ca^{2+} sensor at the exocytic site.

That sensor has been thought for some time to be synaptotagmin (Syt), a membrane protein associated with LDCGs and synaptic vesicles (Perin *et al.*, 1990). There is compelling evidence for this idea. In Syt-1-knockout mice, neurons show a marked decrease in Ca^{2+} -dependent neurotransmitter release from synaptic vesicles (Geppert *et al.*, 1994; Fernandez-Chacon *et al.*, 2001), and ACCs show partial reduction in LDCG secretion (Voets *et al.*, 2001b). Exocytosis in ACCs can be broken down into three components: a fast burst, a slow burst, and a refilling or sustained component which are representative of vesicle recruitment from the readily releasable pool (RRP), slowly releasable pool (SRP), and reserve pool (RP), respectively (Neher and Sakaba, 2008). Since Syt-1-deficient ACCs show a selective reduction in the fast burst component of exocytosis, it is most likely that Syt-1 serves as the Ca^{2+} -sensor (Voets *et al.*, 2001b; Sorensen *et al.*, 2003a).

The mechanism that Syt employs to trigger exocytosis wherein it acts as a key regulator for the temporal control of SNARE dependent fusion is still unknown. Clues for the function of Syt binding to the SNARE complex are found in its interplay with complexin, a family of small soluble proteins that bind to SNAREs (Chen *et al.*, 2002; Pabst *et al.*, 2002). The complexin clamp model proposes that complexin binding to the SNAREs clamps fusion (Schaub *et al.*, 2006; Giraudo *et al.*, 2008; Giraudo *et al.*, 2009). Upon rise of Ca^{2+} , Syt then displaces complexin from the SNARE complex allowing the SNARE assembly to become fusion competent. Thus it becomes extremely important to understand

the specific role of Syt in triggering fusion. One problem in studying this is the fact that more than one of the 17 known isoforms of synaptotagmin may be expressed in a given cell type (Südhof, 2002). For example, both Syt-1 and Syt-7 are involved in triggering exocytosis in ACCs (Schonn *et al.*, 2008). On the other hand, a clue comes from the fact that Syt isoforms show distinct concentration ranges for binding Ca^{2+} and initiating exocytosis (Zhang *et al.*, 1998). Furthermore, Syt contains two Ca^{2+} -binding C2 domains that bind to phospholipids, including PIP2, in a Ca^{2+} -dependent manner (Brose *et al.*, 1992; Sutton *et al.*, 1995; Arac *et al.*, 2006). Accordingly, the major targets of Syt appear to be phospholipids (Sugita *et al.*, 2002; Sugita, 2008). Following Ca^{2+} binding, Syt can also interact with the SNARE proteins syntaxin1 (Bennett *et al.*, 1992; Shao *et al.*, 1997) and SNAP-25 (Zhang *et al.*, 2002). In PC12 cells, Syt-1 specifically binds to the C-terminal residues of SNAP-25 and LDCG secretion is decreased if those residues are mutated. Other studies performed by Reinhard Jahn and colleagues have suggested that at physiological ion concentrations, Ca^{2+} -dependent Syt binding is limited to PIP2 containing membrane patches on the plasma membrane rather than SNARE proteins thereby triggering exocytosis (Park *et al.*, 2015).

In ACCs, GTP can also serve as a trigger for exocytosis independent of the presence of Ca^{2+} (Bittner *et al.*, 1986; Ahnert-Hilger *et al.*, 1992; Burgoyne and Handel, 1994). In fact, GTP triggers exocytosis without increasing intracellular Ca^{2+} in a range of other secretory cells, including: PC12 cells

(Klenchin *et al.*, 1998), pancreatic β -cells (Regazzi *et al.*, 1989), and mast cells (Gomperts, 1983; Fernandez *et al.*, 1984). In PC12 cells, this GTP-triggered form of exocytosis does not require cytosolic proteins, ATP, or Ca^{2+} (Klenchin *et al.*, 1998).

Fusion: The fusion step in exocytosis requires that the LDCG come into direct contact with the plasma membrane, allowing lipids to flow from one bilayer to the other. To accomplish this, the energetically unfavorable process of displacing water from between the two hydrophilic bilayers must be overcome. The SNARE proteins are thought to catalyze and play an important role in this final fusion step (Jahn and Scheller, 2006). The SNARE complex essentially consists of four SNARE motifs; one from syntaxin1, two from SNAP-25 and one from synaptobrevin. These motifs are aligned in parallel, with their transmembrane domains next to each other (Sutton *et al.*, 1995). The current view is that the zippering of the helical SNARE motifs provides the energy necessary to pull the two bilayers together.

Many studies have tested this idea in ACCs. Any mutations designed to impair the zippering of SNAREs lead to a decrease in exocytosis in these cells (Sugita, 2008). Furthermore, studies where the C-terminus of SNAP-25 is mutated reveal a decrease in the fast burst phase of exocytosis. This suggests that the C-terminal region of the SNARE complex is strongly coupled to triggering exocytosis. Conversely, mutations in the N-terminal region do not affect exocytosis (Borisovska *et al.*, 2005; Sørensen *et al.*, 2006).

1.6 Modes of fusion pore expansion

ACCs secrete their granular contents following fusion of the LDCGs with the plasma membrane. Fusion leads to formation of a passage called the fusion pore, connecting the granule lumen to the exterior of the cell. Following formation, the fusion pore either expands completely, whereby the granule membrane collapses onto the plasma membrane (full fusion exocytosis) (Heuser and Reese, 1973), or remains constricted and closes, allowing the granule to be recycled (kiss-and-run or transient exocytosis) (Ceccarelli *et al.*, 1973). The fusion pore can also fluctuate between an open and a closed state within a period of milliseconds (flickering) before fully fusing (Fernandez *et al.*, 1984). Thus, fusion pore behavior can lead to two separate modes of exocytosis based on whether the dense-core of the granule is completely or incompletely released. The exocytic mode is thought to be heavily influenced by sympathetic activity (Takiyyuddin *et al.*, 1990; Watkinson *et al.*, 1990; Perrais *et al.*, 2004; Fulop *et al.*, 2005; Anantharam *et al.*, 2011). One implication of these results is that the various constituents within the granule can be released in a selective manner. Intense stimuli result in full fusion and complete release of all granule contents (Viveros *et al.*, 1969). Conversely, more modest levels of stimulation lead to the kiss-and-run mode, which is characterized by a transient release of smaller cargo through a restricted fusion pore (~4 nm in diameter) (Klyachko and Jackson, 2002). In this case the granules remain intact after exocytosis, and the larger neuropeptide cargos within the granule are retained (Fulop *et al.*, 2005). Thus,

LDCG exocytosis seems to employ a size exclusion mechanism to differentially release catecholamines and neuropeptides that are co-packaged in the same granule (Takiyyuddin *et al.*, 1990; Watkinson *et al.*, 1990; Takiyyuddin *et al.*, 1994). In addition to fusion pore size, pore duration can also significantly affect the amount of transmitter released during the exocytic response. Overall, ACCs may selectively release their granular content by dilating the fusion pore completely, or by closing it following transient fusion (Zhou *et al.*, 1996; Albillos *et al.*, 1997; Ales *et al.*, 1999; An and Zenisek, 2004).

1.7 Summary and Perspective

LDCGs destined to undergo exocytosis transition through stages of docking, priming, triggering, and ultimately fusion. Docking is mediated primarily by Munc18-1 and syntaxin, among other proteins. Priming is ATP-dependent and requires the activity of Munc13-1 and CAPS1, in addition to the phosphorylation of PIP on the plasma membrane. Ca^{2+} entry serves as the trigger for membrane fusion and is mediated through the Ca^{2+} sensing protein synaptotagmin. ACCs express two isoforms of synaptotagmin, Syt-1 and Syt-7; however their independent functions in triggering fusion have been largely unexplored. The focus of this work is to address the role of Syt isoforms in stimulus secretion coupling in the physiological context of adrenal chromaffin cells.

CHAPTER 2 - INTRODUCTION TO CHROMAFFIN CELLS: AN IDEAL SYSTEM FOR THE STUDY OF EXOCYTOSIS

The research work presented in this dissertation was carried out in the bovine adrenal chromaffin cell (ACC). ACCs are often used as a model cell to study exocytosis since they are unique in displaying properties of both neurons and other neuroendocrine secretory cells (Winkler and Fischer-Colbrie, 1998; Garcia *et al.*, 2006). At the time of submission of this dissertation there is a sizeable knowledge base for the ACC. Here I outline the most interesting features of these cells as they provide a foundation for the biological interpretations within this work.

2.1 Brief background

ACCs were first discovered and described in useful detail by Alfred Kohn at the beginning of the 19th century. It was observed that these cells were closely related to neurons in the sympathetic ganglia and have secretory properties (Kohn, 1898, 1902, 1903). Kohn's observation that the cells react with chromium salts, imbuing them with a yellowish-brown staining pattern resulted in the term 'chromaffin' being used to name them (Hingerty and O'Boyle, 1972). The advancement in microscopy technologies in the 1960's provided scientists a means to begin describing the structural, developmental and functional characteristics of these cells (Coupland, 1965a, b; Coupland and Hopwood, 1966; Coupland, 1989). By the end of the 1960's William Douglas had first postulated his theory of stimulus-secretion coupling based on data from cat adrenals, which underscored the importance of Ca²⁺ ions as a trigger linking

cellular excitation with the initiation of exocytosis (Douglas, 1968). In the 1970's following refinement of tissue culture techniques to isolate ACCs, the previously performed *in situ* or *in vivo* studies could be extended further as ACCs became amenable to molecular biology, fluorescence microscopy, biochemical and electrophysiological techniques. In the early 1980's through the turn of the next century, powerful electrochemical and electrophysiological methods for single cell recordings of exocytosis emerged. Techniques like patch clamp capacitance (Neher and Marty, 1982); amperometry (Leszczyszyn *et al.*, 1990) and patch amperometry (Albillos *et al.*, 1997) have all employed ACCs as a model cell to better understand exocytosis.

2.2 Basic anatomy and physiology

Chromaffin cells are found within the adrenal medulla where they comprise the majority of the tissue (Figure 2.1). Ganglionic and other sustentacular cells are also present in the medulla, but to a smaller extent. These supporting cells surround the clusters of medullary ACCs (O'Connor, 2003). Within the ACCs are secretory granules called large dense core granules (LDCGs), which store catecholamines. Catecholamines contained within these granules are released from the cells by the process of exocytosis. During this process, other contents contained within granules, including chromogranins, various peptides (e.g. Neuropeptide Y), and enzymes are also released simultaneously into the circulation. Catecholamines are cleared primarily by reuptake into the cell. Following reuptake, cytosolic catecholamines may either

be repackaged into granules via active transport or deaminated and metabolized by the process of O-methylation or oxidation. Once released into the bloodstream, catecholamines have a short half-life of about 1-2 minutes and are cleared from circulation primarily by reuptake or renal excretion (Fung *et al.*, 2008).

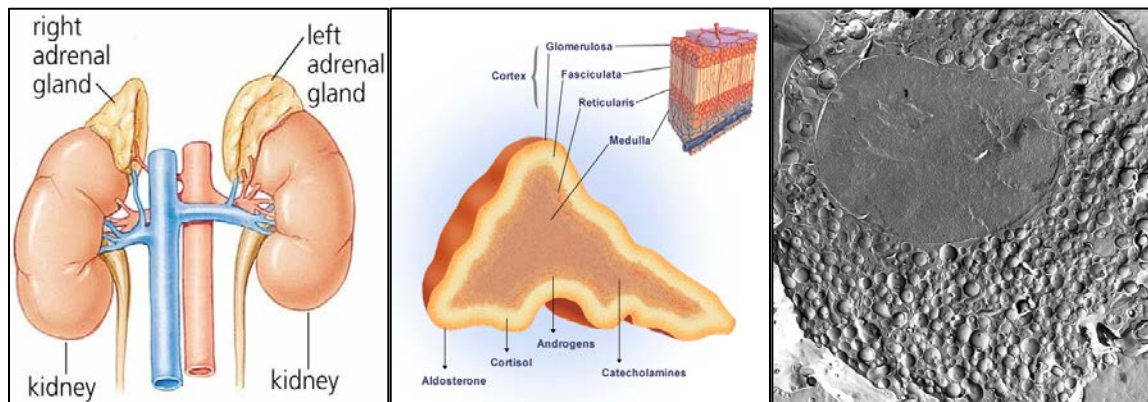


Figure 2.1. Structure and location of adrenal chromaffin cells (ACCs) residing within the adrenal medulla.

The adrenal glands are located just above the kidneys (left panel) and are comprised of the inner medulla, where the ACCs reside, and an outer cortical layer (middle panel). An electron micrograph of a section from an isolated bovine chromaffin cell is shown in the (right panel) with a large number of Large Dense Core Granules (LDCGs). (Figure adapted from Carmichael, S.W. 1979-84. The adrenal medulla. In Eden Press; Agent, Montreal, Quebec, Canada; Buffalo, N.Y. and Grabner *et al.*, 2005)

2.3 Neurogenesis of ACCs

ACCs are embryonically derived from neural crest ectoderm and innervated by the preganglionic sympathetic fibers of splanchnic nerves, which secrete acetylcholine (Le Douarin, 1982). During development, specific guidance factors are responsible for the migration of chromaffin stem cells from the dorsal surface of the neural tube (Le Douarin *et al.*, 1994). In the developing adrenal

gland, nerve fibers and neuroblasts migrate from the neural crest and penetrate between the cortical cells (Crowder, 1957). These invading neuroblasts originate from cords of pheochromoblasts during differentiation (Hervonen, 1971; Coupland, 1989), and contain islets of cortical cells. Both pheochromoblasts and cortical cells remain interrelated during the fetal stage (Wilburn and Jaffe, 1988). Postnatally, the cells of the fetal cortex degenerate and the final cortex begins to form. Islands of neuroblasts then settle against the central vein, and eventually form a highly compact, vascularized structure within the medulla of the adrenal gland. The reticular zone now begins to develop, and cortical cells appear amongst the group of chromaffin cells (Díaz-Flores *et al.*, 2008).

2.4 Chromaffin granules and secretory products

LDCGs within ACCs contain most of the known neuropeptides, though often at low concentrations (Toth and Hinson, 1995). LDCGs also contain other contents like catecholamines, epinephrine or norepinephrine, as well as serotonin, amylin, ATP, and various enzymes (Winkler and Fischer-Colbrie, 1998; Chen *et al.*, 2005). LDCGs of chromaffin cells are similar to those found in neurons with respect to their content, morphology, biogenesis, life cycle, and membrane composition (De Camilli and Jahn, 1990; Thomas-Reetz and De Camilli, 1994).

Depending on the type of cargo they contain (e.g. epinephrine or norepinephrine); LDCGs display heterogeneity in size, shape, and electron density. Variability in these parameters differs between species. For example, in

mice, rats, and dogs LDCGs are highly diverse (Coupland, 1965a, b; Carmichael *et al.*, 1987; Grabner *et al.*, 2005), while in primates the variability is nominal (Al-Lami, 1969; al-Lami and Carmichael, 1991). Epinephrine LDCGs vary by species and range between 150 and 350 nm in diameter. They have a round morphology, present a moderate electron density with a fine granular content appearance, and tend to exhibit a narrow, uniform halo around cells. Alternatively, norepinephrine LDCGs have a larger diameter and an irregular, oval, or elliptical shape with higher electron density (Coupland, 1965a, b; Grabner *et al.*, 2005).

In addition to the catecholamines, LDCGs contain abundant amounts of the granule matrix protein chromogranin, which are precursors to the neuropeptides catestatin and pancreastatin. Amongst these are chromogranins A, B (also called secretogranin I), and C (also called secretogranin II) (Winkler and Fischer-Colbrie, 1992; Montero-Hadjadje *et al.*, 2008). LDCGs also contain neuropeptides and enkephalins (Kataoka *et al.*, 1985), adenine nucleotides, high concentrations of Ca^{2+} (Winkler and Westhead, 1980; Carmichael and Winkler, 1985; Winkler, 1993), syntaxin 1A, synaptotagmin (Yoo *et al.*, 2005), and plasminogen activator (Parmer *et al.*, 1997). ACCs also express adrenomedullin (Kobayashi *et al.*, 2003), and enzymes such as dopamine β -hydroxylase and tyrosine hydroxylase. Additionally, ACCs secrete trophic factors that promote survival of various types of neurons (Schumm *et al.*, 2004). ACCs also contain a population of microvesicles that are closely related to neuronal synaptic vesicles and store acetylcholine but not catecholamines.

2.5 Physiologic effects of secretory products

From a physiological perspective, the two most important functions performed by ACCs are synthesis and secretion of epinephrine and nor epinephrine. Following release into the bloodstream, these monoamines bind to α or β -adrenergic receptors on target cells of various organs. Upon binding, they essentially induce a secondary messenger cascade that drives downstream signaling within the cell. Their release from ACCs leads to a much broader and longer lasting effect since they can cause changes in cells and tissues not directly innervated by blood vessels. Adrenergic receptors belong to the family of seven-pass transmembrane proteins known as G-protein coupled receptors (GPCRs), which stimulate or inhibit intracellular signaling pathways via second messengers such as cyclic adenosine monophosphate (cAMP) and Ca^{2+} . The complexity of the physiological response following stimulation of the ACC varies based on the differential expression of multiple receptor subtypes on the surface of cells and tissues. The major effects mediated by catecholamine release include increased heart rate and heart muscle contraction, constriction of blood vessels, dilation of bronchioles, initiation of lipolysis in fat cells, increased basal metabolic rate and glycolysis in skeletal muscle, dilation of the pupils, and inhibition of specific parasympathetic activities such as gastrointestinal secretion and motor activity (Guyton and Hall, 2000, 2006). In addition to the catecholamines, neurologically active proteins and peptides are also released from ACCs. For example, the chromogranins, which can be cleaved into

catestatins following exocytosis, negatively modulate the neuroendocrine activity of themselves or other nearby ACCs. Neuropeptide Y (NPY) can modulate vasoconstriction and enkephalins can serve as an endogenous opioid, acting as an analgesic to allow an organism to focus on escape or defense during the sympathetic stress response (“fight or flight”) (O'Connor and Frigon, 1984; O'Connor *et al.*, 2007).

2.6 Regulation by the sympathetic nervous system and “tone”

Preganglionic acetylcholine-secreting nerves originating in the spinal cord control release from ACCs by a mechanism similar to that observed in neurons of the sympathetic system. Sympathetic neurons have finer axons that extend into their target organs, and exert localized control at axon terminals. On the contrary, secretion of hormones from ACCs elicits a more widespread response. Exercise, hypoglycemia, hemorrhage, and emotional distress are some of the common factors leading to increased secretion. A key feature of the autonomic nervous system is the requirement of very low frequency stimulation to maintain complete activation of its targeted effectors. Under resting conditions, commonly known, as the “breed and feed” or “rest and digest” state, the parasympathetic and sympathetic nervous systems are continually active at low basal rates. The term “tone” refers to the level of nervous system activation. Gauging the tone at any given time allows the nervous system to regulate the activity of an effector organ appropriately. For example, under resting conditions, sympathetic tone maintains systemic arterioles constricted to half their maximal diameter. By increasing the

degree of sympathetic activation above normal (supertonic) during stress, the arterioles can be further constricted. On the contrary, in a subtonic state the vessels dilate (Guyton and Hall, 2000, 2006). During higher rates of stimulation (supertonic sympathetic activation), ACCs also secrete neuropeptides, in addition to elevated levels of catecholamines, into circulation (Fulop *et al.*, 2005).

CHAPTER 3 - DISTINCT FUSION PROPERTIES OF SYNAPTOTAGMIN-1 AND SYNAPTOTAGMIN-7 BEARING DENSE CORE GRANULES

This chapter has been published.

Tejeshwar C. Rao, Daniel R. Passmore, Andrew R. Peleman, Madhurima Das, Edwin R. Chapman, and Arun Anantharam (2014) Distinct fusion properties of synaptotagmin-1 and synaptotagmin-7 bearing dense core granules. *Molecular Biology of the Cell*. 25(16): 2416-27. doi: 10.1091/mbc.E14-02-0702. This article is distributed by the American Society for Cell Biology, under license from the author(s), which permits unrestricted use, distribution and reproduction in any medium, provided the original author and source are credited.

ABSTRACT

Adrenal chromaffin cells release hormones and neuropeptides that are essential for physiological homeostasis. During this process, secretory granules fuse with the plasma membrane and deliver their cargo to the extracellular space. It was once believed that fusion was the final regulated step in exocytosis, resulting in uniform and total release of granule cargo. Recent evidence argues for non-uniform outcomes after fusion, in which cargo is released with variable kinetics and selectivity. The goal of this study was to identify factors that contribute to the different outcomes, with a focus on the Ca^{2+} -sensing synaptotagmin (Syt) proteins. Two Syt isoforms are expressed in chromaffin cells: Syt-1 and Syt-7. We find that overexpressed and endogenous Syt isoforms are usually sorted to separate secretory granules and are differentially activated by depolarizing stimuli. In addition, overexpressed Syt-1 and Syt-7 impose distinct effects on fusion pore expansion and granule cargo release. Syt-7 pores usually fail to expand (or reseal), slowing the dispersal of luminal cargo proteins and granule membrane proteins. On the other hand, Syt-1 diffuses from fusion

sites and promotes the release of luminal cargo proteins. These findings suggest one way in which chromaffin cells may regulate cargo release is via differential activation of synaptotagmin isoforms.

INTRODUCTION

It was once believed that exocytosis occurred in an all-or-none manner, in which, after a secretory granule fused, it was committed to release all of its contents. More recent evidence suggests that in the adrenal chromaffin cell, mechanisms have evolved to regulate content release after fusion by controlling the rate or the extent of fusion pore expansion (Taraska *et al.*, 2003; Perrais *et al.*, 2004; Taraska and Almers, 2004; Fulop *et al.*, 2005; Fulop *et al.*, 2008; Anantharam *et al.*, 2011). The fusion pore is the aqueous passage through which essential signaling molecules (neurotransmitters, hormones, neuropeptides, etc.) are expelled into the extracellular space. Control over the sieving properties of the fusion pore greatly expands the physiological range of exocytosis. It allows, for example, cells to release contents selectively on the basis of size exclusion; smaller hormones leave small pores more readily than larger proteins, which are retained. Such selective content release may be relevant to different functions of the adrenal medulla as part of the sympathetic nervous system. Under basal conditions, chromaffin cells release catecholamines (epinephrine and norepinephrine) at a low basal rate set by the sympathetic tone (de Diego *et al.*, 2008b). Basal secretion is linked with the cavicapture fusion mode, in which granules fuse and release contents through a transient opening, which reseals

(Taraska *et al.*, 2003; Perrais *et al.*, 2004). Acute stress dramatically up-regulates not only the level of catecholamines in the circulation, but also a variety of neuropeptides with roles in the peripheral response (Damase-Michel *et al.*, 1993; Edwards and Jones, 1993; de Diego *et al.*, 2008b). The increased sympathetic activation of the adrenal medulla during stress is linked with full-collapse fusion. In this mode, the pore expands widely, allowing for more thorough release of granule lumen constituents. Despite these observations, there is a gap in our knowledge with respect to the molecular events that regulate fusion pore expansion and concomitant content dispersal. Because of the importance of adrenal hormones for physiological homeostasis, this is a major limitation.

In chromaffin cells, the trigger for stimulus-evoked exocytosis is a rise in intracellular Ca^{2+} . The level of intracellular Ca^{2+} accumulation varies with the stimulus intensity and secretagogue (Augustine and Neher, 1992; Garcia *et al.*, 2006; de Diego *et al.*, 2008b). Ca^{2+} regulates release by acting on the Ca^{2+} -binding synaptotagmin (Syt) protein family (Brose *et al.*, 1992; Voets *et al.*, 2001b; Schon *et al.*, 2008), driving their association with membranes that harbor anionic lipids (Tucker *et al.*, 2004). This interaction between the Syt- Ca^{2+} complex and the membrane is proposed to serve as a critical step in excitation–secretion coupling (Brose *et al.*, 1992). Although there are at least 17 Syt isoforms, chromaffin cells express only two: Syt-1 and Syt-7 (Schon *et al.*, 2008). The two isoforms differ in their affinity for Ca^{2+} in the presence of anionic phospholipids and their rate of disassociation from phospholipids (Sugita *et al.*,

2002; Tucker *et al.*, 2003; Bhalla *et al.*, 2005; Hui *et al.*, 2005). The goal of the present study was to determine whether the divergent biochemistry of the two Syt isoforms expressed in chromaffin cells imposes functionally divergent effects on dense core granule exocytosis. That the roles of Syt isoforms in chromaffin cells are distinct is suggested by previous studies in the PC12 cell line. PC12s express 4 Syt isoforms: 1, 4, 7, and 9 (Fukuda *et al.*, 2002; Fukuda, 2004; Fukuda *et al.*, 2004). Overexpression studies suggest that isoforms harbor a size preference for secretory granules (Zhang *et al.*, 2011) and endow the fusion event with different functional and kinetic properties (Moghadam and Jackson, 2013). Syt-4, for example, negatively regulates exocytosis, increasing the probability that pores will reseal after fusion (Wang *et al.*, 2001; Zhang *et al.*, 2011). Syt-1 fusion also produces more cavicapture events than either Syt-7 or Syt-9 (Wang *et al.*, 2001; Wang *et al.*, 2003a; Bai *et al.*, 2004b; Wang *et al.*, 2006). Suppression of Syt-1 and Syt-9 expression abolishes Ca^{2+} -dependent release, suggesting that these two isoforms account for all regulated exocytosis in PC12 cells (Lynch and Martin, 2007).

In this study, we identify fundamentally different roles for Syt-1 and Syt-7 in chromaffin cell exocytosis. We find that endogenous Syt-1 and Syt-7 rarely co-localize on granules, with most expressing only one isoform or the other. Syt isoform effects on fusion, fusion pore expansion, and endocytosis were also distinct. When overexpressed, Syt-1 enables the rapid expansion of fusion pores and promotes the release of granule membrane and luminal proteins. On the

other hand, Syt-7 fusion pores usually fail to expand (or reseal) and restrict cargo release. Consistent with these results, granules with Syt-1 overwhelmingly undergo the full-collapse mode of fusion, whereas those with Syt-7 exhibit higher rates of endocytosis. Finally, we find that isoforms have different requirements for activation. A more strongly depolarizing stimulus, and a correspondingly greater increase in intracellular Ca^{2+} , is necessary to activate Syt-1 than it is to activate Syt-7. On the basis of these results, we propose that selective, stimulus-dependent activation of the Syt isoforms play an important role in controlling chromaffin cell fusion modes.

MATERIALS AND METHODS

Polarized Total Internal Reflection Fluorescence Microscopy

Detailed description for the specialized excitation system used to create the orthogonal p- and s-polarized 561-nm beams and further superimpose them onto the 488-nm beam is provided elsewhere (Anantharam *et al.*, 2010). The system uses Lambda SC smart-shutter controllers (Sutter Instruments, Novato, CA) that allow for rapid selection of three shutter openings sequentially—p- and s-polarized 561 nm excitation and the 488-nm excitation (one at a time)—and repeats the cycle using MetaMorph software (Molecular Devices, Sunnyvale, CA). The common beam path was focused through a custom side port to a side-facing filter cube placed below the objective turret of an Olympus IX81 (inverted) microscope (Center Valley, PA) to produce objective-based TIRF illumination. The dichroic mirror/emission filter cube combinations used for the experiments

were as follows: z488/561 rpc and z488/561m_TIRF for syt-pHl/ DiD or CgB pHl/syt-Cherry imaging and z488/640 rpc and z488/640m for imaging antibody staining in TIRF (Chroma Technology, Brattleboro, VT). For directing the incident beam at $\sim 70^\circ$ from the normal on the coverslip, the beam was focused on the periphery of the back focal plane of a 60 \times /1.49 numerical aperture (NA) oil immersion objective (Olympus), thereby giving a decay constant for the evanescent field of ~ 110 nm.

Two additional lenses (1.6 \times and 2 \times) in the emission path between the microscope and electron-multiplying charge-coupled device (EM CCD) camera give a final pixel size of ~ 80 nm. Images were acquired using a cooled EM CCD camera (iXon3, Andor Technology, South Windsor, CT). The acquisition of the digital image was in synchrony with opening of the smart shutters specific for the individual beams. The images were acquired at ~ 5 Hz with 25-ms exposures and 300 gain (EM setting). One complete cycle of three exposures lasted ~ 200 ms.

Chromaffin Cell Preparation and Transfection

The chromaffin cells were isolated from bovine adrenal medulla, and transient transfections were performed as described earlier (Wick *et al.*, 1993). To facilitate cell adhesion, cells were plated on 35-mm tissue culture dishes with cover glass bottom (refractive index, 1.51; World Precision Instruments, Sarasota, FL) pre-coated with poly-d-lysine and bovine collagen. Cells were transiently transfected by electroporation with plasmid(s) using the Neon transfection system (Invitrogen, Carlsbad, CA). The procedure for electroporation

was standardized, and the cells were transfected with a single pulse of 1100 mV for a period of 40 ms. The Syt-1-pHluorin and Syt-7-pHluorin constructs in pCI vector were transfected alone in DiD experiments. The Syt-1-mCherry and Syt-7-mCherry constructs were co-transfected with CgB-pHluorin or VMAT2-pHluorin. The VMAT2-pHluorin plasmid was a gift from Robert Edwards (University of California, San Francisco, CA). Syt isoform sorting was determined in two ways: 1) expression of NPY-Cer alone, followed by immunocytochemistry using antibodies toward the Syt isoforms; or 2) co-transfection of Syt-1-Cherry, Syt-7-GFP, and NPY-Cer. The parent NPY plasmid was a gift from Wolfhard Almers (Vollum Institute, Oregon Health and Science University, Portland, OR). Stimulation-evoked surface distribution was visualized by TIRF microscopy of cells by co-expression of Syt-1-WT and myc-tagged Syt-7 (gift of Thomas Sudhof, Stanford University, Palo Alto, CA) with immunocytochemistry. All experiments were performed 2–5 d after transfection.

Cell Stimulation

Before imaging, cells were stained with diD added directly to cells bathed in PSS at 1:200 dilution. The cells were quickly washed several times in PSS to get rid of the excessive dye and then used immediately. All TIRF experiments were performed in PSS containing 145 mM NaCl, 5.6 mM KCl, 2.2 mM CaCl₂, 0.5 mM MgCl₂, 5.6 mM glucose, and 15 mM 4-(2-hydroxyethyl)-1-piperazineethanesulfonic acid (HEPES), pH 7.4. A computer-controlled perfusion system, ALA-VM4 (ALA Scientific Instruments, Westbury, NY), was used to

perfuse individual cells with a needle (100- μm inner diameter) under positive pressure. Normally, cells were perfused with PSS for 10 s and then stimulated with high- K^+ -containing solution to secrete (95 mM NaCl, 56 mM KCl, 5 mM CaCl_2 , 0.5 mM MgCl_2 , 5.6 mM glucose, 15 mM HEPES, pH 7.4) for ~60 s to trigger exocytosis. Endocytosis was measured as previously described (Anantharam *et al.*, 2011). Briefly, cells were first perfused with elevated- K^+ PSS at pH 7.4 for 30 s and then exposed to pH 5.5 PSS (HEPES was substituted by 2-(N-morpholino) ethane sulfonic acid buffer) to quench the fluorescence of any extracellular facing pHluorin. The cells were then again exposed to normal PSS at pH 7.4, and the cycle was repeated every 10 s. Bafilomycin (Santa Cruz Biotechnology, Santa Cruz, CA), an inhibitor of vacuolar-type H^+ -ATPase that reacidifies endocytosed granules, was added to PSS at a final concentration of 5 μM . Experiments were performed at ambient temperatures of 30–32°C.

Image Analysis

The Syt-pHluorin, diD s- and p-polarization emission images were captured sequentially using MetaMorph software. The P/S and P+2S ratios were calculated after normalization on a pixel-to-pixel basis for every image, and custom software written in IDL (ITT, Boulder, CO) was used to align the transformations to the Syt-pHluorin images. Individual granules undergoing exocytosis were evident by increase in the pHluorin intensity after fusion with the plasma membrane as a result of change in pH of the granule. The P/S and P+2S changes were calculated by centering the region of interest over localized

increase in P/S ratio at the site of exocytosis in a radius of ~240 nm. Multiple factors, such as relative intensities of the p- and s-polarized excitations, biases in optical system, and certain interference fringes, can result in variations in the P/S ratio. To reduce this discrepancy and further allow for a theoretical comparison, a solution of 10 mM rhodamine 6G (Invitrogen), a dye predicted to be randomly oriented, was used to normalize the P/S data from DiD emission. The spatial mean of rhodamine 6G emission excited by each of the p- and s-polarized 561-nm beams was used for normalization of data. Similarly, for correcting the P+2S values, the amplitudes of p relative to s were calculated by calibration of rhodamine 6G. Topological changes were considered significant if P/S and P+2S increased above 7% (3× SD of the mean) with respect to baseline within five frames of the fusion event (indicated by pHluorin or GFP intensity changes). Emission intensity changes that did not cross the 7% threshold were not included in the data set for analysis. The average fluorescence change of gCaMP5G in response to different depolarizing stimuli (10, 25, and 56 mM KCl) was estimated not as $[Ca^{2+}]$, but as the pseudo ratio $\Delta F/F = (F - F_{base}) / (F_{base} - B)$, where F is the measured fluorescence intensity of the genetically encoded Ca^{2+} indicator, F_{base} fluorescence intensity of Ca^{2+} indicator in the cell before stimulation, and B the background signal determined from average of areas adjacent to the cell.

Immunocytochemistry

For immunofluorescence microscopy to detect synaptotagmin isoform distribution in cells expressing NPY Cerulean, isolated chromaffin cells on the

glass cover dish were fixed with 4% paraformaldehyde in phosphate-buffered saline (PBS) for 30 min. The cells were then rinsed and quenched with 50 mM NH_4Cl in PBS. After washing, the cell membrane was permeabilized for 7 min with acetone to preserve the cell cytoskeleton. The cells were further washed with Tris-buffered saline (TBS) and blocked with 1% gelatin in TBS and 4% donkey serum for 30 min each. Primary and secondary antibodies were diluted in a solution of 2–4 mg/ml BSA. Cells were incubated for 2 h at room temperature with a combination of the following antibodies: monoclonal anti-Syt-1 antibody (antibody 41.1) and polyclonal anti-Syt-7 antibody (Synaptic Systems, Göttingen, Germany). The cells were then washed five times in TBS and incubated for 70 min with Alexa-conjugated anti-rabbit and anti-mouse secondary antibodies (Molecular Probes/Invitrogen, Eugene, OR). The cells were washed five times after the incubation and imaged by confocal microscopy.

Alternatively, to visualize the stimulation-evoked surface distribution of the Syt isoforms, the cells expressing Syt-1 WT and myc-tagged Syt-7 were first washed with PSS at room temperature, followed by stimulation with either a high- K^+ -containing PSS solution (56 mM KCl) or low- K^+ -containing PSS solution (10 mM KCl) for 1 min at room temperature. All activity within the cell after stimulation was arrested using cold PSS. The cells were further incubated with the following antibodies for 2 hr. on ice (4°C): monoclonal anti-Syt-1 antibody and myc-tag antibody for Syt-7 (Cell Signaling Technology, Danvers, MA). The cells were washed five times with TBS and then fixed at 37°C using the

procedure described. After blocking, the cells were stained by incubation with Alexa-conjugated anti-rabbit and anti-mouse secondary antibodies (Molecular Probes/Invitrogen) for 70 min at room temperature as previously described.

Confocal Microscopy

For transfected and immuno-stained cells showing a fluorescence signal, images were acquired on a Leica TCS SP5 confocal microscope with a 63×/1.40 NA oil objective. For imaging, a 405-nm diode laser, an argon 488-nm laser, and a HeNe red 594-nm laser were used. The images obtained were analyzed with Image J software (National Institutes of Health, Bethesda, MD). Statistical calculations were performed using Prism 6 software (GraphPad, La Jolla, CA).

RESULTS

Synaptotagmin isoforms are sorted to different granule populations

Chromaffin cells express two protein isoforms of synaptotagmin (Syt-1, Syt-7). An important question is whether they are sorted to the same or separate secretory granules. A recent study in PC12 cells, which express Syt-1, 4, 7, and 9, showed there to be significant differences in isoform sorting (Zhang *et al.*, 2011). Therefore our first goal was to visualize chromaffin cell granules and determine how frequently they express one or both isoforms. We transfected cells with neuropeptide Y–Cerulean (NPY-Cer) to label granules and identified isoforms using antibodies against Syt-1 and Syt-7. We then counted the number of fluorescent Syt-1 and/or Syt-7 puncta that co-localized with NPY. The data are shown in Figure 3.1, A and B.

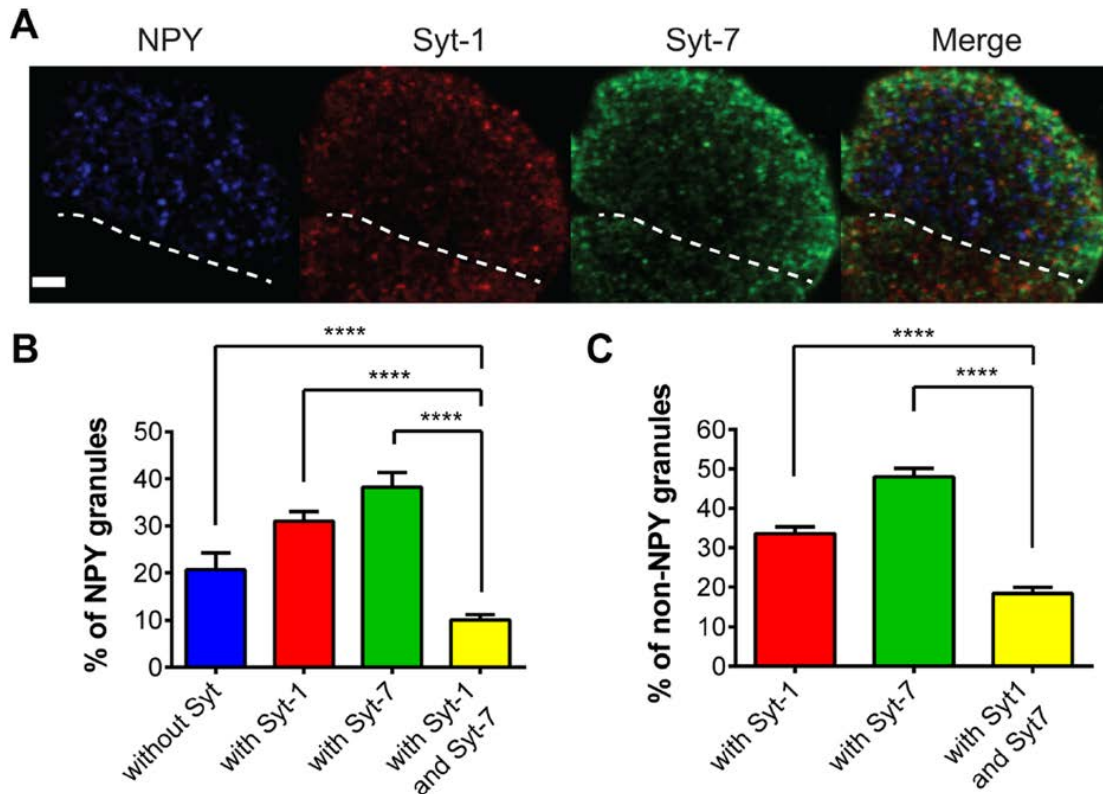


Figure 3.1. Confocal imaging of Syt isoform expression on NPY-containing granules.

(A) Chromaffin cells cultured on glass coverslips were transfected with a plasmid encoding NPY-Cer. At 3–4 d after transfection, cells were fixed, permeabilized, and exposed to Syt-1 and Syt-7 antibodies. Confocal sections of 0.5 μm were taken through the cell. The region closest to the coverglass was imaged. The dotted line indicates the boundary of the transfected NPY-Cer cell from a non-transfected cell below. Scale bar, 3 μm. **(B)** The percentage co-localization of NPY granules with any synaptotagmin or with Syt-1, Syt-7, and Syt-1 plus Syt-7. Differences between groups were assessed with the Student's t test ($n = 17$ cells, **** $p < 0.0001$). **(C)** Synaptotagmin isoforms were sometimes detected in regions without obvious NPY-Cer fluorescence. Co-localization of isoforms in non-NPY granules was determined. Differences between groups were assessed with the Student's t test ($n = 17$ cells, **** $p < 0.0001$).

Across 17 cells, almost 69% of NPY-labeled granules expressed either Syt-1 or Syt-7. Fewer than 20% of NPY granules did not have any Syt-protein, whereas an even smaller number (<10%) expressed both isoforms. We also

examined whether overexpression altered the distribution of synaptotagmin resulting in increased co-localization of isoforms on granules. Cells were transfected with NPY-Cer, Syt-1–green fluorescent protein (GFP), and Syt-7–mCherry and analyzed as before. We found that even when overexpressed, synaptotagmin isoforms were usually segregated within cells, with only 9.5% of NPY-Cer granules harboring both Syt-1 and Syt-7 (Supplemental Figure S3.1 A). When overexpressed, the amount of synaptotagmin on granules is approximately two times higher than it is in non-transfected cells (Supplemental Figure S3.1 D).

Many granules expressing synaptotagmins did not express NPY-Cer, which may either reflect inefficiencies inherent in the expression of exogenous proteins via transfection or true heterogeneity in the distribution of NPY across granules. Nonetheless, in the population of granules without NPY-Cer, the co-localization of endogenous Syt-1 and Syt-7 (Figure 3.1 C) or overexpressed Syt-1–GFP and Syt-7–mCherry (Supplemental Figure S3.1 C) remained low.

Finally, to verify these results, we stained for endogenous Syt-1 in cells expressing Syt-7–mCherry and endogenous Syt-7 in cells expressing Syt-1–mCherry. As the data in Supplemental Figure S3.2 C show, only a fraction of granules with Syt-7–mCherry harbor endogenous Syt-1, and similarly, only a small number of granules with Syt-1–mCherry harbor endogenous Syt-7. Overall, these experiments demonstrate that Syt-1 and Syt-7 are usually sorted to separate secretory granules—even when overexpressed—with a minority of granules expressing both isoforms.

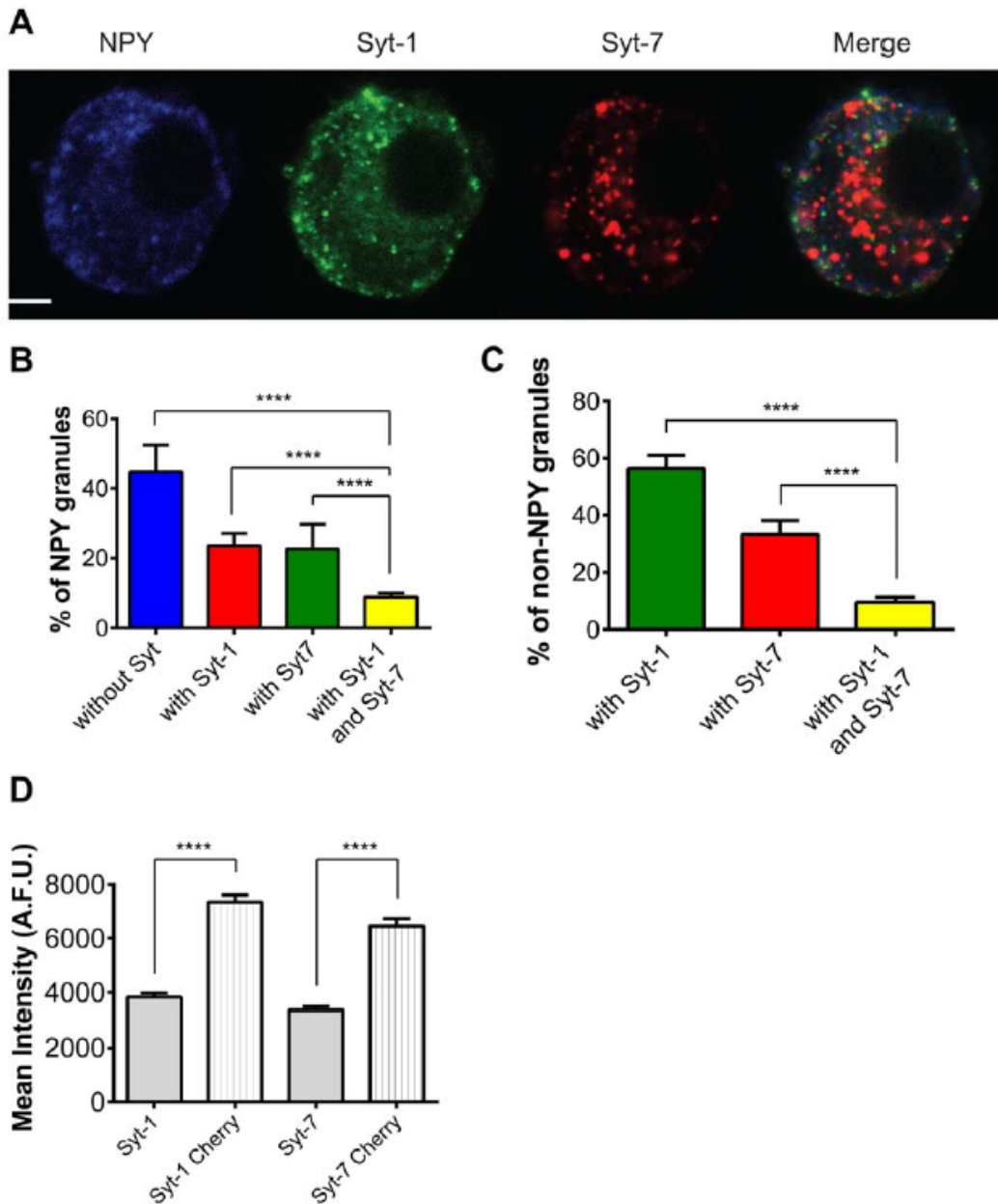


Figure S3.1. Confocal imaging of overexpressed Syt isoforms and NPY Cerulean.

(A) Confocal imaging of overexpressed Syt-1 GFP, Syt-7 Cherry, and a granule lumen protein, NPY-Cer. Scale bar, 3 μ M. (B) Percent co-localization of NPY-Cer granules with Syt-1, Syt-7, or both Syt-1 and Syt-7. Differences between NPY-Cer + Syt-1 + Syt-7 and other groups are significant (**** $p < 0.0001$, Student's t-test). (C) The co-localization of Syt isoforms in granules without NPY is shown. Statistical differences were assessed with the Student's t-test (**** $p < 0.0001$). (D) Expression level of transfected Syt isoforms compared to endogenous protein. Chromaffin cells were transfected with plasmids encoding Syt-1 Cherry

or Syt-7 Cherry and stained with the anti-Syt-1 (cytoplasmic domain) or anti-Syt-7 antibody, respectively. The mean pixel intensity for individual granules ($n > 100$ for 6 cells) with Cherry fluorescence (indicating presence of exogenous Syt) was significantly different from that of granules without Cherry fluorescence (indicating only endogenous protein; **** $p < 0.0001$, Student's t test).

Stimulation-evoked surface distribution of synaptotagmin isoforms is distinct

We next examined the functional consequences of isoform segregation on secretory granule exocytosis. We reasoned that if Syt isoforms drive different modes of granule fusion in chromaffin cells, as previously reported in PC12 cells (Zhang *et al.*, 2011), their stimulus-evoked appearance on the cell surface should also be distinct. To test this idea, we stimulated cells expressing Syt-1 (wild type [WT]) and c-myc–Syt-7 with 56 mM KCl for 30 s. This treatment depolarizes the membrane potential and triggers exocytosis (Anantharam *et al.*, 2011). Cell activity was rapidly arrested with an ice-cold (4°C) physiological saline solution followed by incubation with a solution of bovine serum albumin (BSA) containing the N-terminal luminal domain primary antibody to Syt-1 or anti-myc (to bind transfected c-myc–Syt-7). These antibodies recognize portions of the Syts that are exposed to the extracellular solution after granule fusion. The cells were then washed to remove primary antibodies, fixed, and exposed to fluorescent secondary antibodies. The cell footprint (i.e., the part of the cell affixed to the cover glass and observable in the field of view) was subsequently imaged with a total internal reflection fluorescence (TIRF) microscope. The immunocytochemistry revealed that after fusion, most Syt-1 is distributed diffusely along the plasma membrane (Figure 3.2 A).

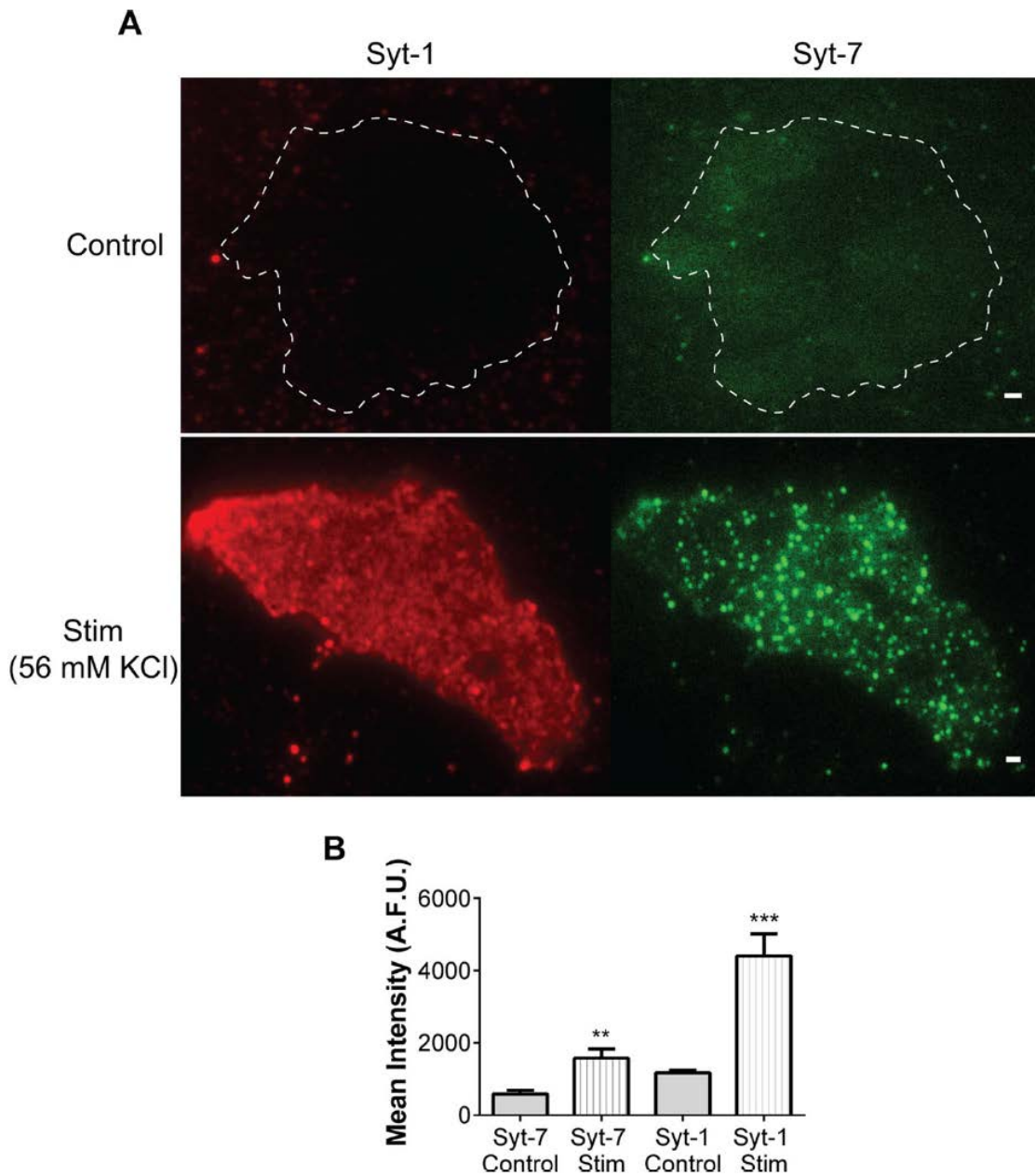


Figure 3.2. TIRF imaging of Syt isoforms to visualize surface distribution following depolarization.

Chromaffin cells were exposed to physiological saline solution (control) or 56 mM KCl PSS for 30 s. Cell activity was arrested with ice-cold saline solution. The cells were then incubated with N-terminal luminal domain antibody to Syt-1 or anti-myc (recognizes transfected c-myc-Syt-7), stained with fluorescent secondary antibodies, and imaged with a TIRF microscope. **(A)** In the absence of stimulation, little surface Syt fluorescence is visible. Top, dotted white line is the membrane outline of the imaged cell. With stimulation, Syt-7 appears on the

surface with a punctate distribution, whereas Syt-1 distribution is more diffuse. **(B)** Quantification of the entire cell footprint (i.e., the part of the cell adhered to the coverglass and imaged) of control (unstimulated) and stimulated (Stim) cells expressing Syt-1 WT or c-myc Syt-7 (from six cells). Data are averages \pm SEM (** $p < 0.01$, *** $p < 0.001$, Student's t test). Surface intensity increased by 2.7 times for stimulated Syt-7 cells and 3.7 times for stimulated Syt-1 cells.

On the other hand, Syt-7 is confined to discrete clusters (puncta) on the plasma membrane (Figure 3.2 A). To verify that the antibody was only binding to surface Syts and not to protein within the cytosol, we used a confocal microscope to visualize the cell interior. As we focused away from the focal plane closest to coverglass and further into the cell, little fluorescence was evident (Supplemental Figure S3.2 C). In the absence of stimulation, there was minimal plasma membrane fluorescence attributable to Syt-1 or Syt-7 when imaged with either the confocal (Supplemental Figure S3.2 C) or TIRF (Figure 3.2 A) microscope.

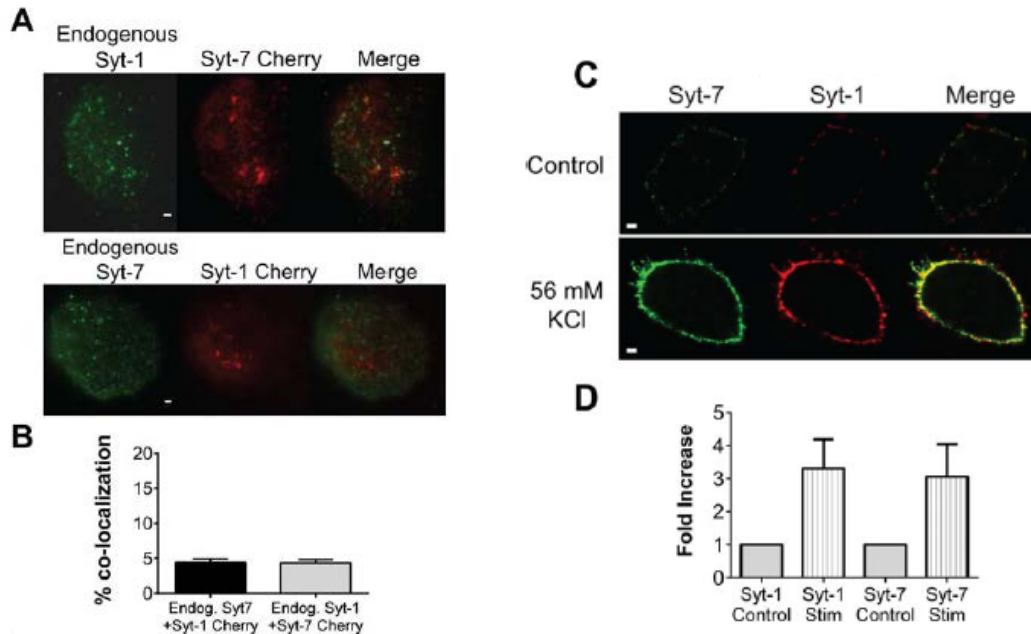


Figure S3.2. Confocal imaging of Syt isoforms both within cells and on membrane following depolarization.

(A) Chromaffin cells were stained for endogenous Syt-1 in cells transfected with Syt-7 Cherry or endogenous Syt-7 in cells transfected with Syt-1 Cherry. Scale

bar, 1 μM . **(B)** The “merge” image of the two channels shows very little co-localization (approximately 4%) between overexpressed Syt-7 and endogenous Syt-1 or overexpressed Syt-1 and endogenous Syt-7. **(C)** Confocal images of unstimulated (control) or 56 mM KCl PSS. Non-permeabilized cells were exposed to N-terminal luminal domain antibody to Syt-1 or anti-myc antibody to Syt-7 and fluorescent secondary antibodies. The control cell without stimulation shows very little membrane fluorescence while the cell depolarized with 56 mM KCl shows strong fluorescence around the membrane. Scale bar, 4 μm . **(D)** The bar graph represents the fold change in membrane intensity of stimulated (Stim) over unstimulated cells (Control). Stim data have been normalized with respect to the mean membrane intensity in the Control cells.

Syt-1 spreads out of fusion sites, whereas Syt-7 persists at the pore

The clustered surface distribution of Syt-7 could reflect protein confined to a partially open fusion pore or domains of protein aggregation on the plasma membrane after collapse of the granule membrane. To distinguish between these possibilities, we monitored Syt-7–pHluorin (pHluorin is on the N-terminal luminal domain) intensity changes after fusion, as well as the underlying topology of the fused granule membrane with polarization and total internal reflection fluorescence microscopy (pTIRFM). Transfected cells were labeled with diD, a fluorophore that intercalates in the plasma membrane with its transition dipole moments roughly parallel to the membrane plane. Local perfusion of a 56 mM KCl solution depolarizes the cell membrane and triggers exocytosis. During experiments, cells were sequentially exposed to 488-nm TIR illumination (to excite pHluorin) and 561-nm TIR illumination (to excite diD) that is either p or s polarized. Details on how the polarizations are generated are given elsewhere (Anantharam *et al.*, 2010). From the P and S emissions, we calculated pixel-to-pixel P/S and P+2S images. The P/S images report on diD-labeled membrane

curvature. P/S is expected to increase immediately upon granule fusion as diD diffuses from the plasma membrane into the granule membrane. Its decay over time reflects the rate of granule membrane collapse into the plasma membrane. P+2S reports on total diD emission. Computer simulations indicate that P+2S will increase if the geometry results in more diD-labeled membrane close to the glass interface, as when a fused granule is attached to the plasma membrane by a neck. P+2S will decrease if diD diffuses into a post-fusion membrane indentation (placing diD farther from the substrate and thereby in a dimmer evanescent field intensity). Thus together P/S and P+2S provide information on the changing geometry of the fusion pore as it expands, reseals, or remains stable (Anantharam *et al.*, 2010).

Using this approach, we found that Syt-7 remains clustered after fusion (Figure 3.3 A) at indentations whose P/S and P+2S emissions are consistent with a granule connected to the plasma membrane via a short neck (Figure 3.3 E; (Anantharam *et al.*, 2010; Anantharam *et al.*, 2011)).

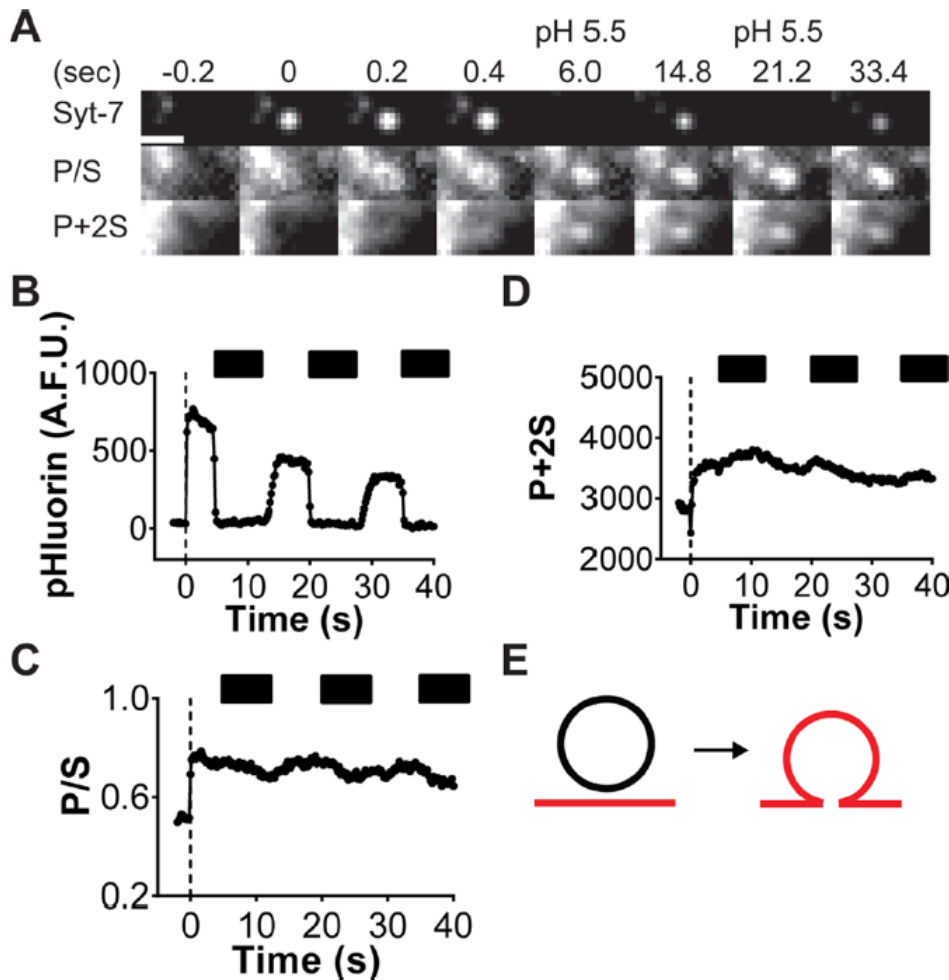


Figure 3.3. Syt-7 fluorescence persists at sites of fusion for tens of seconds.

(A) The fusion of a Syt-7–pHLuorin granule and concomitant increases in diD-labeled membrane curvature (P/S) and concentration (P+2S). Scale, 960 nm. **(B–D)** Intensity vs. time for images in A. Dotted line at time 0 indicates the perfusion. Black bars indicate duration of pH 5.5 PSS washes. **(E)** Based on computer simulations (as described in (Anantharam *et al.*, 2010), the increases in P/S and P+2S are consistent with a fusion pore that fails to expand.

Spreading of Syt-7 out of these indentations is restricted, suggesting that the protein is anchored to structures in either the membrane or the cytoplasm. To determine how long Syt-7 was on the cell surface and exposed to the extracellular space, we stimulated cells expressing Syt-7–pHLuorin for 30 s,

followed by periodic washes with physiological salt solution (PSS) at pH 7.4 and 5.5 (Figure 3.3, B–D, black bars). This treatment quenches the pHluorin fluorescence (Figure 3.3 B). Because diD is also pH sensitive, P+2S emission diminishes during the pH 5.5 washes (Figure 3.3 D).

Overall, the pH switching method revealed that 71% (36 of 51 events; six cells) of Syt-7 fusion pores were accessible to the extracellular space for at least 40 s. For some Syt-7 events (15 of 51 events), the pHluorin signal is evident but suddenly no longer quenched by low pH—consistent with endocytosis having occurred. An example of an endocytic event is shown in Figure 3.4. Before stimulation with 56 mM KCl, no Syt-7 pHluorin fluorescence is evident either within the circled region or at the arrow (Figure 3.4 A). On depolarization, fluorescent spots suddenly appear as the granule lumen is exposed to the neutral extracellular pH. Subsequent washes with a pH 5.5 solution reveal that one of the spots is insensitive to quenching (within the circled region in Figure 3.4 A and graph in Figure 3.4 B). The granule within the circled region has most likely undergone endocytosis at the site of fusion.

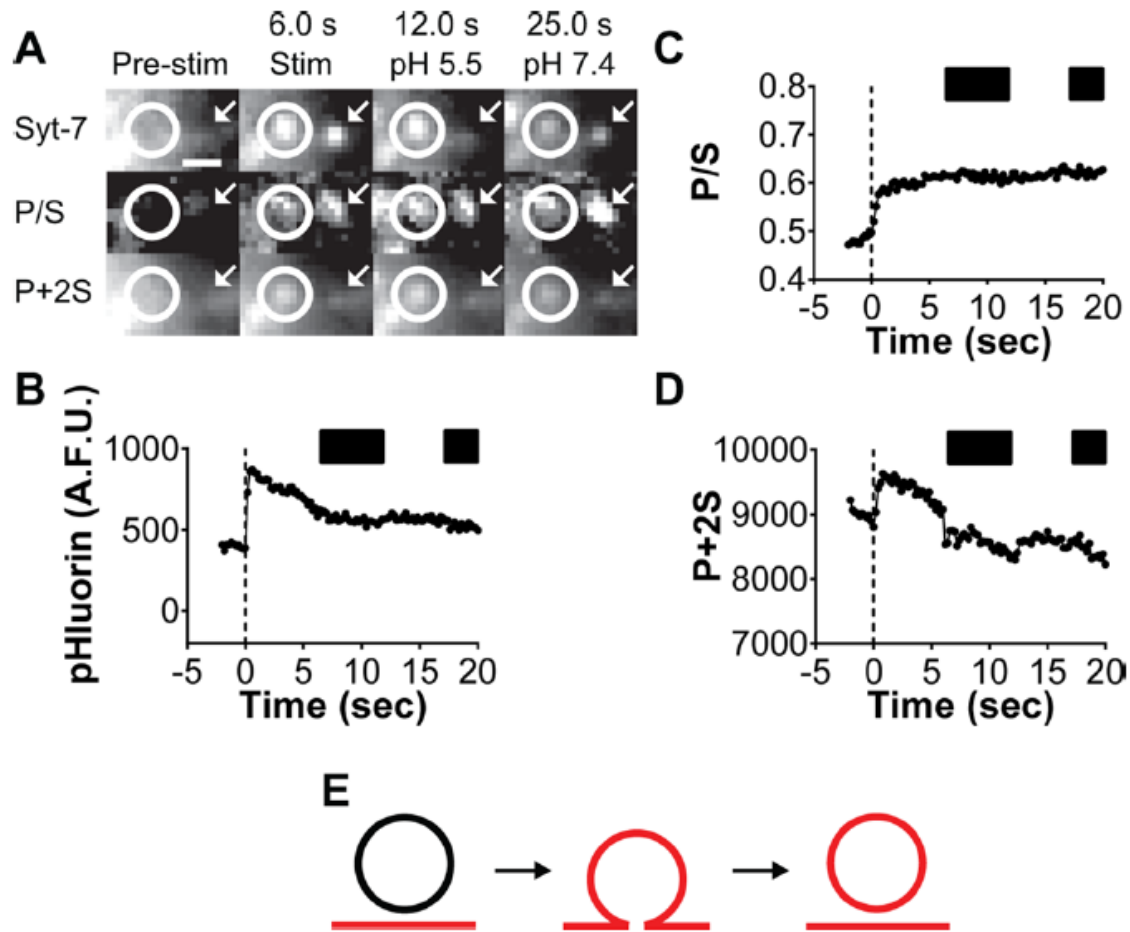


Figure 3.4. Fusion of Syt-7 granules sometimes results in cavicapture.

(A) Two Syt-7 pHluorin fusion events (circle and arrow). Before fusion (Pre-stim) no fluorescence is visible at either site. With stimulation (6.0 s), puncta are evident within the circled region and at the arrow. Syt-7 fluorescence within the circled region is not quenched by pH 5.5 PSS, suggesting that this event has undergone endocytosis at the site of fusion (cavicapture). Syt-7 fluorescence at the arrow is sensitive to a wash of pH 5.5 PSS, suggesting that the granule lumen is accessible to the extracellular space via a pore. Scale, 960 nm. **(B–D)** Graphs for pHluorin, P/S, and P+2S emission images within circled region of **A**. **(E)** The emission intensity changes observed are consistent with an endocytosed membrane remaining within the evanescent field, yielding increases in P/S and P+2S.

Measurements of membrane topology independently support this conclusion (Figure 3.4, C and D). Both P/S and P+2S increase as the granule and plasma membranes fuse. Periodic dips in P+2S are observed during low-pH

application, but after accounting for photo bleaching, the trend is for P+2S at fusion sites to remain elevated (Figure 3.4 D). P/S does not change in response to low pH because the P and S emissions are reduced proportionately (Figure 3.4 C). Computer simulations predict that the persistent increases in P/S and P+2S are most consistent with a diD-labeled endocytosed membrane remaining within the evanescent field after fusion (Figure 3.4 E). This is independently supported by the insensitivity of the pHluorin signal to low-pH perfusion.

Conversely, Syt-1-pHluorin diffuses from sites of granule fusion. One example of this is shown in Figure 3.5, A and B. The spreading fluorescence of Syt-1 in the plane of the plasma membrane was further analyzed by calculating the diffusion coefficient (D) for a subset of events. D was calculated from the slope of the plot of w^2 versus time, where w^2 is the variance of the Gaussian fit of the Syt-1 fluorescence (Figure 3.5 C). The diffusion coefficient for the event shown in Figure 3.5 A was calculated to be $0.53 \times 10^{-2} \mu\text{m}^2/\text{s}$. The mean diffusion coefficient from 17 Syt-1 fusion events with approximately linear increases in w^2 versus time was calculated as $0.63 \times 10^{-2} \pm 0.15 \mu\text{m}^2/\text{s}$. This value is more than an order of magnitude smaller than that calculated for vesicular monoamine transporter (VAMP) in chromaffin cells (Allersma *et al.*, 2004). This suggests that even when Syt-1 diffuses out of fusion sites, it does so slowly. Only 8% (3 of 36) of Syt-1 pHluorin fusion events are punctate for 40 s or more.

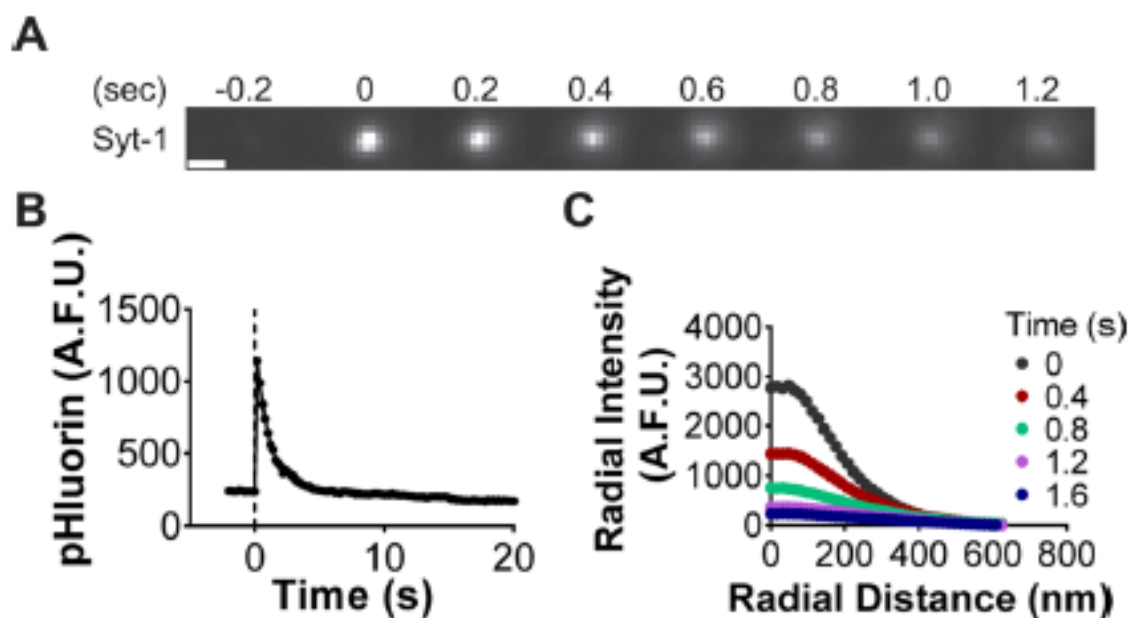


Figure 3.5. Syt-1 diffusion.

(A) Syt-1-pHluorin diffusing from a fusion site. Scale, 960 nm. **(B)** Syt-1-pHluorin intensity decay. **(C)** The diffusion coefficient **(D)** of Syt-1 was calculated from the variance (w^2) vs. time of Gaussian fits by using $D = \Delta w^2 / 4\Delta t$. The diffusion coefficient for the Syt-1 fusion event shown was calculated to be $0.53 \times 10^{-2} \mu\text{m}^2/\text{s}$. For clarity, radial intensity profiles every 400 ms are shown (images were actually acquired at 5 Hz).

Post-fusion topological changes are associated with distinct fusion modes for Syt-1 and Syt-7 granules

Averaged pHluorin intensities show that whereas Syt-1 disperses from fusion sites, Syt-7 tends to stay clustered (Figure 3.6 A). Measurements of endocytic frequency and membrane topological changes suggest fundamentally different outcomes for Syt-1 and Syt-7 after fusion (Figure 3.6, A–D). Post-fusion P/S signals (representing the indented fused granule/plasma membrane domain) decay to baseline within 5 s for the majority of Syt-1 events (27 of 36 events, or 75%; Figure 3.6 C). Meanwhile, 82% (42 of 51 events) of Syt-7 post-fusion indentations persist (i.e., show no evidence of decay or collapse) for the duration

of the imaging period. This ranged from 40 to ~80 s, depending on when the granule fused with respect to time of stimulus application. For 31 granules that fused soon after the stimulus was applied, the indentations (P/S increase) lasted for at least 80 s. This stands in stark contrast to Syt-1 post-fusion indentations, which lasted for the duration of the imaging period in only three of 36 cases.

Topological changes were also monitored during fusion of vesicular monoamine transporter-2 (VMAT-2) pHluorin-expressing granules. These events exhibit an intermediate phenotype, with 38% (nine of 24) of P/S signals decaying to baseline within 5 s (Supplemental Figure S3.3 B). This is not surprising, as ostensibly VMAT-2 is expressed on Syt-1 and Syt-7 granules. Most fusion events with a P/S change were also accompanied by a change in P+2S, which indicates total diD emission from a region of interest. This was true for 37 of 51 Syt-7 events, 23 of 36 Syt-1 events (Figure 3.6 D), and 17 of 24 VMAT-2 events (Supplemental Figure S3.3 C). P+2S changes associated with Syt-1 granule fusion were overwhelmingly short lived. In only one instance did a P+2S change persist for >5 s. When observed, P+2S also tended to decrease rather than increase, suggesting a widening pore. In contrast, at sites of Syt-7 fusion, P+2S usually increased (34 of 37) rather than decreased (3 of 37), with most lasting for >5 s. P+2S changes after VMAT-2 granule fusion were again intermediate, with roughly equivalent numbers of events associated with increases and decreases (Supplemental Figure S3.3 C).

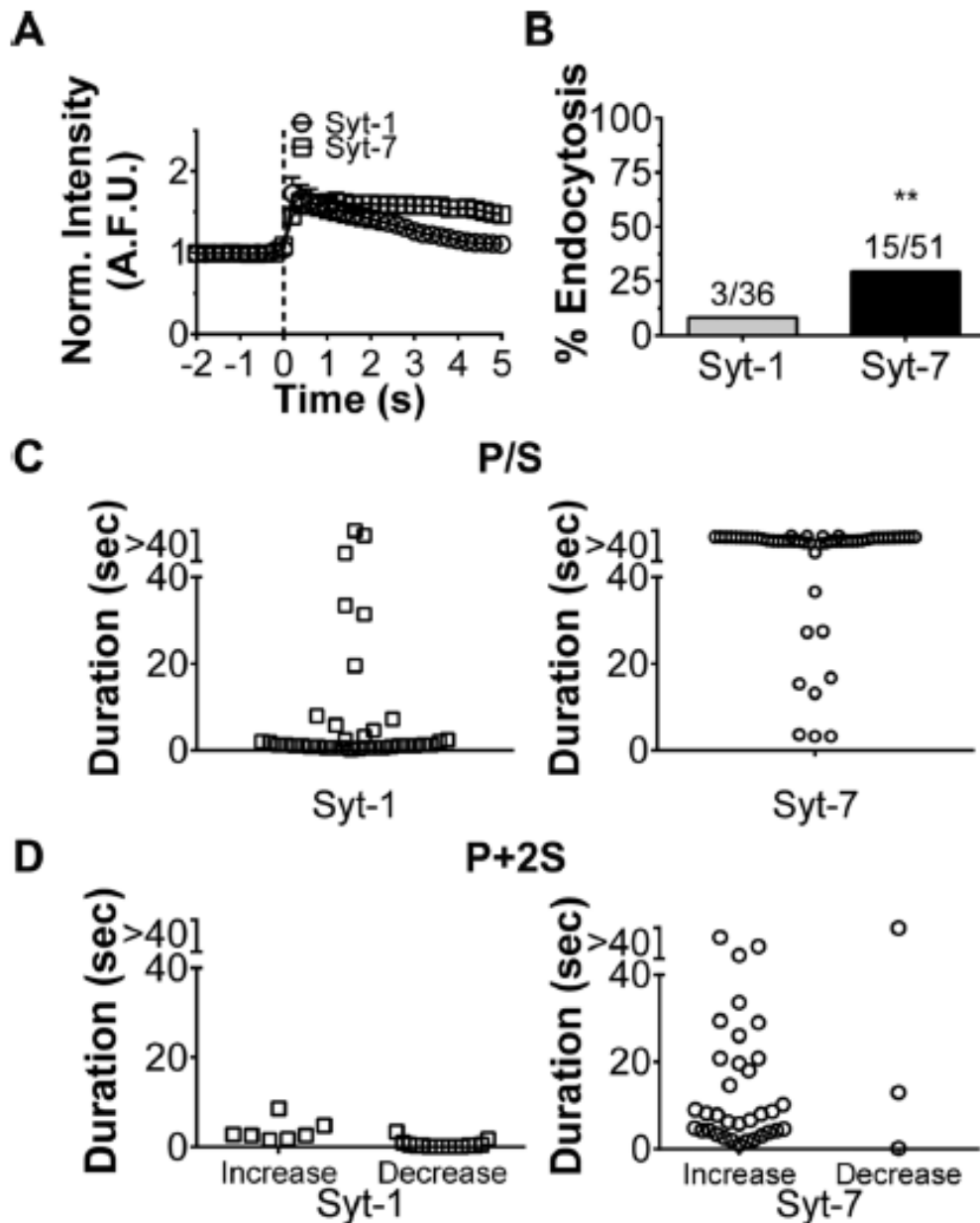


Figure 3.6. Changes in membrane curvature following Syt fusion.

(A) Averaged, normalized intensities of Syt-1 (n = 36; seven cells) and Syt-7 (n = 51; six cells) fusion events \pm SEM. Means are significantly different after 2.8 s (* $p < 0.05$, Student's t test). (B) Chromaffin cells expressing Syt-1 or Syt-7 pHluorin were exposed to low-pH (5.5) PSS for ~ 8 -s intervals after an initial 30-s stimulation with 56 mM KCl in the presence of bafilomycin. Low-pH-insensitive events were assumed to have undergone endocytosis and are expressed as percentage of total fusion events. The probability of a fusion event undergoing endocytosis (cavapture) with Syt-7 (six cells) was significantly different from

that with Syt-1 (seven cells; $**p < 0.01$, binomial probability). P/S **(C)** and P+2S **(D)** lifetimes for individual Syt-1 and Syt-7 fusion events. Syt-1 events are short lived. Only nine of 36 P/S increases and one of 23 P+2S changes (increases and decreases) persist for >5 s for Syt-1. In contrast, most Syt-7 fusion events are associated with P/S (48 of 51 events) and P+2S (22 of 37 events) changes lasting >5 s.

Thus fusion of Syt-7 granules results in the formation of a pore that frequently reseals, resulting in endocytosis (29% of events). The remaining 71% of events may either be progressing to cavicapture or, alternatively, full-collapse fusion with slower kinetics. In contrast, Syt-1 pores expand widely after fusion. A small minority of these fusion events end in endocytosis (8% of events; Figure 3.6 B). When a much larger number of events are considered— that is, from cells expressing Syt-1 or Syt-7 pHluorin but not stained with diD—the frequency of endocytosis remains considerably lower for Syt-1 than for Syt-7. Three of 289 Syt-1 fusion events resulted in endocytosis versus 68 of 310 Syt-7 fusion events (Supplemental Figure S3.3 D). This demonstrates that diD staining did not, on its own, change the prevailing fusion mode for Syt-1 and Syt-7 granules.

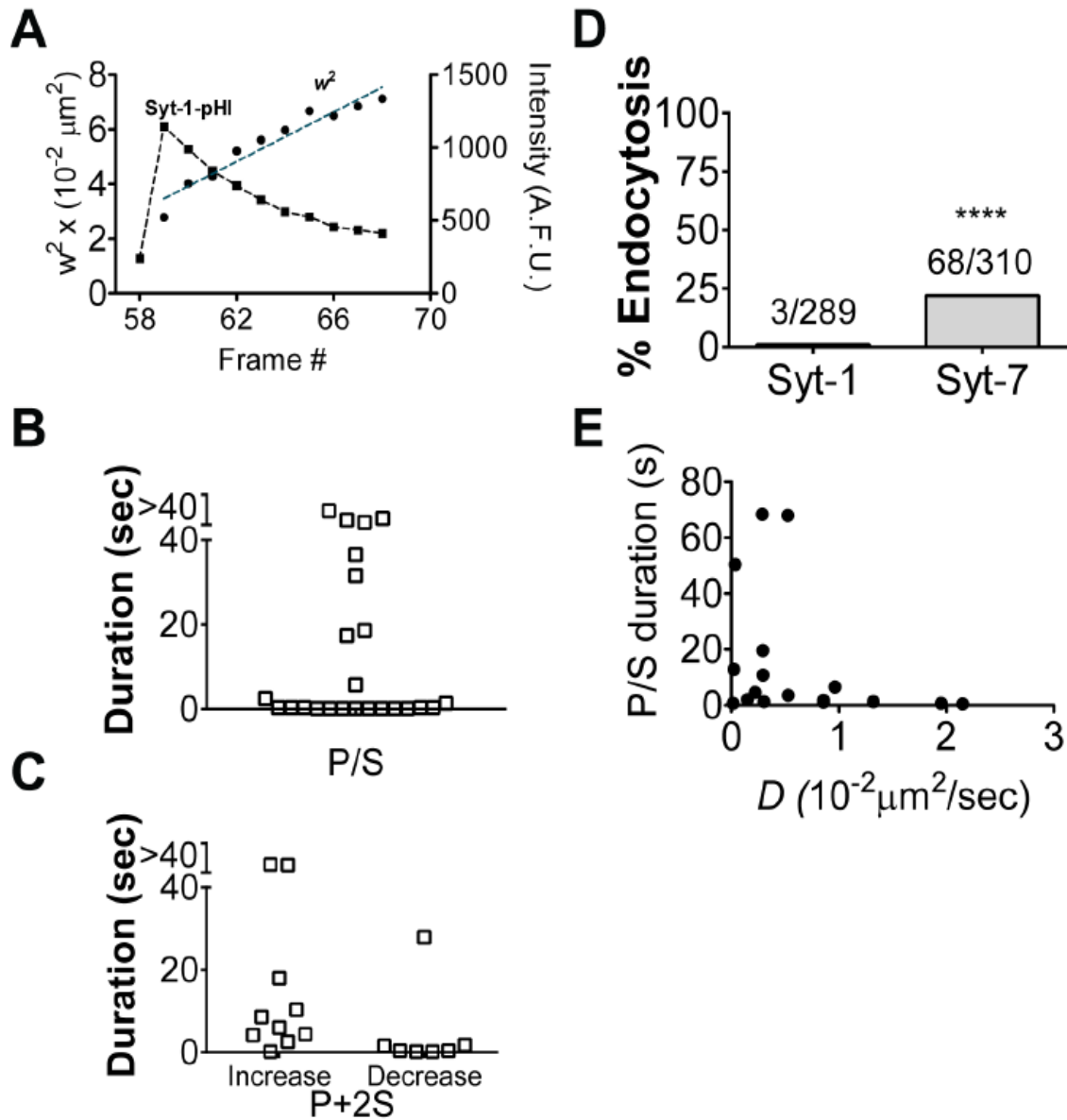


Figure S3.3. Percentage endocytosis for Syt isoforms and changes in membrane curvature for VMAT-2 following fusion.

(A) For the event in Figure 3.5 A, the total intensity of Syt-1-pHl and width squared w^2 of the radially averaged Gaussian fit of the intensity profile are plotted. P/S (B) and P+2S (C) lifetimes for individual VMAT-2 fusion events. (D) Endocytic frequency of Syt-1 and Syt-7 pHluorin granules stimulated with 56 mM KCl. Events were tabulated from cells not stained with diD. Syt-7 granules undergo endocytosis with a higher frequency than Syt-1 granules (**** $p < 0.0001$; binomial probability). (E) Scatter plot of curvature duration versus diffusion (D) for individual Syt-1 fusion events

Syt-7 slows dispersal of granule cargo proteins and membrane proteins

The topological changes observed in Figure 3.6 demonstrate that Syt-7 fusion pores widen slowly (or reseal), whereas Syt-1 pores expand widely. If the presence of Syt-7 on the granule retards pore expansion, the dispersal of luminal granule contents should also be slowed. To determine whether this was the case, we transfected cells to express Syt-1 or Syt-7-mCherry and chromogranin B (CgB) pHluorin. We monitored the release of CgB out of granules with either Syt-1 or Syt-7. Representative CgB-pHluorin release events from Syt-1 and Syt-7 granule are shown in Figure 3.7, A–D. On average, CgB release from Syt-1 granules (circles in graph) occurred more rapidly than from Syt-7 granules (squares in graph).

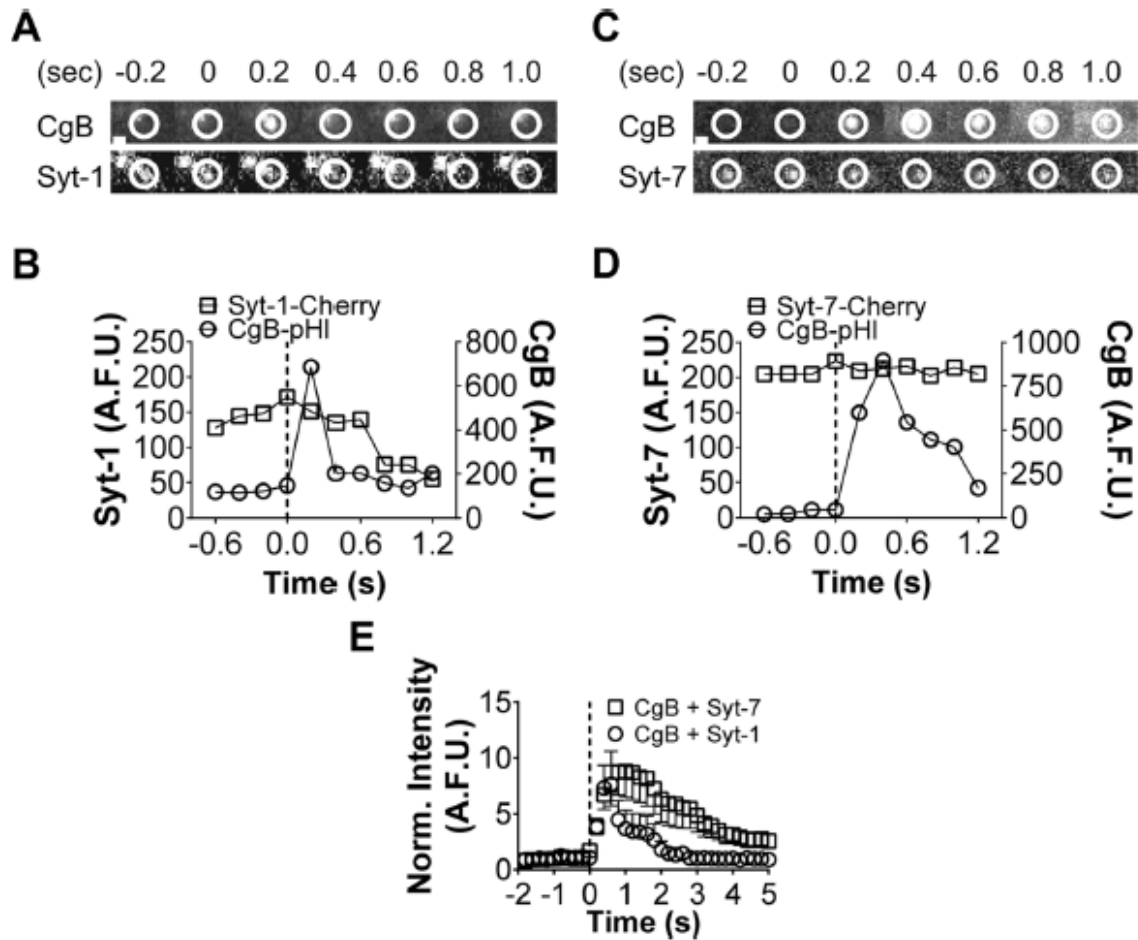


Figure 3.7. Syt-1 granules release luminal contents more quickly than Syt-7 granules.

(A) Fusion of a Syt-1-Cherry granule. CgB-pHluorin intensity increases (indicating fusion) at time 0.2 s (within circled region). Syt-1 and CgB disperse quickly after fusion (dotted line). Note the loss of fluorescence within circled region **(A, B)**. **(C)** Syt-7 remains punctate after fusion (bottom). CgB is released slowly. **(D)** Graphs for C. **(E)** On average, CgB is more rapidly released from fusing Syt-1 rather than Syt-7 granules. $n = 19$ for Syt-1 plus CgB; $n = 21$ for Syt-7 plus CgB. After 2 s, averages \pm SEM are significantly ($*p < 0.05$) different by Student's *t* test. Scale bar, 960 nm.

We also studied the effects of Syt-7 expression on the diffusion of a granule membrane protein, VMAT-2, out of the fused granule/plasma membrane domain. VMAT2-pHluorin ordinarily diffuses rapidly from sites of Syt-1 granule fusion, exhibiting a roughly two-fold higher diffusion coefficient than Syt-1 (Figure

3.8, A and B, and Supplemental Figure S3.3 D). However, when VMAT-2 is co-expressed with Syt-7, its movement out of fusion sites is significantly disrupted (Figure 3.8, C and D).

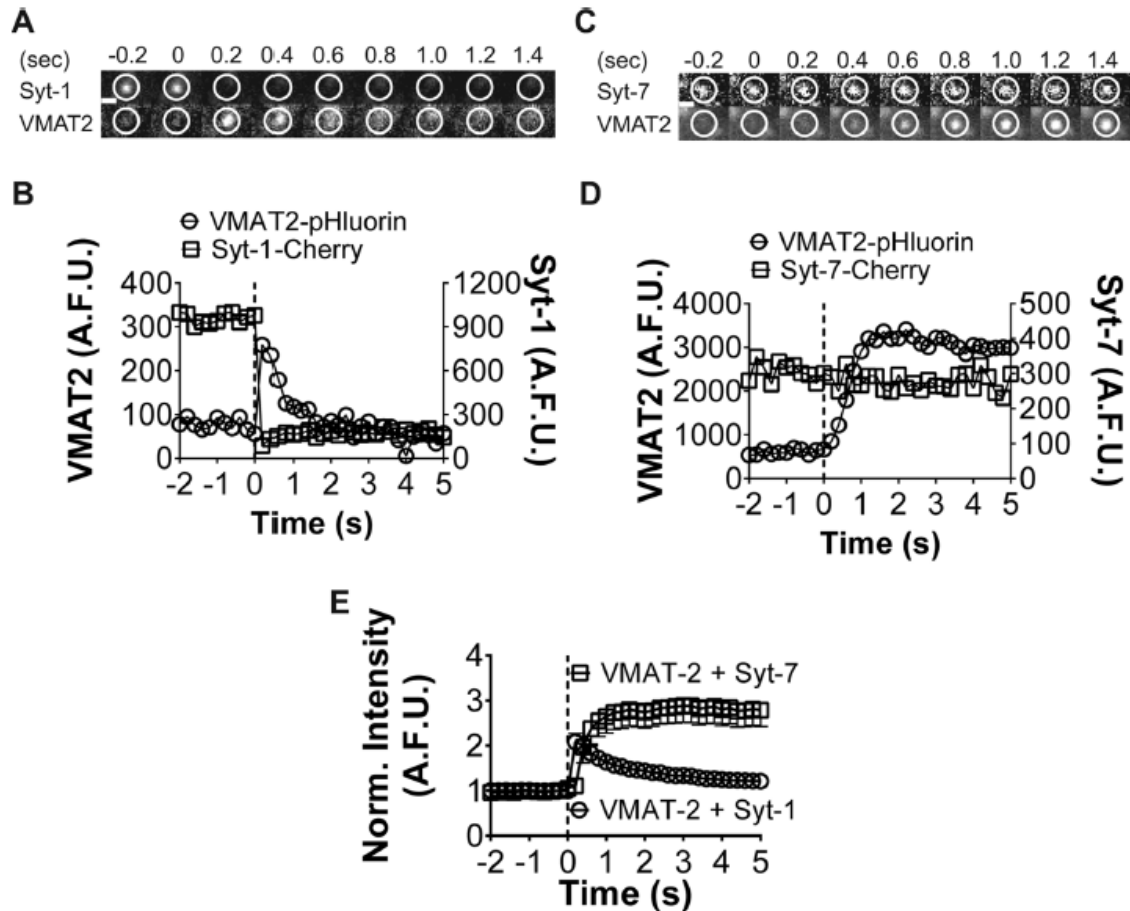


Figure 3.8. A granule membrane protein is released slowly from Syt-7 granules upon fusion.

(A) VMAT2-pHluorin fluorescence rapidly disperses from fusing Syt-1 granules (within circled region). **(B)** Graph for A indicates Syt-1 intensity diminishes after fusion (dotted line), whereas VMAT2 intensity increases and then diminishes. **(C, D)** VMAT2 movement is restricted from fused Syt-7 granules **(D)**. $n = 24$ for Syt-1 plus VMAT2; $n = 17$ for Syt-7 plus VMAT2. Averages \pm SEM are significantly different after 1 s ($*p < 0.05$) by Student's *t* test. Only negative (-) error bar is shown for VMAT2 plus Syt-7 and positive (+) error bar for VMAT2 plus Syt-1. Scale bar, 960 nm.

Indeed, VMAT-2 fluorescence shows a strong tendency to persist at the fusion site along with Syt-7. The post-fusion fluorescence intensity from many fusion events is shown in Figure 3.8 E. Fluorescence intensity decays to baseline in roughly 4 s for VMAT-2 + Syt-1 events, whereas it is resistant to decay in the case of VMAT-2 + Syt-7 events.

Synaptotagmins are differentially activated by depolarizing stimuli

Membrane depolarization opens voltage-gated channels, allowing Ca^{2+} to accumulate within cells and trigger exocytosis. The level of Ca^{2+} accumulation is commensurate with stimulus intensity (Augustine and Neher, 1992). Changes in stimulus intensity are tied to two different fusion modes for chromaffin cell secretory granules (Fulop *et al.*, 2005). Therefore the goal of the following experiments was to determine whether Syt isoforms were differentially activated by elevations in intracellular Ca^{2+} to promote these different fusion modes. To perform these studies, we first monitored qualitative changes in near-membrane Ca^{2+} in cells transfected with gCaMP5G (Tucker *et al.*, 2003) and exposed to 10, 25, and 56 mM KCl for 50–60 s. The greatest increases in Ca^{2+} were observed with 56 mM KCl. This demonstrates that Ca^{2+} accumulation at the membrane and near fusion sites is sensitive to how strongly the cell is depolarized (Figure 3.9 A). With decreasing amounts of KCl in the depolarizing solution, the $\Delta F/F$ is significantly lower (averaged $\Delta F/F$ data are shown \pm SEM). Next we transfected cells with Syt-1–GFP or Syt-7–GFP and monitored whether granules expressing fluorescent isoforms were differentially responsive to KCl depolarization. At the

lowest KCl concentration, only a handful of fusion events (seven of 2041 docked granules across 25 cells) were observed for Syt-1, and a similar number (35 of 1994 docked granules across 25 cells) were observed for Syt-7. With a moderate 25 mM KCl stimulation, ~17% of docked Syt-7 granules fused, whereas the number of recorded Syt-1 events remained low. Large numbers of fusion events for Syt-1 were only observed with 56 mM KCl, which also evokes the greatest increases in near-membrane Ca^{2+} (Figure 3.9, A and B). In fact, the 56 mM stimulation is more effective at activating Syt-1 than Syt-7, with 32% of docked Syt-1 granules fusing as compared with 25% of docked Syt-7 granules. These experiments demonstrate that activation of Syt isoforms is strongly Ca^{2+} dependent. Mild depolarization and small elevations in intracellular Ca^{2+} preferentially trigger Syt-7 granule fusion. Although higher elevations in Ca^{2+} activate both isoforms, it is the Syt-1 granules that fuse with greater frequency.

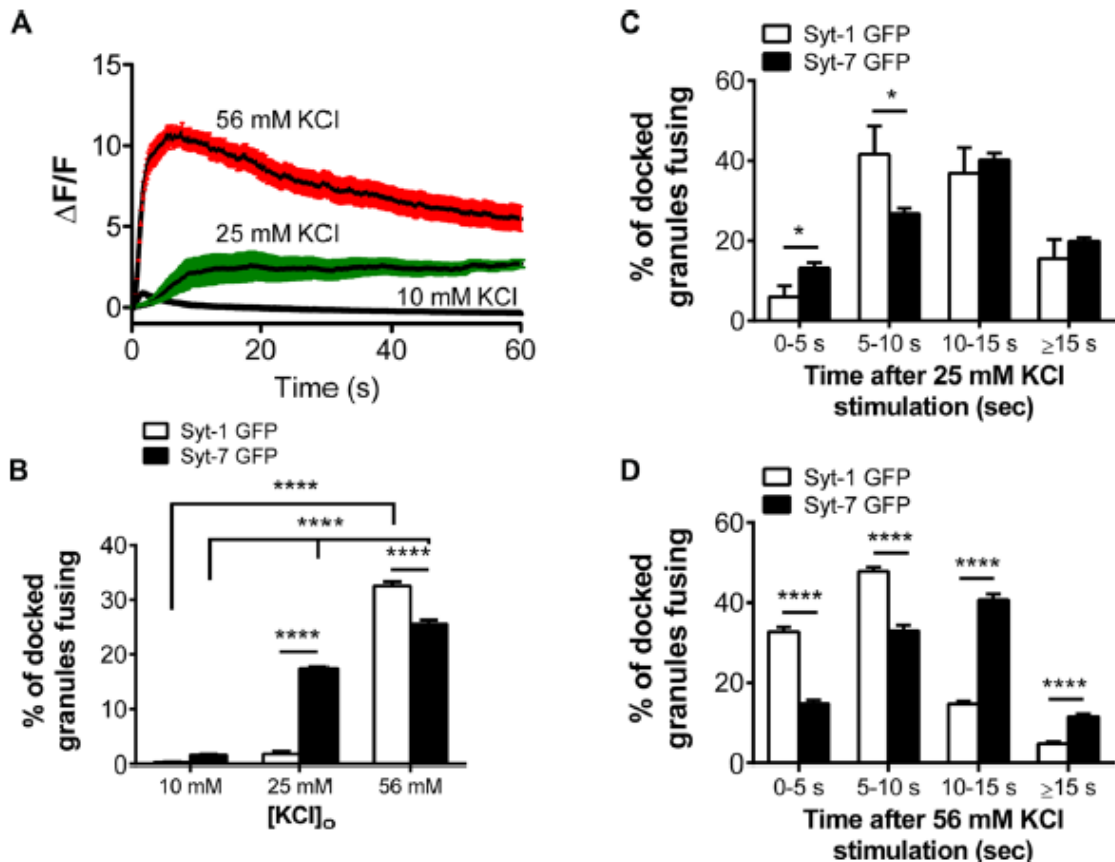


Figure 3.9. Syt-1 and Syt-7 are differentially activated by depolarization.

(A) Near-membrane $\Delta F/F$ in cells ($n = 5$, all groups) transfected with gCaMP5G and imaged in TIRF was calculated as described in Materials and Methods. Means (solid black lines) of 10 and 25 mM KCl are statistically significant compared with 56 mM KCl (t test, $***p < 0.001$). (B) Syt-1-GFP and Syt-7-GFP were expressed separately in chromaffin cells. The number of fusing Syt-1 or Syt-7 granules for each condition is expressed as a percentage of granules resident in the evanescent field (“docked”) at least 10 s before the start of the stimulus. Raw counts of number of events/number of docked granules ($n = 25$ cells for Syt-1 and Syt-7). For Syt-1, 7/2041 (10 mM), 51/2373 (25 mM), and 1089/3273 (56 mM). For Syt-7, 35/1994 (10 mM), 371/2149 (25 mM), and 662/2556 (56 mM). Statistical differences in percentage fusion at 10, 25, and 56 mM KCl (Syt-1 and Syt-7) were assessed with two-way analysis of variance ($****p < 0.0001$). (C, D) The time delay between application of KCl and fusion was calculated for Syt-1- or Syt-7-GFP granules and binned into intervals as indicated. Raw data of number of fusion events in each bin/total number of fusion events. For Syt-1 at 25 mM KCl, 6/51 (0–5 s), 18/51 (5–10 s), 18/51 (10–15 s), and 9/51 (>15 s). For Syt-7 at 25 mM KCl, 48/371 (0–5 s), 99/371 (5–10 s), 150/371 (10–15 s), and 74/371 (>15 s). For Syt-1 at 56 mM KCl, 347/1089 (0–5 s), 529/1089 (5–10 s), 156/1089 (10–15 s), and 57/1089 (>15 s). For Syt-7 at 56

mM KCl, 103/662 (0–5 s), 217/662 (5–10 s), 265/662 (10–15 s), and 77/662 (>15 s). Statistical differences between groups were calculated using the Student's t test (* $p < 0.05$; **** $p < 0.0001$).

We further examined the data in Figure 3.9 B to determine whether the time between stimulus application and fusion was different for the two isoforms. As shown in Figure 3.9, C and D, we separated events into bins, with the first bin constituting events occurring within the first 5 s of stimulus, the next between 5 and 10 s of stimulus, and so on. With 25 mM KCl, although the total number of Syt-1 fusion events was small (51 events across 25 cells), ~50% of granules that fused did so within the first 10 s of stimulus. Forty percent of Syt- 7–GFP granules fused in the same period (Figure 3.9 C). More dramatic effects were observed with 56 mM KCl. With this stimulus, there was a significantly shorter time delay between KCl application and fusion for Syt-1 than Syt-7 in all the bins (Figure 3.9 D). Indeed, almost 80% of Syt-1 granules fused within the first 10 s of the stimulus, compared with only 48% for Syt-7. Only 20% of docked Syt-1 granules fused 10 s or more after the stimulus, compared with 52% of Syt-7 granules. Thus, with a strongly depolarizing stimulus, Syt-1 granules not only fuse more readily than Syt-7 granules, they also tend to fuse earlier.

DISCUSSION

The major findings of this study are that 1) synaptotagmin isoforms Syt-1 and Syt-7 are usually sorted to different secretory granules; 2) the isoforms drive different fusion modes of exocytosis, with Syt-1 favoring rapid and wide fusion pore expansion and Syt-7 slowing or limiting this process; 3) when Syt-1 drives

fusion, luminal and membrane constituents of the granule are released more rapidly and more thoroughly than when Syt-7 granules fuse; and 4) the isoforms are differentially activated by membrane depolarization and concomitant intracellular Ca^{2+} elevations. These results are summarized in Figure 3.10.

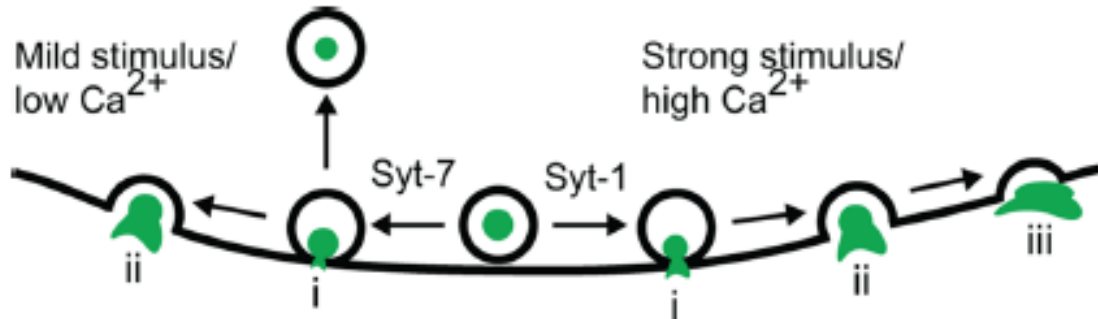


Figure 3.10: Model for Syt isoform mediated exocytosis in chromaffin cells. On the basis of membrane topological data, measurements of endocytosis, and imaging of luminal/membrane protein release, we propose that Syt isoforms favor different fusion modes in adrenal chromaffin cells. The isoforms themselves are preferentially activated by mild (Syt-7) and strong (Syt-1) depolarization. Post fusion topologies of Syt-1 granules are consistent with a rapid transition between an initial and wide pore (i \rightarrow iii), thereby promoting the release of granule lumen and membrane constituents. On the other hand, post fusion topologies of Syt-7 granules indicate a slow transition between an initial and wide pore (i \rightarrow ii), thereby restricting the release of granule lumen and membrane constituents. In addition, Syt-7 fusion events more frequently result in endocytosis at the site of fusion (i.e., cavicapture) than do Syt-1 events.

This study began with the surprising observation that in bovine chromaffin cells, unlike PC12 cells (Zhang *et al.*, 2011), there is little co-localization of synaptotagmin isoforms on secretory granules. Even with overexpression, both proteins are detected together on only a fraction of granules screened. A significant functional consequence of isoform segregation is that individual granules are endowed with unique Ca^{2+} sensitivities, allowing for rapid, local control of the fusion mode based on local Ca^{2+} levels. Thereby stimuli that

differentially elevate cytosolic Ca^{2+} (Augustine and Neher, 1992; Garcia *et al.*, 2006; Fulop and Smith, 2007; de Diego *et al.*, 2008b; Moghadam and Jackson, 2013) can differentially activate granules that will release only some (in the case of Syt-7) or more/all of their contents (in the case of Syt-1). There is consequently a strong Ca^{2+} - dependent component to pore expansion, which may be regulated by the synaptotagmins.

Mild KCl depolarization (25 mM), which moderately elevates intracellular Ca^{2+} , selectively triggers the fusion of docked Syt-7 granules (Figure 3.9 B). We define “docked” as a granule resident in the evanescent field for at least 10 s before the stimulus is applied. KCl 56 mM depolarization and correspondingly higher elevations in intracellular Ca^{2+} activate both isoforms but favor fusion of Syt-1 granules. In addition, with this stimulus, differences in the time of isoform activation become apparent. Specifically, the latency between KCl application and fusion is significantly shorter for Syt-1 than Syt-7. Almost 80% of docked Syt-1 granules fuse within 10 s of 56 mM KCl application as opposed to 48% of docked Syt-7 granules during the same period of time (Figure 3.9 D).

Syt-1 and Syt-7 are differentially responsive to the strength of stimulation with varying time courses for activation even in response to the same depolarizing stimulus (56 mM KCl). One therefore wonders whether Syt-1 and Syt-7 are the Ca^{2+} sensors for functionally distinct granule “pools.” Such pools are believed to account for the distinct kinetic components of membrane capacitance increases evoked by depolarizing voltage pulses or flash photolysis

of Ca^{2+} (Neher and Zucker, 1993; Chow *et al.*, 1994; Heinemann *et al.*, 1994; Chow *et al.*, 1996; Voets *et al.*, 1999b; Neher and Sakaba, 2008). The fast kinetic component of the capacitance burst is suggested to reflect an immediately releasable pool (IRP) of granules, which require only mild depolarization for release. Whereas there are important kinetic differences between electrophysiological measurements and imaged secretory responses, the selective activation of Syt-7 in response to mild KCl depolarization is qualitatively consistent with its sorting to the IRP. These granules may be closely localized to Ca^{2+} channels, providing basal catecholamine secretion at a minimal metabolic expense (Voets *et al.*, 1999b). With strong depolarization and a higher global change in $[\text{Ca}^{2+}]_i$, both Syt-1 and Syt-7 fusion events are observed. Syt-1 granules, however, fuse more readily and fuse earlier than Syt-7 granules (Figure 3.9, B and D). Thus it is possible that both Syt-1 and Syt-7 granules are found in a ready releasable pool, with differences in their relative distances to Ca^{2+} channels/microdomains accounting for differences in their time courses of activation (Voets *et al.*, 1999b).

Despite these similarities, absolute comparisons between electrophysiological and optical measurements are difficult to make for several reasons. For example, differences in release kinetics between the granule pools defined by capacitance are already apparent within tens of milliseconds after depolarization (Horrigan and Bookman, 1994; Voets *et al.*, 1999b). This undoubtedly reflects the ability of the electrophysiological approaches to

measure early events. In our study, temporal differences in latency to fusion using the high-K⁺ stimulation are not apparent for at least 1 s to several seconds (Figure 3.9, C and D). In addition, the duration of imaged cavicapture events (Figure 3.4) is slower than the tens of milliseconds-long “stand-alone feet” detected by amperometry (Zhou *et al.*, 1996). Our data may be on the time scale of longer stepwise capacitance changes measured by Lindau and colleagues (Albillos *et al.*, 1997) and “kiss and-run” events in PC12 cells imaged by Jackson, Chapman, and colleagues (Zhang *et al.*, 2011). The reason for these discrepancies is not clear. An answer will likely require a systematic comparison of optical and electrical measurements in the same group of cells or combinatorial approaches capable, for example, of imaging fusion at the same time as amperometric detection of catecholamine release (Hafez *et al.*, 2005).

Syt-1 and Syt-7 granules diverge not only in their depolarization dependence of activation, but, as noted earlier, in the rate at which they release luminal and membrane constituents. For instance, Syt-1 releases CgB with more rapid kinetics than Syt-7. Likewise, VMAT-2 is released and spreads along the membrane after fusion of Syt-1 granules, with a diffusion coefficient ($8.92 \pm 1.61 \times 10^{-2} \mu\text{m}^2/\text{s}$, $n = 25$) that is roughly 10 times that of Syt-1 itself. VMAT-2 diffusion out of Syt-7 granules, however, is negligible. The differences in release properties result from the divergent post-fusion fates of fused Syt-1 and Syt-7 granules. These fates were monitored with pTIRFM. We previously used dil and polarized excitation light from a 514-nm laser to detect the rapid changes in

membrane topology that occur with granule fusion (Anantharam *et al.*, 2010; Anantharam *et al.*, 2011). In this study, the instrument setup was modified so that a polarized 561-nm beam excited the fluorescence of a different membrane probe—diD. DiD was used because its red-shifted emission spectrum enables two-color imaging studies requiring GFP or pHluorin, which the overlapping emission spectra of dil and GFP/pHluorin all but preclude. Indeed, in earlier studies, two-color imaging was performed with dil and Cerulean (Anantharam *et al.*, 2010). Although brighter than cyan fluorescent protein, Cerulean has a lower extinction coefficient and quantum yield and exhibits decreased pH sensitivity compared with pHluorin or even GFP (Rizzo *et al.*, 2004). Most important, the modification we now introduced makes it possible to extract topological data from fusion events while directly monitoring the recycling kinetics of a protein of interest (e.g., Syt-1, Syt-7, VMAT-2, and CgB). This protein is fused to pHluorin and detects changes in luminal pH that occur normally during cavicapture (i.e., re-acidification) or when a fused granule is experimentally exposed to a low-pH extracellular solution (Anantharam *et al.*, 2010).

Our data show that when Syt-1 drives fusion, the overwhelming outcome is rapid curvature decay of the fused granule/plasma membrane domain. Indeed, 75% (27/36) of Syt-1 events show curvature decay to prefusion levels within 5 s of fusion. The overall probability of endocytosis is accordingly quite low. On the other hand, when Syt-7 drives fusion, indentations representing the fused granule can be remarkably stable. In the majority of cases, they were observed

to persist for >80–90 s, the duration of the imaging protocol. Whether the indentation eventually collapses into the plasma membrane or is retrieved via a form of clathrin-dependent endocytosis that occurs at or near the site of fusion (Bittner *et al.*, 2013) was not investigated.

The divergent effects of the isoforms on fusion pore expansion may be a functional consequence of their distinct biochemistry. Syt-1 and Syt-7 exhibit different affinities for Ca^{2+} in the presence of phospholipid membranes. In biochemical assays, the Syt cytoplasmic domains are predicted to vary >10-fold in their $[\text{Ca}^{2+}]_{1/2}$ (<1 μM for Syt-7 and 14 μM for Syt-1; (Wang *et al.*, 2005)). Once bound to Ca^{2+} , the Syts also release membranes with different kinetics (Sugita *et al.*, 2002; Bhalla *et al.*, 2005; Hui *et al.*, 2005). The disassembly of the Syt-1– Ca^{2+} –membrane complex occurs more quickly than disassembly of the Syt-7– Ca^{2+} –membrane complex in membranes containing phosphatidyl serine. Thus, when intracellular Ca^{2+} increase to trigger chromaffin cell exocytosis, Syt-7 may insert into and hold the plasma membrane more avidly than Syt-1, thereby stabilizing the fusion pore. The pore would be expected to expand as Syt-7 slowly released the membrane or to reseal as additional proteins (possibly dynamin; (Fulop *et al.*, 2008; Chan *et al.*, 2010; Anantharam *et al.*, 2011)) are recruited to facilitate fission. In *in vitro* assays, Syt-1 releases membranes with rapid kinetics. After exocytosis in chromaffin cells, it generally departs the fusion site. It is interesting to note that there is no correlation between the rate of Syt-1 diffusion after fusion and the rate of fusion pore expansion (Supplemental Figure

S3.3 E). Once Syt-1 disperses from fusion sites, the underlying granule/plasma membrane domain collapses with a varying time course.

The actions of Syt-7 during secretory granule exocytosis are consistent with its previously reported actions during lysosomal exocytosis in fibroblasts. Lysosomal granules remain as puncta after fusion, with vesicle membrane collapse only observed when Syt-7 is absent (Chakrabarti *et al.*, 2003; Jaiswal *et al.*, 2004; Andrews and Chakrabarti, 2005). The presence of Syt-7 on fused granules prevents the release of large lumenal cargo through the fusion pore or diffusion of membrane proteins along the membrane (Jaiswal *et al.*, 2004). Similarly, in chromaffin cells, the finding that Syt-1 and Syt-7 are rarely found together on granules and favor discrete fusion modes for exocytosis raises the possibility that the post-fusion fate of the granule is largely influenced by which isoform it harbors. Alternatively, the Syt isoform may predispose a given granule to fuse under one or another stimulus condition but work together with other regulatory factors to stabilize or destabilize the fusion pore. Considerable evidence has shown that actin dynamics (either disruption or stabilization; (Jaiswal *et al.*, 2009)), inhibition of myosins (Doreian *et al.*, 2008; Neco *et al.*, 2008; Berberian *et al.*, 2009; Gonzalez-Jamett *et al.*, 2013), inhibition of calcineurin (Engisch and Nowycky, 1998; Sun *et al.*, 2010; Zanin *et al.*, 2013), and disruption of dynamin function by pharmacologic or genetic means (Fulop *et al.*, 2008; Chan *et al.*, 2010; Gonzalez-Jamett *et al.*, 2010; Anantharam *et al.*, 2011; Gonzalez-Jamett *et al.*, 2013) all alter fusion pore expansion. These

elements may be heterogeneously distributed across the cell membrane or preferentially localized to sites of Syt-1 or Syt-7 fusion. The stable or expanding pore may therefore represent a confluence of stimulus-dependent activities of synaptotagmin and other regulators at the fusion site.

Overall, this study provides strong evidence that molecular heterogeneity, rather than homogeneity, may be a defining feature of chromaffin cell secretory granules. Given that this is the case, the obvious question is, to what end? The implication here is that heterogeneity with respect to synaptotagmins provides cells with a tunable, Ca^{2+} -dependent mechanism to control and define the properties of regulated exocytosis. The regulation of the secretory response via synaptotagmin diversity and segregation may also be generalizable to other systems. The design is eminently scalable, so that for cells (e.g., neurons) that receive more complex stimuli, only a greater number of synaptotagmin isoforms is required to regulate release.

ACKNOWLEDGEMENTS

The authors would like to thank Ronald W. Holz, Daniel Axelrod, and Mary Bittner for helpful suggestions on all aspects of this study. We also thank James T. Taylor, Johan Edvinsson, Rachel L. Aikman, and Praneeth Katrapati for technical assistance. This research was supported by National Institutes of Health Grant MH 61876 (to E.R.C.), American Heart Association Grant 13SDG14420049, and start-up funds from Wayne State University (to A.A.).

CHAPTER 4 - CHROMAFFIN CELL SYNAPTOTAGMIN ISOFORMS FORM FUNCTIONALLY AND SPATIALLY SEPARABLE GRANULE POOLS

This chapter is being prepared for submission to Journal of General Physiology. Rao T. C., Bourg J., Bai H., Dahl, P.J., Ranski, A.H., Schmidtke M.W., Veatch S.L., Chapman E. R., Giovannucci, D.R., Anantharam A. 2016. Chromaffin cell synaptotagmin isoforms form functionally and spatially separable granule pools

ABSTRACT

Current models for the adrenal chromaffin cell secretory response rely on the assumption that secretory granules are functionally homogenous. However, there is growing evidence that heterogeneity may define fundamental properties of granules, including their kinetics and Ca^{2+} -dependence of fusion. In this context, a key difference between granules appears to be whether they express synaptotagmin-1 (Syt-1) or synaptotagmin-7 (Syt-7). To understand the implications of this difference for the secretory response, we first investigated the morphological distribution of Syt-bearing granules within cells. In addition to the fact that isoforms are rarely co-expressed (<10%), Syt-1 and Syt-7-bearing granules are heterogeneously distributed within cells and show evidence for spatial segregation with respect to the plasma membrane. We next investigated functional differences between granules with Syt-1 or Syt-7 in cells depolarized with elevated K^+ . First, we found that with mild depolarization, the Syt-7 granule population shows far greater fusion efficacy. However, strong depolarization is equally effective at driving fusion of both types of Syt-bearing granules. When cells are challenged to secrete again immediately following a strong depolarization, Syt-1 granules require less time to transition to a fusion

competent state. Irrespective of the fusion efficacy, Syt-7 granules fuse with faster kinetics across all stimulation conditions tested. These findings were validated in cells permeabilized with digitonin and exposed directly to high intracellular Ca^{2+} . While Syt-7 granules fuse with greater efficacy at low $[\text{Ca}^{2+}]_{\text{in}}$, higher $[\text{Ca}^{2+}]_{\text{in}}$ is equally effective at activating isoforms. Overall, our results show that Syt-1 and Syt-7 are sorted to functionally and spatially distinguishable granule pools. We posit that the heterogeneity in chromaffin granule fusion modes and release kinetics may therefore arise from intrinsic differences in granules themselves.

INTRODUCTION

Depolarization of adrenomedullary chromaffin cells leads to Ca^{2+} influx through voltage-gated channels, with stronger stimuli leading to higher Ca^{2+} levels in the cell (Douglas and Rubin, 1961; Neher and Augustine, 1992; Fulop and Smith, 2007; de Diego *et al.*, 2008b). Ca^{2+} in turn drives exocytosis by interacting with the Ca^{2+} -binding synaptotagmin (Syt) protein family (Brose *et al.*, 1992; Voets *et al.*, 2001a; Schon *et al.*, 2008). The Syt protein family currently includes 17 isoforms, however only two of these isoforms (Syt-1 and Syt-7) are known to be expressed in chromaffin cells (Schon *et al.*, 2008). Structurally, both Syt isoforms harbor an N-terminal transmembrane domain that extends into the lumen of the chromaffin granule, followed by two cytosolic C2 domains (C2A and C2B) connected by a short linker region (Perin *et al.*, 1990; Perin *et al.*, 1991; Chapman, 2002). The Ca^{2+} binding properties of these isoforms are

primarily determined by the amino acid sequence within the tandem C2 domains located near the protein's C-terminus (Sutton *et al.*, 1995; Ubach *et al.*, 1998; Fernandez *et al.*, 2001). Biochemical studies have established a number of differences in how these isoforms respond to Ca^{2+} . For example, Syt-7 is capable of binding a total of six Ca^{2+} ions while Syt-1 can only bind to five (Südhof and Rizo, 1996; Ubach *et al.*, 1998). Additionally, Syt-7 has a roughly 10 fold higher affinity for Ca^{2+} ions compared to Syt-1 (Sugita *et al.*, 2002; Bhalla *et al.*, 2005).

At one time, all chromaffin granules within a cell were viewed as being functionally homogeneous, with uniform rates of fusion and content discharge. This idea is challenged by our recent work (Rao *et al.*, 2014) in which we discovered that expression of one or the other isoform of synaptotagmin endows granules with distinct fusion properties. A key finding was that fusion pores of granules harboring Syt-1 expand more rapidly than pores of granules expressing Syt-7. The result is that Syt-1 granules “collapse” more frequently into the plasma membrane following fusion than Syt-7 granules.

In this study, to probe deeper into the notion of granule heterogeneity, we extensively characterized the distribution of Syt-1 and Syt-7 granules within chromaffin cells. Direct comparison of granules expressing Syt-1 or Syt-7 revealed that Syt-7 granules are located closer to the plasma membrane. Using automated image analysis approaches, we confirmed that these isoforms are largely sorted to different granules. In addition to the differences in spatial distribution, we also sought to address whether the previously established in vitro

differences between these isoforms translate into functional differences during exocytosis. To do so, we first focused our attention on understanding the dynamic behavior of Syt isoforms following stimulation. Syt-7 granules require only mild stimulation to initiate fusion and fuse earlier following application of the stimulus. On the contrary, Syt-1 requires stronger stimulation to initiate exocytosis, and these granules undergo greater lateral displacement prior to fusion. Following depletion of the release competent granules, the remaining docked Syt-1 granules require less time to transition into a “fusion-competent” state during repeated stimulation. Also, when comparing docked versus newcomer granules, a greater proportion of Syt-1 events belong to the newcomer population.

Since the strength of KCl used to depolarize cells is related to local Ca^{2+} accumulation, we next adopted a more direct approach to trigger exocytosis by directly manipulating intracellular Ca^{2+} levels. In agreement with the use of KCl, applying lower amounts of Ca^{2+} directly to permeabilized cells favors fusion of Syt-7 in comparison to Syt-1 granules and does so with less delay following Ca^{2+} application. Strikingly, these observed differences in the activation and fusion kinetics of Syt granules are predicted by the in vitro differences in Ca^{2+} affinity previously reported for Syt isoforms (Bhalla *et al.*, 2005; Hui *et al.*, 2005; Bhalla *et al.*, 2008). Furthermore, blocking of voltage-gated Ca^{2+} channels reduces the fusion probability of each Syt granule population based on the channel subtype(s) blocked.

The physiological importance of LDCG exocytosis is to release hormones and signaling peptides from within granules. Therefore, we investigated the release kinetics of the luminal protein neuropeptide Y (NPY). Following stimulation, Syt-1 allows rapid release of NPY from granules and quickly diffuses from the site of fusion, whereas Syt-7 substantially slows the rate of NPY release and persists at the site of fusion. The rate at which these compounds are released is directly related to the post-fusion behavior of Syt isoforms on the plasma membrane. Syt-7 remains clustered on the plasma membrane and may therefore contribute to the maintenance of an intact fusion pore. In agreement with this idea, Syt-7 also shows slower dissociation kinetics from liposomes in vitro in comparison with Syt-1.

In sum, our results support the notion that chromaffin cell granules are not homogeneous but can be distinguished spatially, kinetically, and functionally based on which of the two synaptotagmin isoforms they harbor. These findings argue that granule heterogeneity may serve as a means to tune release of hormones and neuropeptides from neuroendocrine cells based on the level of physiological stimulation.

MATERIALS AND METHODS

Chromaffin Cell Preparation and Transfection

The chromaffin cells used for these experiments were isolated from the adrenal medullae of adult cows (*Bos taurus*) obtained from JBS Packing Company (Plainwell, Michigan, USA). Transient transfections were performed as

described earlier (Wick *et al.*, 1993). Briefly, cells were plated on 35-mm glass bottom tissue culture dishes (refractive index, 1.51; World Precision Instruments, Sarasota, FL) pre-coated with poly-D-lysine and bovine collagen. Coating promotes adherence of cells to the glass surface. Cells were transiently transfected by electroporation with plasmid(s) using the Neon transfection system (Invitrogen, Carlsbad, CA). Following standardization of the electroporation protocol, the chromaffin cells were transfected with the desired plasmid with a single pulse of 1100 mV for a period of 40 ms. Untransfected cells or cells transfected with NPY cerulean were used for the immuno-staining experiments. NPY pHluorin (pHI) was co-transfected with either Syt-1 or Syt-7 mCherry for the experiments to determine the rates of content release. Syt-1 or Syt-7 fusion proteins either with a GFP (Green fluorescent protein) or pHI tag were transfected separately for determining the motion of the granules and the digitonin permeabilization experiments. The media on the cells was changed after overnight incubation and all the experiments were performed 48 hrs following transfection to ensure expression of the fusion protein. All procedures were performed following approval from the Wayne State University Institutional Animal Care and Use Committee (IACUC).

Immunocytochemistry

Immunofluorescence microscopy was performed to detect the distribution of synaptotagmin isoforms within chromaffin cells. For this procedure, isolated chromaffin cells were first transfected with NPY cerulean and then plated on a

pre-coated 35 mm glass bottom cover dish. Non-transfected cells were also plated to stain for endogenous Syts. The cells were first fixed with 4% paraformaldehyde in phosphate-buffered saline (PBS) for 30 mins at 37 °C. The cells were quickly rinsed following the incubation and quenched using a solution of 50 mM NH₄Cl in PBS and incubated again for 30 mins at 37 °C. After washing off the quenching solution, the cells were permeabilized using acetone solution for 7 mins. After the incubation, the cells were washed with Tris-buffered saline (TBS) twice and blocked with 1% gelatin in TBS for 20 mins followed by 4% donkey serum for 30 mins both at 37 °C. A solution of 2-4 mg/ml BSA made in TBS was used to dilute the primary and secondary antibodies. Cells were incubated for 2 hrs at 37 °C with a combination of the following primary antibodies: monoclonal mouse anti-Syt-1 antibody (antibody 41.1, Cat. No. 105 011) and polyclonal rabbit anti-Syt-7 antibody (Cat. No. 105 173) from Synaptic Systems, Göttingen, Germany. Following incubation the cells were washed five times with TBS and incubated for 70 min with Alexa-conjugated anti-rabbit and anti-mouse secondary antibodies (Molecular Probes/Invitrogen, Eugene, OR). Finally the cells were washed five times after the secondary incubation and imaged by confocal microscopy.

Confocal Microscopy

Images of the NPY transfected cells immuno-stained for the endogenous Syt proteins were acquired on a Leica TCS SP5 confocal microscope with a 63x/1.40 NA oil objective. Images for cells stained for endogenous Syt alone

were acquired on a Zeiss LSM 780 confocal microscope with a W Plan-Apochromat 63x/1.0 NA M27 water immersion objective. For imaging, a 405-nm diode laser, a 488-nm Argon laser, and a HeNe red 633-nm laser were used on both the confocal microscopes.

Cell Stimulation

Cells were quickly washed 2-3 times in basal physiological salt solution (PSS) to get rid of any residual media and then used for the secretion experiments. For the TIRF experiments, cells were perfused with PSS containing 145 mM NaCl, 5.6 mM KCl, 2.2 mM CaCl₂, 0.5 mM MgCl₂, 5.6 mM glucose, 15 mM HEPES, pH 7.4 for 10 sec and then stimulated with high K⁺ solution containing either 56 mM (95 mM NaCl, 56 mM KCl, 5 mM CaCl₂, 0.5 mM MgCl₂, 5.6 mM Glucose, 15 mM HEPES, pH 7.4) or 25 mM KCl (126 mM NaCl, 25 mM KCl, 5 mM CaCl₂, 0.5 mM MgCl₂, 5.6 mM Glucose, 15 mM HEPES, pH 7.4) to trigger exocytosis for about 60 sec. Individual cells were perfused with a needle (100 μm inner diameter) under positive pressure applied using the ALA-VM4 perfusion system (ALA Scientific Instruments, Westbury, NY, USA).

For repeated stimulation experiments, chromaffin cells transfected with GCaMP5G, Syt-1, or Syt-7 GFP were depolarized with elevated K⁺ (56 mM KCl) during subsequent rounds of stimulation. The cells were initially perfused with 56 mM KCl for 30 s and then exposed to basal PSS for either 10 s or 60 s to allow clearance of Ca²⁺ from within the cytoplasm. Following this recovery period, the

cells were again exposed to elevated K^+ one or more times for a period of 15 s with intermittent application of basal PSS (10 s; See Figure 4.5).

TIRF Microscopy

TIRF imaging was performed on an inverted microscope (IX81; Olympus, Center Valley, PA, USA) equipped with an oil 60X objective (NA 1.49), two additional lenses (1.6X and 2X) in the emission path between the microscope, and a cooled electron-multiplying charge-coupled device (EM CCD) camera (iXon3, Andor Technology, South Windsor, CT, USA). Two-color TIRF microscopy was performed by illuminating the samples using a 488-nm Argon ion laser and a 561-nm solid state Sapphire Coherent laser (Santa Clara, CA, USA). Detailed description for the TIRF setup used is provided elsewhere (Passmore *et al.*, 2014). Lambda SC smart-shutter controllers have been employed for rapid switching between the excitation wavelengths (Sutter Instruments, Novato, CA, USA). Images were acquired with Metamorph software (Molecular Devices, LLC, Sunnyvale, CA, USA) successively in the green and the red channels with an exposure time of 30 ms and an EM gain of 300. The frame acquisition rate was ~ 5 Hz for a pair of images. The final pixel size was approximately 80 nm.

Determination of $[Ca^{2+}]_i$ using TIRF microscopy

We used the genetically encoded Ca^{2+} indicator GCaMP5G (Akerboom *et al.*, 2012) to determine changes in cytosolic free Ca^{2+} evoked by different depolarizing solution challenges. Chromaffin cells transfected with GCaMP5G were plated on a 35 mm glass cover dish and imaged by TIRF microscopy (see

TIRF Microscopy above). The standard bath solution was a basal PSS (see cell stimulation above). To depolarize the cells in order to evoke changes in cytosolic Ca^{2+} , the standard bath solution was adjusted to contain 5.6, 10, 25, 40, 56, 80, or 100 mM KCl while maintaining overall osmolarity of the solution. Calculations for determining the intracellular Ca^{2+} concentrations were performed as described previously (Neher and Augustine, 1992; Neher, 1995; Maravall *et al.*, 2000). A brief explanation for the same has been provided here. The average fluorescence change of GCaMP5G in response to the different depolarizing stimuli was estimated as the ratio $\Delta F/F = (F - F_{\text{base}})/F_{\text{base}}$, where F is the peak fluorescence intensity of GCaMP5G following stimulation and F_{base} is the average fluorescence intensity in the same cell prior to stimulation. The averaged $\Delta F/F$ values from all KCl concentrations were used to estimate the fold change in fluorescence at GCaMP5G- Ca^{2+} binding saturation (see below $(\Delta F/F)_{\text{plateau}}$). Calcium concentrations were then calculated using the following equations (Maravall *et al.*, 2000):

$$\frac{\Delta[\text{Ca}^{2+}]}{K_d} = \frac{F_{\text{max}}}{F_0} (1 - R_f^{-1}) \frac{\Delta F/F}{((\Delta F/F)_{\text{max}} - \Delta F/F) \cdot (\Delta F/F)_{\text{max}}}$$

where, $\Delta[\text{Ca}^{2+}]$ is the rise in calcium concentration

K_d is the dissociation constant. We used a K_d value of 447 ± 10 nM for GCaMP5G (Chen *et al.*, 2013b)

F_{max} is the peak fluorescence value for each cell

F_0 is the average baseline fluorescence prior to stimulation for each cell

R_f is the dynamic range of the indicator. We used an R_f value of 45.4 ± 0.9 for GCaMP5G, (Chen *et al.*, 2013b)

$\Delta F/F$ is the change in fluorescence divided by the baseline fluorescence

$(\Delta F/F)_{\max}$ is the corrected $\Delta F/F$ at saturation (see below)

$(\Delta F/F)_{\max}$ was calculated based on the equation below. Saturation of GCaMP5G occurred at 80 and 100 mM KCl (Figure 4.6 A), and these values were used to determine the correction factor, x:

$$(\Delta F/F)_{\max} = (\Delta F/F)_{\text{plateau}} * 100/x$$

where x is a correction factor:

$$x = 100 * \frac{1 - Q * \left(\frac{u_1}{u_2}\right)}{1 - (u_1/u_2)}$$

where u_1 and u_2 are the lower and higher KCl concentrations driving stimulation (80, 100 mM) at GCaMP5G saturation, and Q is the ratio of plateau fluorescence at higher and lower KCl stimulus (Maravall *et al.*, 2000).

The average resting calcium concentration ($[Ca^{2+}]_0$) within control unstimulated cells was determined using the equation below (Maravall *et al.*, 2000):

$$\frac{[Ca^{2+}]_0}{K_d} = \frac{1 - R_f^{-1}}{(\Delta F/F)_{\max}} - R_f^{-1}$$

Ratiometric Ca^{2+} Imaging for determination of intracellular $[Ca^{2+}]$

We used the ratiometric Ca^{2+} indicator fura-2 (TEFLabs, Austin, TX, USA) to determine changes in cytosolic free Ca^{2+} evoked by different depolarizing solution challenges. Cells cultured on glass coverslips were used to form the

bottom of a recording chamber and loaded at room temperature for 45 min with 2 μM fura-2 AM in physiological saline. Local application of bath or stimulus solutions through small-bore glass capillary tubing was achieved using a pressure-driven reservoir. The standard bath solution was a basal PSS (see cell stimulation above). To depolarize the cells in order to evoke changes in cytosolic Ca^{2+} , the standard bath solution was adjusted to contain 10, 25 or 56 mM KCl while maintaining overall osmolarity of the solution. Dye fluorescence was monitored using a monochromator-based system digital imaging system (T.I.L.L.-Photonics, Hillsboro, Oregon, USA) coupled to a Nikon TE-2000 microscope. Cells were alternately excited at $340/380 \pm 15$ nm reflected onto the plane of focus using a DM400 dichroic mirror and Super Fluor 40x, 1.3 NA oil immersion objective. The emitted fluorescence was collected through a 510 ± 25 nm band pass filter (Chroma, Bellow Falls, VT, USA).

For dye calibration we used the in vivo procedure where the calibration constant values for R_{min} , R_{max} and K_{eff} were determined from 3 to 5 cells dialyzed through patch pipette with standard internal recording solution adjusted to contain either minimal Ca^{2+} (10 mM EGTA, no added Ca^{2+}) or saturating Ca^{2+} (3 mM Ca^{2+}) concentrations and containing 150 μM fura-2 (Giovannucci and Stuenkel, 1997). Values for R_{min} , R_{max} and K_{eff} were 0.44, 5.52 and 972 nM, respectively.

Digitonin Permeabilization Experiments:

Permeabilized chromaffin cell experiments were performed as described elsewhere (Bittner and Holz, 1992). First the nutrient media was washed off the dish and replaced with sodium glutamate solution (NaGEP) containing 139 mM sodium glutamate, 20 mM PIPES, 2 mM MgATP, and 0.2 mM EGTA, pH 6.6, with no added Ca^{2+} . The EGTA in the bath solution helps control the levels of free calcium in a precise and reproducible manner. To extend the range of concentrations tested above 30 μM , NTA was used in place of EGTA to chelate Ca^{2+} . Individual cells were then perfused with NaGEP solution (0.2 mM EGTA) for 10 sec and then permeabilized by switching to NaGEP solution (5 mM EGTA) containing 40 μM digitonin for 50 sec with varying concentrations of free Ca^{2+} (1, 5, 10, 30, 100 μM). The amount of free Ca^{2+} in the solution was calculated using the Martell and Smith constants for EGTA-Ca binding. A stock NaGEP solution with 30 μM free Ca^{2+} was made using 4.693 mM CaCl_2 (total Ca^{2+}). Other concentrations of Ca^{2+} were made by mixing the Ca-free and the 30 μM Ca^{2+} stock solutions together in the appropriate ratios. NaGEP solution with 100 μM free Ca^{2+} was also made using 4.97 mM CaCl_2 (total Ca^{2+}).

Channel Blocker Experiments

Stock Solution of nifedipine (L-type; Sigma, Saint Louis, Missouri) was prepared in DMSO at a concentration of 10 mM and diluted with the bath solution (PSS, see cell stimulation) to the required final concentration of 3 μM . ω -Conotoxin GVIA (N-type) and ω -conotoxin MVIIC (N/P/Q-type; Sigma, Saint Louis, Missouri) were prepared in distilled water to a stock concentration of 1

mg/ml and kept in aliquots at -20 °C until use. Ω -conotoxin GVIA and ω -conotoxin MVIIC were used at a final concentration of 1 μ M and 3 μ M in PSS, respectively. Chromaffin cells transfected separately with GCaMP5G, Syt-1, or Syt-7 GFP were incubated with the above listed Ca^{2+} channel blockers alone or in combination. The effect of channel blockers was then determined using TIRF microscopy following stimulation of exocytosis with 56 mM KCl. The control cells were imaged prior to application of the blockers. The percentage reduction in exocytosis is based on the difference in the number of fusion events between control and treated cells.

Super-resolution Imaging

For this procedure, isolated chromaffin cells transfected separately with Syt-1 or Syt-7 pHluorin were plated on a pre-coated 35 mm glass bottom cover dish. Cells were first washed with PSS, followed by stimulation with either a high- K^{+} -containing PSS solution (56 mM KCl) or basal PSS solution (5.6 mM KCl) for 20 s at room temperature. All activity within the cell following the stimulation period was arrested using ice-cold PSS and the cells were fixed immediately with 4% paraformaldehyde in phosphate-buffered saline (PBS) for 30 min. The cells were then rinsed and quenched for 30 min with 50 mM NH_4Cl in PBS. Cells were immunostained with biotinylated anti-GFP, rabbit IgG fraction antibody (Life Technologies) and streptavidin conjugated AlexaFluor 647 (Invitrogen). Cells were finally imaged in a buffer containing: 50mM Tris, 10mM NaCl, 10% w/v glucose, 10mM Cysteamine hydrochloride (Sigma, Saint Louis, Missouri), 50mM

β -mercaptoethanol, $40\mu\text{g mL}^{-1}$ catalase (Sigma, Saint Louis, Missouri), $500\mu\text{g mL}^{-1}$ glucose oxidase (Sigma, Saint Louis, Missouri), pH 9.0.

Imaging was performed using TIRF microscopy with an Olympus IX81-XDC inverted microscope with a cell TIRF module, a 100X APO objective (NA = 1.49), and active Z-drift correction (ZDC) (Olympus America). Excitation of Alexa-Fluor 647 was accomplished using a 647-nm diode laser (OBIS 647 LX-100FP, Coherent). Excitation and emission were filtered using the quadband filter cube set ET-405/488/561/647 (Chroma). Images were acquired on an iXon Ultra EMCCD camera (Andor Nanotechnology).

Stopped-Flow Rapid Mixing Experiments

For stopped-flow experiments, cytoplasmic domains (C2AB) of Syt-1 and Syt-7 were subcloned into pTrcHisA vector (Invitrogen) generating an N-terminal His-6 tag. His-6-tagged proteins were purified on a Ni-nitrilotriacetic acid-agarose (Qiagen, Valencia, CA) column, as described previously (Chapman *et al.*, 1995). His-6-tagged proteins were eluted from the beads by using imidazole (Chapman *et al.*, 1996). Synthetic 1,2-dioleoyl-sn-glycero-3-phospho-l-serine (phosphatidylserine, PS), 1,2-dioleoyl-sn-glycero-3-phosphocholine (phosphatidylcholine, PC), 1,2-dioleoyl-sn-glycero-3-phosphoethanolamine (phosphatidylethanolamine, PE), and 1,2-dioleoyl-sn-glycero-3-phosphoethanolamine-N-(5-dimethylamino-1-naphthalenesulfonyl) (dansyl-PE) were purchased from Avanti Polar Lipids. FRET was used to monitor the time course of Ca^{2+} -dependent Syt-liposome interactions by using an SX.18MV

stopped-flow spectrometer (Applied Photophysics, Surrey, U.K.) as described previously (Wang *et al.*, 2003b). Native tryptophan residue(s) in Syt and dansyl groups attached to phospholipids in the liposomes serve as energy donors and acceptors, respectively. Liposomes (100 nm; 5% dansyl-PE; 25% PE; 15, 25 or 35 % PS; and 55, 45 or 35 % PC) were premixed with Syt-1 or Syt-7 in the presence of Ca^{2+} and then rapidly mixed with HEPES buffer containing excess EGTA. The Trp residues in the cytoplasmic domain of each Syt isoform were excited at 285 nm, and the emission from the dansyl-PE acceptor was collected by using a 470-nm cutoff filter. The dead time was ≈ 1 ms. The chelation of Ca^{2+} by EGTA results in a rapid loss of the fluorescent signal.

Image Analysis

The images obtained from confocal microscopy were analyzed using a software-based approach with Imaris software (Bitplane, Zurich, Switzerland) using the “spot function” module for object based co-localization analysis. To determine the distance of the Syt granules from the nearest point on the cell surface, confocal z-sections were used to render a 3D surface in Imaris. The Syt GFP granules within the evanescent field were tracked using a custom-script (Degtyar *et al.*, 2007) developed in IDL (ITT, Boulder, CO, USA).

The images obtained from TIRF microscopy were analyzed in multiple ways. Determination of NPY or Syt GFP fusion events was based on changes in GFP fluorescence. NPY fusion events were identified by one of the following two criteria: (1) upon fusion, the release of NPY GFP from granules resulted in decay

of the fluorescent signal as the protein was lost from the granule, or (2) a transient rise in GFP fluorescence occurred at the moment of fusion and was followed by decay as mentioned above (Taraska *et al.*, 2003; Perrais *et al.*, 2004).

On the other hand, Syt GFP fusion events were identified primarily based on the increase in fluorescence following fusion with the plasma membrane (See explanation below). We selected events based on a minimum 20% increase in GFP fluorescence following fusion. In some cases the initial rise in fluorescence was followed by a decrease as Syt GFP diffuses along the plasma membrane. Fusion of GFP containing granules with the plasma membrane results in brightening of fluorescence for two reasons: (1) GFP (pKa 5.9) present within the granule lumen encounters the neutral pH (7.4) of the extracellular medium causing slight dequenching of the fluorophore, and (2) the increased strength of the evanescent field at the plasma membrane–coverslip interface, causes greater excitation of the GFP molecules (Kneen *et al.*, 1998; Tsien, 1998; Campbell and Choy, 2001).

The Syt-1 pHluorin/Syt-7 pHuji and NPY pHluorin/Syt mCherry emission images were captured sequentially using the Metamorph software (Molecular Devices, LLC, Sunnyvale, CA). Individual granules undergoing exocytosis were evident by an increase in the pHluorin/pHuji intensity following fusion with the plasma membrane due to the change in pH of the granule. The changes in the fluorescence intensity over time for the different fusion events were calculated

after normalization for every fusion event using custom software written in IDL (ITT, Boulder, CO, USA)

For the super-resolution images, captured single molecules were identified in individual image frames. Localized centers were identified by the use of a multi-emitter algorithm that compensates for events that do not fit to a single emission profile (Huang *et al.*, 2011) using the open source thunderSTORM ImageJ plug-in (Ovesný *et al.*, 2014). Localizations were then processed to remove outliers in intensity, width, or localization error. Localized centers from at least 5,000 images were used to reconstruct final high resolution images.

High resolution reconstructed images were analyzed using a Density Based Spatial Clustering Analysis with Noise (DBSCAN) algorithm (Ester *et al.*, 1996). DBSCAN assigns clusters in the reconstructed images based on the density of localizations in a user defined search radius (r) and a minimum localization threshold.

RESULTS

The subcellular distribution of Syt-1 and Syt-7 isoforms is distinct

The distribution of endogenous Syt-1 and Syt-7 isoforms within chromaffin cells was systematically assessed using isoform-specific antibodies and confocal microscopy (Figure S4.1). The analysis performed here differs from our previous approach (Rao *et al.*, 2014) in that it uses an automated object-based identification method which reduces the uncertainties associated with visual spot counting of granules and variable antibody staining.

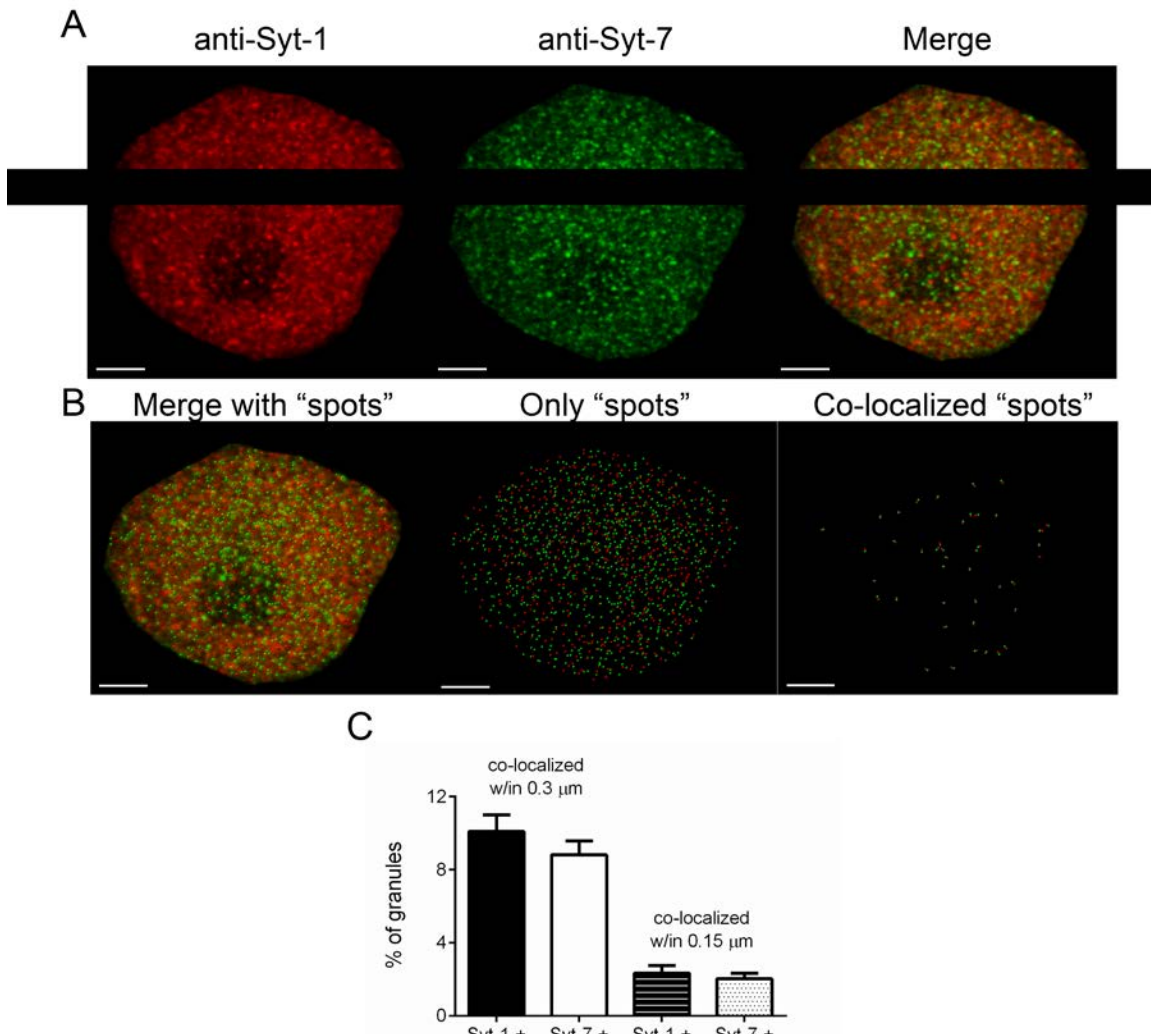


Figure S4.1. Confocal imaging of endogenous Syt isoform distribution within chromaffin cells.

(A) A representative image of a chromaffin cell stained for endogenous Syt-1 and Syt-7. Scale bar, 5 μm . (B) Syt-1 and Syt-7 puncta are identified by spheres generated by the spot function in Imaris (Bitplane). (C) The percent co-localization of synaptotagmin isoforms was calculated using a threshold distance of 0.3 μm or 0.15 μm ($n = 8$ cells).

This approach also provides a platform for analyzing the spatial arrangement of punctate granular proteins within the cell and allows us to better resolve individual granules and the distances between them. Endogenous

synaptotagmin exhibits a punctate pattern of distribution within cells – consistent with its presence on dense core granules.

A key question we wished to address was the extent to which isoforms are expressed together on granules. Therefore, we assessed the degree of co-localization of the fluorescent synaptotagmin puncta in the colored channels in several ways. First, we performed a pixel-by-pixel Pearson's correlation analysis after thresholding based on the dimmest pixel in the cell. We applied this schema to multiple cells stained for Syt-1 and Syt-7 and obtained values that ranged between 0.14 and 0.16 (Data not shown). This indicates only a weak correlation between pixel intensities, and therefore suggests there is little co-localization between Syt-1 and Syt-7 on granules.

Applying our object based methodology, fluorescent synaptotagmin puncta were automatically identified based on size and intensity thresholds using the Spot function in Imaris (Bitplane). Examples of puncta represented by spheres are shown in Figure S4.1 B. The displayed spheres are positioned at the center of fluorescence intensity. Next, the number of red and green "spots" (representing Syt-1 and Syt-7, respectively) that are roughly at one granule diameter (300 nm), or within one granule diameter (150 nm), of one another was estimated with a co-localization function. The results of this analysis are shown in Figure S4.1 C. Again, the overall fraction of spots (representing granules) with co-localized synaptotagmins is quite low.

Based on the confocal imaging above, it was apparent that the probability of finding Syt-1 and Syt-7 on the same granule was considerably lower than the probability of finding them on different granules. This finding lends credence to the notion that chromaffin cell synaptotagmin isoforms are largely sorted to different granule populations. We next sought to determine whether those granule populations (i.e., with Syt-1 or Syt-7) differed in their average distance from the cell surface. A reasonable assumption is that the outermost fluorescent Syt puncta approximately demarcate the border of the cell (i.e., the plasma membrane). Based on this assumption, confocal z-sections ($0.71\ \mu\text{m}$) were used to render a 3D surface representing the approximate contours of the cell membrane (Figure 4.1 A).

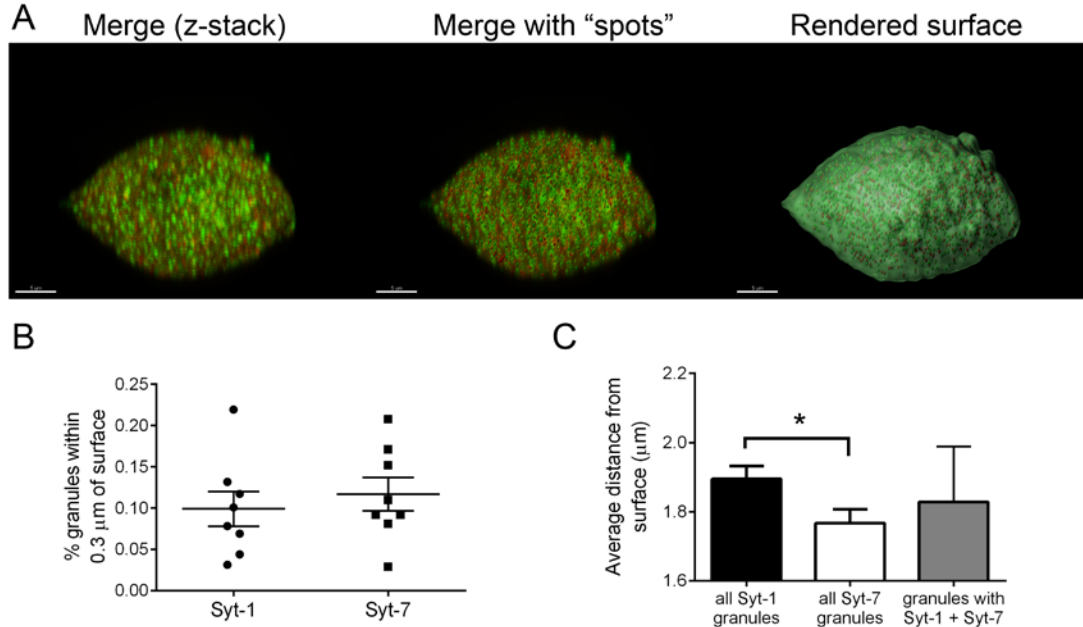


Figure 4.1: Distribution of Syt isoforms with respect to a rendered cell surface.

(A) A 3-dimensional image of a chromaffin cell reconstructed from individual confocal z-sections ($0.71\ \mu\text{m}$). Antibodies were used to identify endogenous Syt-

1 and Syt-7 proteins. The spheres in the middle panel mark stained Syt-1 (Red) or Syt-7 (Green) puncta (generated using the Spot function in Imaris (Bitplane)). The z-sections were used to render a 3D surface representing the approximate contours of the cell surface (right panel). Scale bar, 5 μm . (B) Graph illustrates the percentage of Syt-1 or Syt-7 granules located within a distance of one granule diameter (0.3 μm) from the rendered surface ($n = 8$ cells). Differences between groups were assessed with the Student's t-test ($p > 0.05$, ns). (C) The overall average distances of granules bearing Syt-1, Syt-7, or both isoforms were calculated with reference to the nearest surface. Note, this analysis takes into account all granules, not just those within 0.3 μm of the surface as in (B). Differences between the Syt-1 and Syt-7 granule populations were assessed with the Student's t-test ($n = 8$ cells, $*p < 0.01$).

The distance of individual Syt-1 and Syt-7 puncta – again, identified using isoform specific antibodies (Figure S4.1) – from the nearest surface was measured. Syt-1 puncta were distributed within the cell at greater distances from the surface, on average, than Syt-7 puncta (Figure 4.1 C). This did not depend on whether fluorescence from Syt-1 protein (red emission channel) or from Syt-7 protein (green emission channel) was used in rendering the surface. There is no significant difference between the percentage of Syt-1 and Syt-7 puncta (of the total number of puncta in the cell) that are located within one granule diameter of the rendered surface (Figure 4.1 B). We add that average distance of granules with both Syt-1 and Syt-7 from the membrane is highly variable, and indeed, not statistically different from either the Syt-1 or Syt-7 population.

We can conclude from the analysis presented here that Syt-1 and Syt-7 are differentially distributed in chromaffin cells. Isoforms rarely co-localize and on average, Syt-1 granules appear to be positioned at greater distances from the plasma membrane than Syt-7 granules. However, the fraction of the total labeled

granules that are within one granule diameter of the plasma membrane is not different between groups.

Syt isoforms respond differentially to stimuli

We first transfected cells with Syt-1 GFP or Syt-7 GFP alone and monitored how each isoform responded to different degrees of membrane depolarization using KCl solutions of varying strength. Here, we consider the proportion of fusing granules based on all granules resident within the evanescent field (“docked”) at least 10 s prior to the start of depolarization. At the lowest KCl concentration tested (25 mM KCl), a greater proportion of docked Syt-7 granules fused with the plasma membrane (10%) in comparison to Syt-1 (3%) (Figure 4.2 A). Stronger KCl concentrations lead to a greater number of fusion events for both synaptotagmin isoforms. 56 mM KCl was more effective at activating Syt-1 than Syt-7 granules, with 31% of docked Syt-1 granules fusing in comparison to 28% of Syt-7 granules. When the KCl concentration was elevated even further to 80 mM, isoforms showed similar percentages of fusing granules.

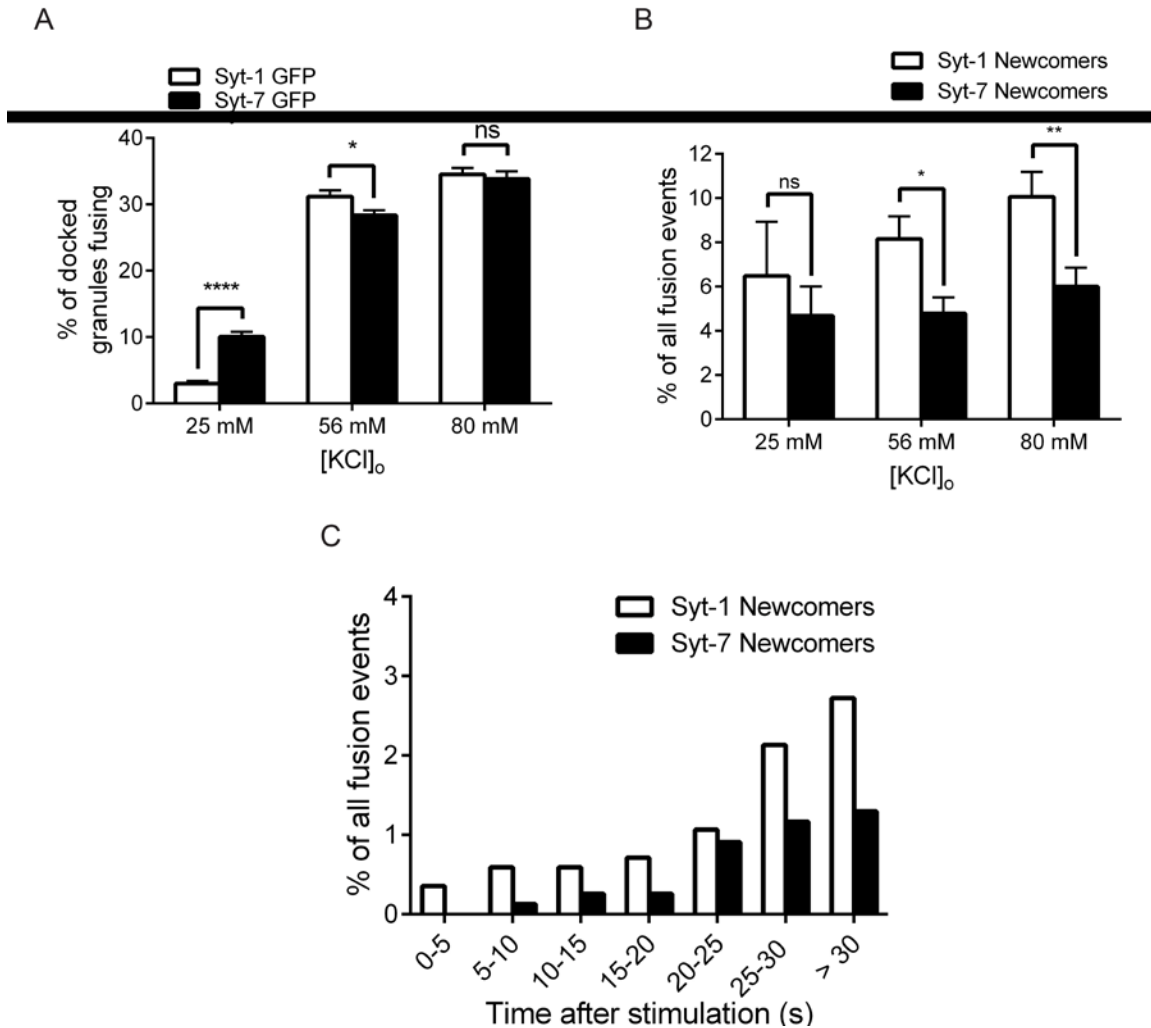


Figure 4.2. Characterization of docked and newcomer granules following membrane depolarization.

Syt-1 or Syt-7 GFP was expressed separately in chromaffin cells and exocytosis was triggered by stimulation with KCl of different strengths (25, 56, 80 mM) (A) The number of fusing Syt granules for each condition is expressed as a percentage of all granules resident in the evanescent field (“docked”) at least 10 s prior to the start of the stimulus ($n = 12$ cells (25 and 80 mM KCl); $n = 18$ (56 mM KCl)). Statistical differences were assessed with Student’s t-test (* $p < 0.05$, **** $p < 0.0001$). (B) Bar graph depicts the percentage of newcomer granules that fuse in relation to the total number of fusion events. Statistical differences were assessed with Student’s t-test (* $p < 0.05$, ** $p < 0.01$). (C) Time course for newcomer Syt-1 and Syt-7 fusion events following stimulation with 56 mM KCl. The percentage of newcomer events is based on the total number of fusion events and binned into 5 s intervals. Note that there is a greater proportion of Syt-1 newcomer fusion in comparison to Syt-7 newcomer fusion at all time points.

These experiments demonstrate that activation of Syt isoforms is dependent on the strength of the stimulus. Mild depolarization results in a smaller rise in intracellular Ca^{2+} (see Figure 4.6 B below) and preferentially triggers Syt-7 granule fusion. Stronger depolarization leads to a larger increase in Ca^{2+} and activates both Syt isoforms to a similar degree.

It is important to note that docked granules do not comprise all fusing granules. Therefore, we sought to characterize the fraction of total fusion events for each Syt isoform that belong to the “newcomer” category. Unlike docked granules, these events are mediated by granules from deeper within the cell (outside of the evanescent field) and only approach the plasma membrane prior to fusion. Upon stronger depolarization (56 or 80 mM KCl), the ratio of Syt-1 newcomers to all Syt-1 fusion events is significantly greater than the ratio for Syt-7 newcomers (Figure 4.2 B). This trend is less prevalent at milder depolarization (25 mM KCl) due to the overall lack of Syt-1 fusion. Furthermore, when factoring in the latency of newcomers following stimulation (binned into 5 s intervals), there are more Syt-1 than Syt-7 newcomer fusion events at all time points (Figure 4.2 C).

In order to shed light on the mechanism of activation of synaptotagmin isoforms within chromaffin cells, we expressed both isoforms simultaneously within cells. Cells were co-transfected with Syt-1 pHl and Syt-7 pHuji, and the timing of their activation was monitored using both strong (56 mM KCl) and mild (25 mM KCl) depolarization. Syt-7 granules fused earlier than Syt-1 following

depolarization, irrespective of KCl strength (Figure 4.3, A-D). This trend can be seen in the representative images and traces of Syt-1 and Syt-7 events from a single co-transfected cell, where Syt-7 pHuji events begin almost immediately following application of 56 mM KCl (Figure 4.3, A and B). We also compared the frequency distribution of all fusion events based on the time at which they occurred following depolarization (Figure 4.3, C and D). The events were binned into 1 s intervals and fit with a Gaussian curve to determine the average time until fusion for Syt-1 pHl (8.66 s) and Syt-7 pHuji (6.52 s) using 56 mM KCl.

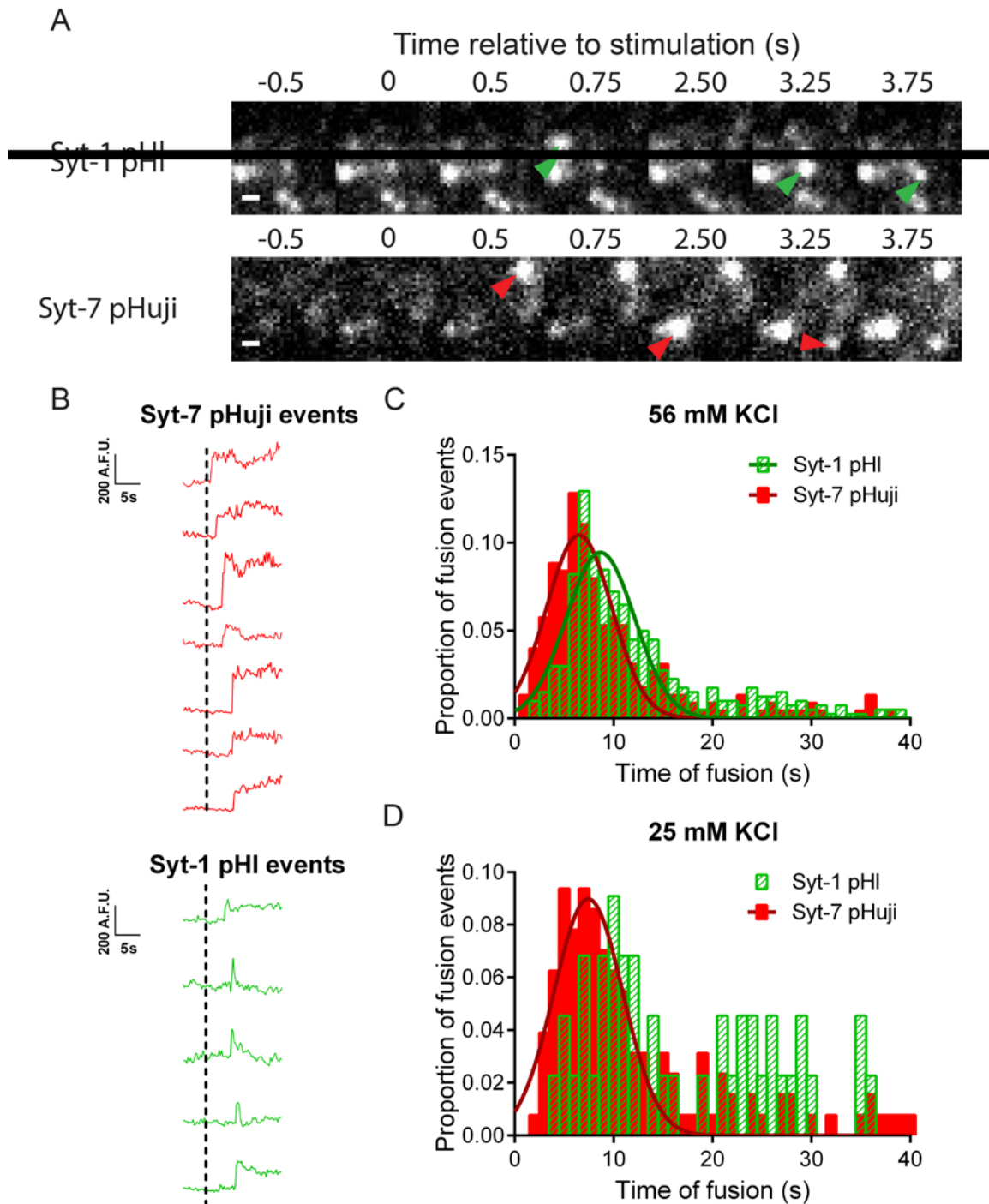


Figure 4.3. Differential time course for activation of Syt isoforms.

Syt-1 pHI and Syt-7 pHuji were co-expressed simultaneously in the same chromaffin cell and exocytosis was triggered by stimulation with KCl of different strengths (25 and 56 mM). (A) Representative fusion events for Syt-1 pHI and Syt-7 pHuji granules. Fusing granules are indicated by a colored arrow corresponding to the fluorophore. Time 0 s represents the start of stimulation.

Scale bar, 400nm. (B) Representative traces for Syt-1 pHl and Syt-7 pHuji fusion events from the same cell all aligned to the start of the stimulation period (dotted line). Syt-7 pHuji granules begin fusing prior to Syt-1 pHl granules following stimulation. (C) Frequency distribution of all fusion events following depolarization with 56 mM KCl binned into 1 s intervals (Syt-1 pHl - 402 events and Syt-7 pHuji - 226 events, $n = 11$ cells). The data was fit with a Gaussian to determine the average time of fusion for Syt-1 pHl (8.661 s) and Syt-7 pHuji (6.515 s) events. (D) Frequency distribution of all fusion events following depolarization with 25 mM KCl binned into 1 s intervals (Syt-1 pHl - 44 events and Syt-7 pHuji - 128 events, $n = 10$ cells). Syt-1 pHl does not show a normal distribution due to small number of fusion events at lower KCl stimulation and hence could not be fit with a Gaussian. The average time of fusion for Syt-7 pHuji events was 7.438 s.

Consistent with what was observed in Figure 4.2 A, mild depolarization resulted in very little fusion of Syt-1 pHl. Therefore, the frequency distribution could not be accurately represented with a Gaussian fit at 25 mM KCl. However, under these conditions Syt-7 pHuji still tended to fuse earlier (average time ~ 7.44 s).

Syt-1 granules move a greater distance to sites of fusion than Syt-7 granules

We next determined whether Syt-bearing granules differed in their general mobility prior to reaching their ultimate fusion sites. Since it is difficult to accurately track the movement of the granules in the z-direction, we instead focused on the lateral displacement of granules in the X-Y plane within the evanescent field. To investigate this question, we expressed Syt-1 or Syt-7 in cells as GFP fusion proteins and tracked granules using TIRF microscopy for tens of seconds before and during membrane depolarization with 56 mM KCl. The time of fusion was evident as a sudden brightening of the granule sometimes

followed by spreading of the fluorescence from the granule membrane into the plasma membrane.

Prior to stimulation, both Syt-1 and Syt-7 granules undergo small x and y (R) motions in the plane of the cell membrane. It is clear from monitoring these motions that granules tend to fuse at sites that are tens to hundreds of nanometers displaced from their initial positions at the start of stimulation (Figure 4.4 A, see solid circle versus dashed circle).

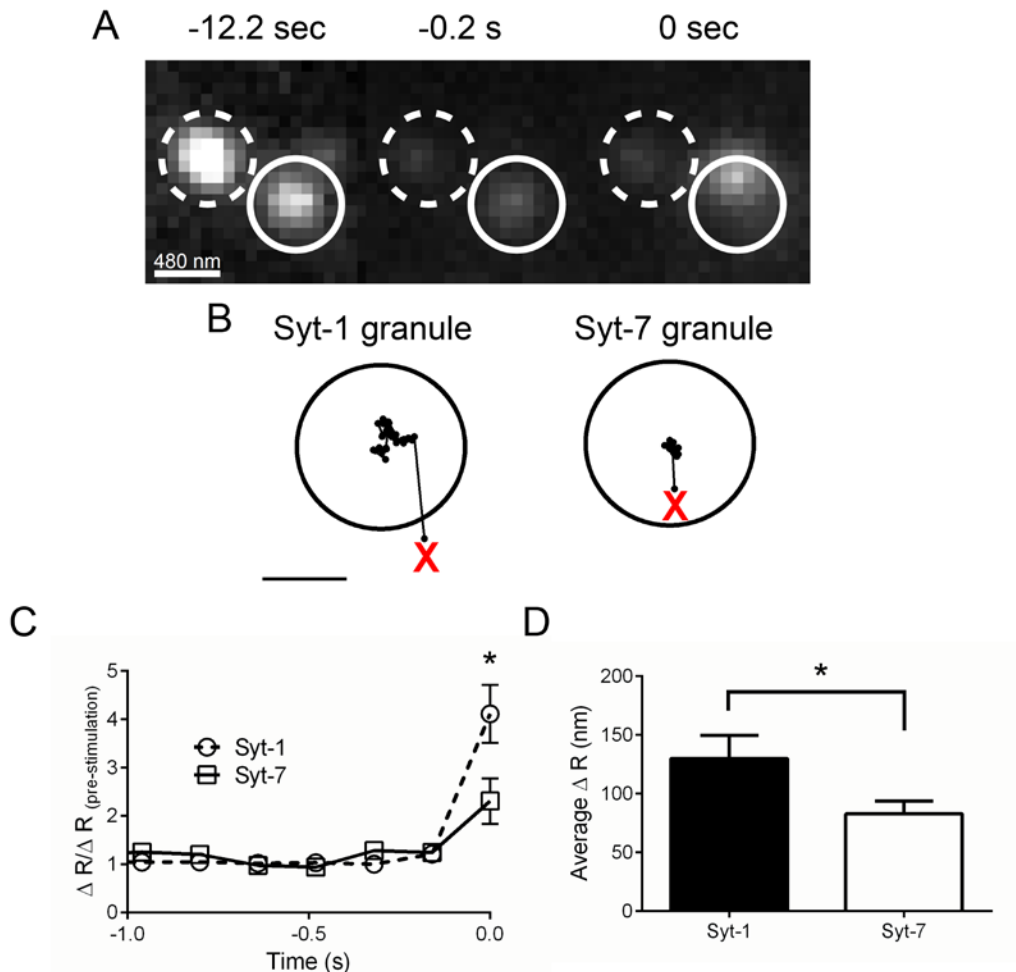


Figure 4.4: Lateral mobility of Syt isoform bearing chromaffin granules.

(A) Images of fusing (solid circle) and non-fusing (dashed circle) Syt-1 GFP granules at the start of stimulation (-12.2 s), immediately prior to fusion (-0.2 s),

and at fusion (0 s). The non-fusing granule remains within the dashed circle even after 12.2 s of stimulation as seen at time 0. The fusing granule significantly increases its motion in the frame immediately before fusion. Note displacement of the fluorescent punctum within the solid circle between -0.2 s and 0 s. (B) Representative frame-to-frame tracks for Syt-1 and Syt-7 GFP during the 3 s prior to fusion (Red X) following stimulation with 56 mM KCl. (C) Average, frame-to-frame motion of fusing Syt-1 and Syt-7 granules in the 1 s before fusion (time 0). Statistical differences were assessed by the Student's t-test (* $p < 0.05$). (D) Average displacement of Syt-1 and Syt-7 granules from the start position to the fusion position in part B. Statistical differences was assessed with the Student's t-test (* $p < 0.05$).

Granules were tracked within the evanescent field using a custom-script developed in IDL (Degtyar *et al.*, 2007). Representative tracks for Syt-1 and Syt-7 granules in the seconds before fusion are shown in Figure 4.4 B. The red X indicates the site of fusion. We quantified this motion by taking the frame-by-frame, post-stimulation ΔR expressed relative to its ΔR before stimulation. This normalization was necessary because it was apparent that certain granules are inherently more mobile than others. Figure 4.4 C shows the average ΔR (post-stim)/ ΔR (pre-stim) for fusing Syt-1 and Syt-7 granules. In the moments leading to fusion, Syt-1 and Syt-7 mobility is similar. However, in the last 200 milliseconds before fusion, Syt-1 granules tend to travel a greater distance than Syt-7 granules. The sudden increased motion is specific to fusing granules. For example, when the motion of non-fusing granules (typically within 2 to 5 granule diameters of fusing granules) was tracked alongside their fusing neighbors, there was no noticeable increase in movement (data not shown). The displacement of individual Syt-1 and Syt-7 granules from the start position to the fusion site was

also measured (Figure 4.4 D). Again, we found that Syt-7 granules tend to travel a shorter distance to fusion sites, on average, than Syt-1 granules.

Syt isoforms differ in their fusion competency during repeated stimulation

Having looked at the granules which fused upon stimulation, we next wanted to determine the fate of the remaining docked granules when challenged again with a depolarizing stimulus. An important factor to consider while designing this experiment was whether Ca^{2+} levels returned to baseline between subsequent rounds of stimulation. To verify this, we first transfected cells with the genetically encoded Ca^{2+} indicator GCaMP5G and subjected them to multiple rounds of depolarization with 56 mM KCl (see methods). Indeed, GCaMP5G fluorescence fell back to baseline when cells were given a 10 s recovery period (Figure 4.5 A, left panel). Using the same stimulation paradigm on cells transfected with either Syt-1 or Syt-7 GFP, we observed that Syt-1 granules show greater fusion competency when compared to Syt-7 granules (Figure 4.5 A, right panel). This led us to question whether there was a difference in the time required for the Syt-1 and Syt-7 granule populations to transition into a fusion ready state. To test this, we increased the recovery period between subsequent stimuli to 60 s. Given this longer recovery window, Syt-1 and Syt-7 granules showed similar fusion competency (Figure 4.5 B, right panel). Therefore, it seems that Syt-1 granules that are not initially capable of undergoing fusion require less time to transition into a fusion competent state.

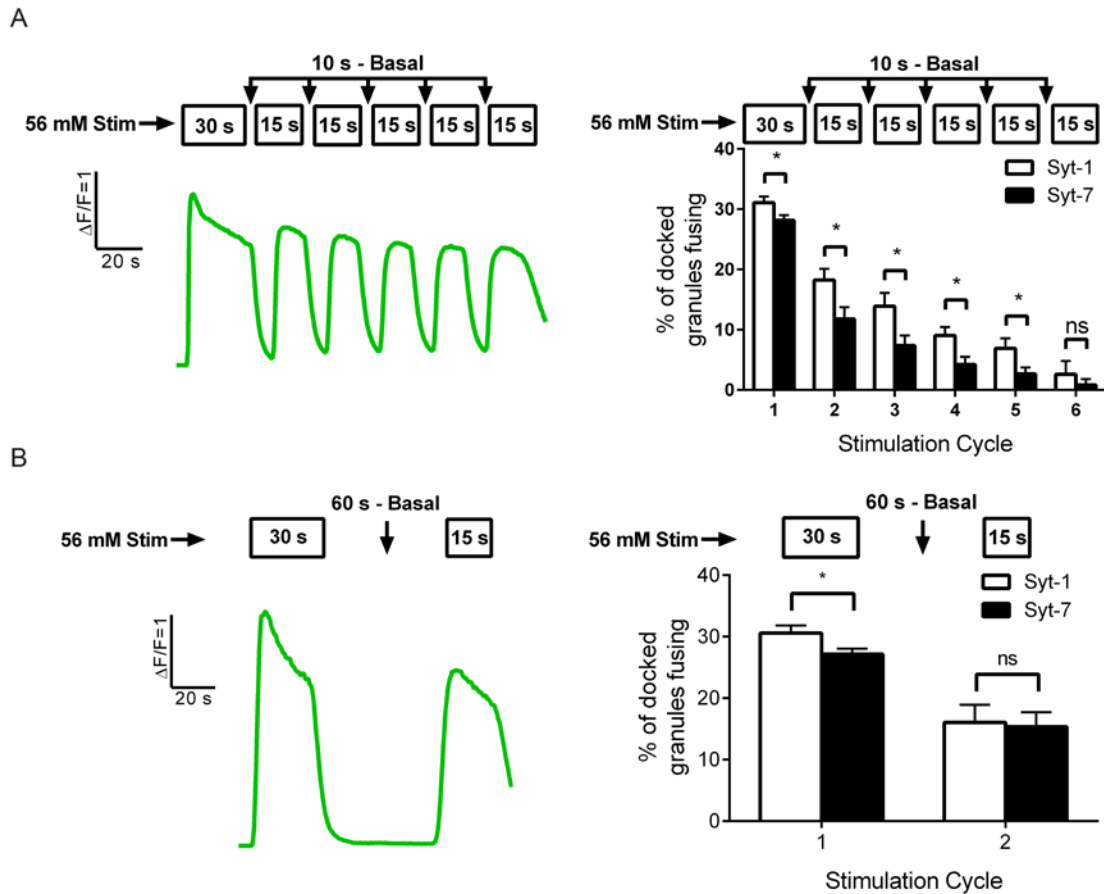


Figure 4.5: Effect of repeated stimulation on Syt fusion competency. Chromaffin cells transfected with GCaMP5G, Syt-1, or Syt-7 GFP were depolarized with 56 mM KCl during multiple rounds of stimulation (depicted on top of each graph). (A) Representative trace (left) indicates the Ca^{2+} influx measured in a single GCaMP5G transfected chromaffin cell following repeated rounds of stimulation (56 mM KCl) with intermittent application of basal PSS (10 s - recovery period). Note that GCaMP5G fluorescence drops to baseline between subsequent stimuli, indicative of Ca^{2+} clearance from the cytoplasm. The percentage of fusing Syt-1 or Syt-7 GFP granules (right) is based on the total number of docked granules present at the beginning of each round of stimulation. Differences between groups were assessed with the Student's t-test ($n = 17$ cells, $*p < 0.05$) (B) Representative trace (left) indicates the Ca^{2+} influx measured during multiple rounds of stimulation with a longer recovery period (60 s - Basal PSS). Bar graph represents the percentage of fusing Syt-1 or Syt-7 GFP granules during application of each stimulus. Differences between groups were assessed with the Student's t-test ($n = 17$ cells, $*p < 0.05$).

Membrane depolarization leads to a concentration-dependent influx of Ca^{2+}

While the depolarization evoked by elevated extracellular KCl is certainly effective in driving exocytosis, what matters most is the effect of depolarization on intracellular free Ca^{2+} around fusion sites. To confirm that depolarization with KCl leads to an influx of Ca^{2+} , we transfected cells with GCaMP5G and measured the changes in fluorescence using TIRF. GCaMP5G fluorescence increases upon Ca^{2+} binding and this increase can be represented as a fold change ($\Delta F/F$) in fluorescence intensity (Figure 4.6 A). Binding of GCaMP5G to Ca^{2+} was saturated upon application of stronger KCl solutions (≥ 56 mM). Using this information we were able to approximate the total internal Ca^{2+} concentration ($[\text{Ca}^{2+}]_i$) resulting from application of each KCl solution based on the equations described in Maravall et al., 2000 (see methods). We observed that the rise in total internal Ca^{2+} was directly related to the concentration of KCl used to depolarize the cell (Figure 4.6 B).

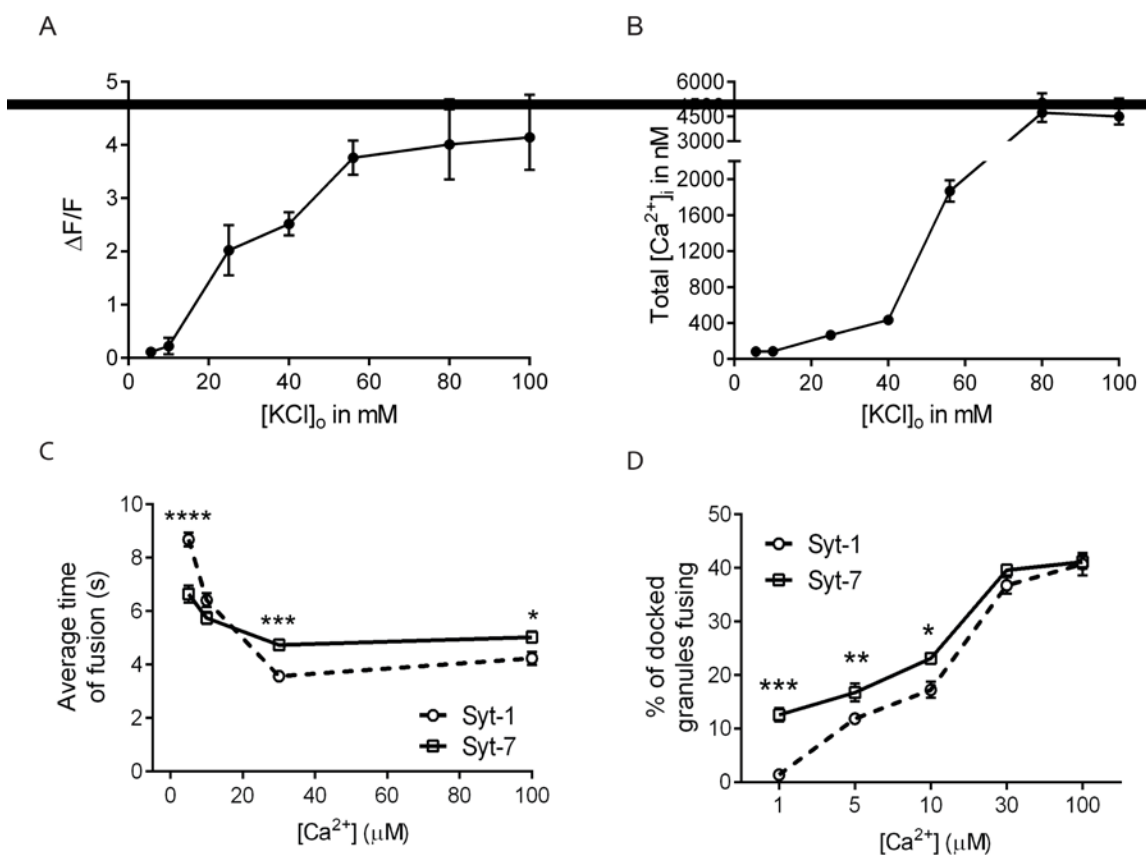


Figure 4.6: Determination of $[Ca^{2+}]_i$ in chromaffin cells using TIRF microscopy and the effects of cytosolic Ca^{2+} on Syt fusion.

(A) Chromaffin cells transfected with GCaMP5G were stimulated with different strengths of KCl (5.6, 10, 25, 40, 56, 80 or 100 mM) to depolarize the membrane. Graph shows the averaged fold changes in GCaMP5G fluorescence ($\Delta F/F$) following KCl depolarization to estimate indicator saturation. Error bars depict S.E.M. ($n = 8$ cells for each depolarization condition) (B) Graph indicates the total intracellular free Ca^{2+} concentration (nM) following depolarization with KCl (as in 7A). Values were estimated using the equations obtained from Maravall et al., 2000. Error bars depict S.E.M. ($n = 8$ cells for each depolarization condition). (C) Syt-1 or Syt-7 GFP was expressed separately in chromaffin cells. The graph indicates the average elapsed time from application of Ca^{2+} (at the indicated concentrations) to the first Syt-1 or Syt-7 fusion event. Differences in fusion times were found to be statistically significant using Student's t-test (* $p < 0.05$, *** $p < 0.001$, **** $p < 0.0001$). (D) Percentage fusion of Syt-1 and Syt-7 granules for each $[Ca^{2+}]$ based on the total number of docked granules at the beginning of stimulation. Raw counts for fusion events/docked granules and cells respectively - 100 μM : Syt-1 (352/856; 10 cells), Syt-7 (366/894; 10 cells); 30 μM : Syt-1 (823/2187; 15 cells), Syt-7 (811/2110; 15 cells); 10 μM : Syt-1 (346/2037; 15 cells), Syt-7 (491/2091; 15 cells); 5 μM : Syt-1 (241/1996; 15 cells), Syt-7 (368/2227; 15 cells); 1 μM : Syt-1 (27/1993; 15 cells), Syt-7 (318/2393; 15 cells).

Statistical differences for the percentage fusion of Syt-1 and Syt-7 granules were assessed with the Student's t-test (* $p < 0.05$, ** $p < 0.01$, *** $p < 0.001$).

We also measured intracellular Ca^{2+} changes using the ratiometric Ca^{2+} indicator fura-2, and observed a similar concentration-dependent change in $[\text{Ca}^{2+}]_i$ levels based on the strength of the KCl solution (Figure S4.2) (Neher, 1995; Giovannucci and Stuenkel, 1997).

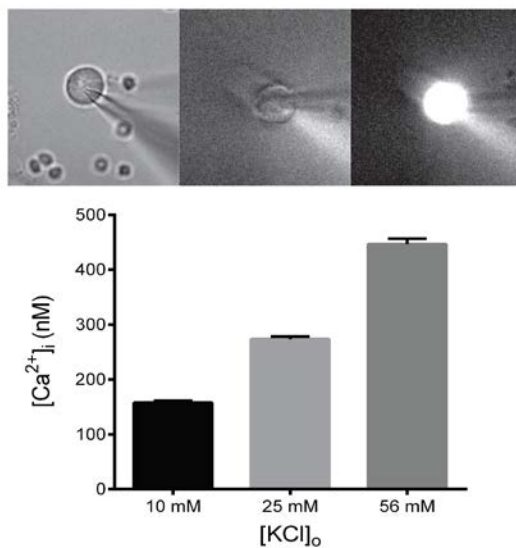


Figure S4.2. Patch-clamped chromaffin cells depolarized with elevated KCl. Ratiometric Ca^{2+} imaging of chromaffin cells using the indicator fura-2 to determine changes in cytosolic free Ca^{2+} evoked by the stimulating solutions (For stimulation with 10 mM KCl, $n = 10$ cells; 25 mM KCl, $n = 7$ cells and 56 mM KCl $n = 5$ cells).

Synaptotagmin isoforms are differentially activated by cytosolic Ca^{2+} changes

We next assessed the role of Ca^{2+} in activating or driving fusion of Syt isoform bearing granules. Cells expressing Syt-1 or Syt-7 GFP were imaged using TIRF microscopy following permeabilization with solutions containing digitonin and Ca^{2+} buffered to varying concentrations from 1-100 μM . Ca^{2+}

concentrations between 1 and 30 μM were buffered by EGTA. To extend the range of concentrations tested to above 30 μM , NTA was used to chelate Ca^{2+} . Ca^{2+} strongly influenced the average time until fusion of individual granules as well as the fusion efficiency of docked granules (Figure 4.6, C and D). We define fusion efficiency as the fraction of docked granules that fuse in response to Ca^{2+} exposure. As one might predict, when permeabilized cells are exposed to increasing amounts of Ca^{2+} , a greater fraction of docked granules undergo exocytosis. However, Syt-7 granules exhibit a lower Ca^{2+} requirement for activation from 1-10 μM as compared to Syt-1 granules (Figure. 4.6 D). These data show that at lower Ca^{2+} concentrations, Syt-7 granules exhibit a greater probability of undergoing fusion and do so with less delay following Ca^{2+} application. In agreement with the results obtained using membrane depolarization, there is no significant difference in isoform activation at higher Ca^{2+} concentrations.

Blockade of Ca^{2+} channels inhibits secretion by Syt isoforms

Given the importance of Ca^{2+} levels on activation of Syt isoforms, we were interested in testing how inhibition of various voltage-gated Ca^{2+} channels would impact Syt fusion efficiency. Based on previous studies, we chose to use the following Ca^{2+} channel blockers: Nifedipine (L-type), ω -conotoxin GVIA (N-type), and ω -conotoxin MVIIC (N/P/Q-type) at concentrations of 3, 1, and 3 μM respectively. (Hernández-Guijo *et al.*, 1998). First, we validated the efficacy of the blockers using GCaMP5G transfected cells. Following application, all

blockers significantly reduced the influx of Ca^{2+} upon membrane depolarization with 56 mM KCl (Figure S4.3 A).

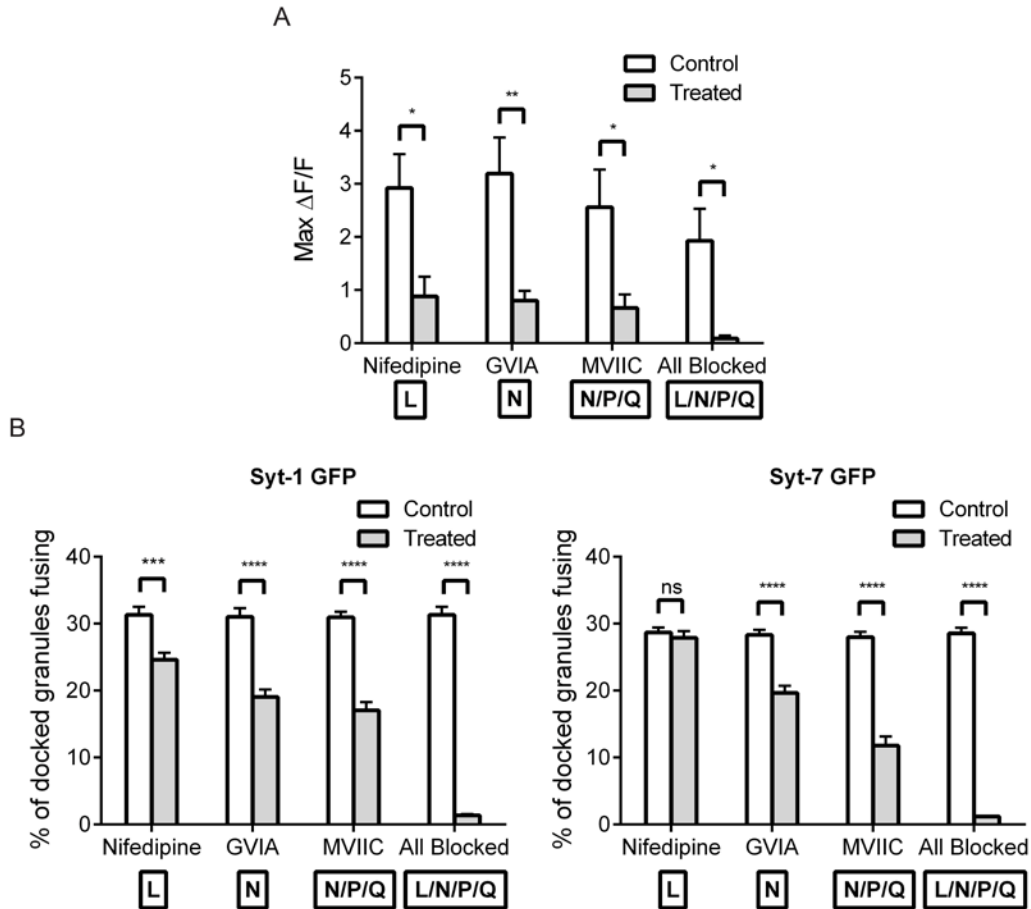


Figure S4.3. Effect of different Ca^{2+} channel blockers (alone or in combination) on Ca^{2+} entry and Syt isoform fusion in chromaffin cells following membrane depolarization.

Chromaffin cells were transfected separately with GCaMP5G, Syt-1 or Syt-7 GFP and exposed to different Ca^{2+} channel blockers at the following concentrations: Nifedipine (L-type blocker) 3 μM , ω -conotoxin GVIA (N-type blocker) 1 μM , ω -conotoxin MVIIC (N/P/Q-type blocker) 3 μM , or all three blockers together. The cells were stimulated with 56 mM KCl following a 10 min incubation with the listed blockers. (A) The graph shows the averaged maximal fold changes in GCaMP5G fluorescence ($\Delta F/F$) following depolarization which estimates the Ca^{2+} influx. Error bars depict S.E.M. (n = 5 cells for all conditions). Statistical differences were assessed with Student's t-test (*p < 0.05, **p < 0.01). (B) The number of fusing Syt-1 or Syt-7 granules for each treatment is expressed as a percentage of all docked granules. Control cells were obtained from the same

plate prior to addition of blockers (n = 18 cells for all conditions except “all blocked” where n = 6 cells). Statistical differences were assessed with Student’s t-test (**p < 0.001, ****p < 0.0001).

Next, we measured the effect of blockers on fusion efficiency in Syt-1 or Syt-7 GFP transfected cells. We observed that all treatments significantly inhibited Syt-mediated fusion with the exception of Nifedipine in Syt-7 cells, which showed small but insignificant inhibition (Figure S4.3 B). The control data was obtained from cells prior to the addition of blockers. We further quantified the reduction in fusion between Syt isoforms. Although all conditions were effective in reducing Syt-1 or Syt-7 fusion, we observed some differences in the degree of reduction based on the blocker applied (Figure 4.7). For example, L-type channel blockade resulted in a greater reduction of Syt-1 fusion, whereas blocking N/P/Q-type channels had a greater effect on Syt-7 fusion.

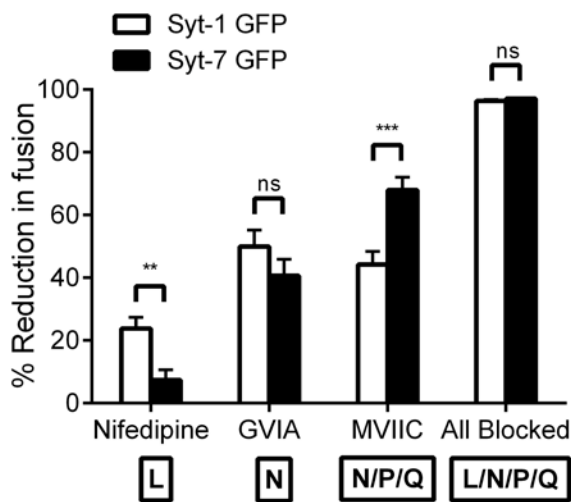


Figure 4.7: Effect of different Ca^{2+} channel blockers (alone or in combination) on Syt isoform fusion in chromaffin cells following membrane depolarization.

Chromaffin cells were transfected separately with Syt-1 or Syt-7 GFP and exposed to different Ca^{2+} channel blockers at the following concentrations:

Nifedipine (L-type blocker) 3 μM , ω -conotoxin GVIA (N-type blocker) 1 μM , ω -conotoxin MVIIC (N/P/Q-type blocker) 3 μM , or all three blockers together. The cells were stimulated with 56 mM KCl following a 10 min incubation with the listed blockers. The percentage reduction is based on the difference in the number of fusion events between control and treated cells (See Figure S4.2 B, $n = 18$ cells for all conditions except “all blocked” where $n = 6$ cells). Statistical differences were assessed with Student’s t-test (** $p < 0.01$, *** $p < 0.001$).

The rate of NPY release is controlled by the synaptotagmin isoform driving fusion

Up to this point, we had observed differences in the spatial distribution and activation requirements of Syt isoforms. These differences led us to speculate that cargo release from Syt granules may be influenced by the particular isoform they harbor. To characterize how cargo is released from these granule populations, we chose to look at the granule content marker Neuropeptide Y (NPY).

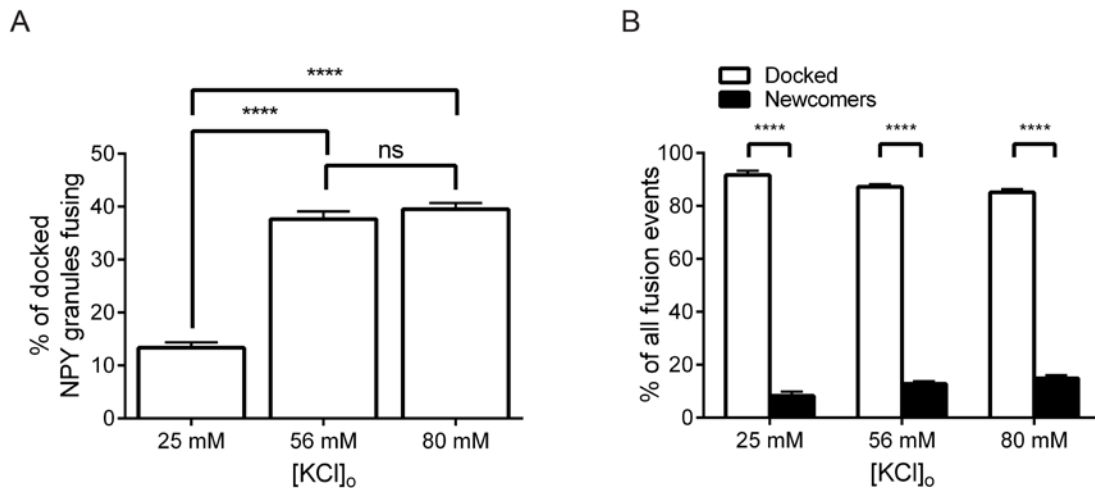


Figure S4.4. Fusion of NPY GFP granules following differential stimulation. NPY GFP transfected chromaffin cells were stimulated with KCl of different strengths (25, 56, 80 mM) to trigger exocytosis. (A) The number of fusing NPY granules for each condition is expressed as a percentage of all docked granules ($n = 12$ cells for each condition). Statistical differences were assessed with Student’s t-test (**** $p < 0.0001$) (B) Bar graph depicts the percentage of docked and newcomer granules that fuse in relation to the total number of fusion events.

Note that only the fusing granules are used to calculate the percentage here. Statistical differences were assessed with Student's t-test (**** $p < 0.0001$).

We first wanted to see how NPY-containing granules responded to differing levels of membrane depolarization using varying concentrations of KCl (Figure S4.4 A). Similar to what was observed when looking at Syt isoforms, we found that cells overexpressing NPY GFP fused in a concentration-dependent manner, with mild depolarization (25 mM KCl) resulting in significantly less exocytosis (13%) compared to stronger depolarization (~ 40%). We also found that the vast majority of fusing NPY GFP granules were docked prior to fusion, with only ~ 10% of them being newcomers (Figure S4.4 B). Using the Spot function analysis described earlier, we also measured the co-localization of endogenous Syt isoforms in cells overexpressing NPY Cerulean (NPY Cer) (Figure S4.5, A and B). The probability of finding both isoforms on the same NPY granule was significantly lower than that of finding a single isoform, with co-localization values ranging from 0.8 - 3.1 % in the 6 cells analyzed (Figure S4.5 C).

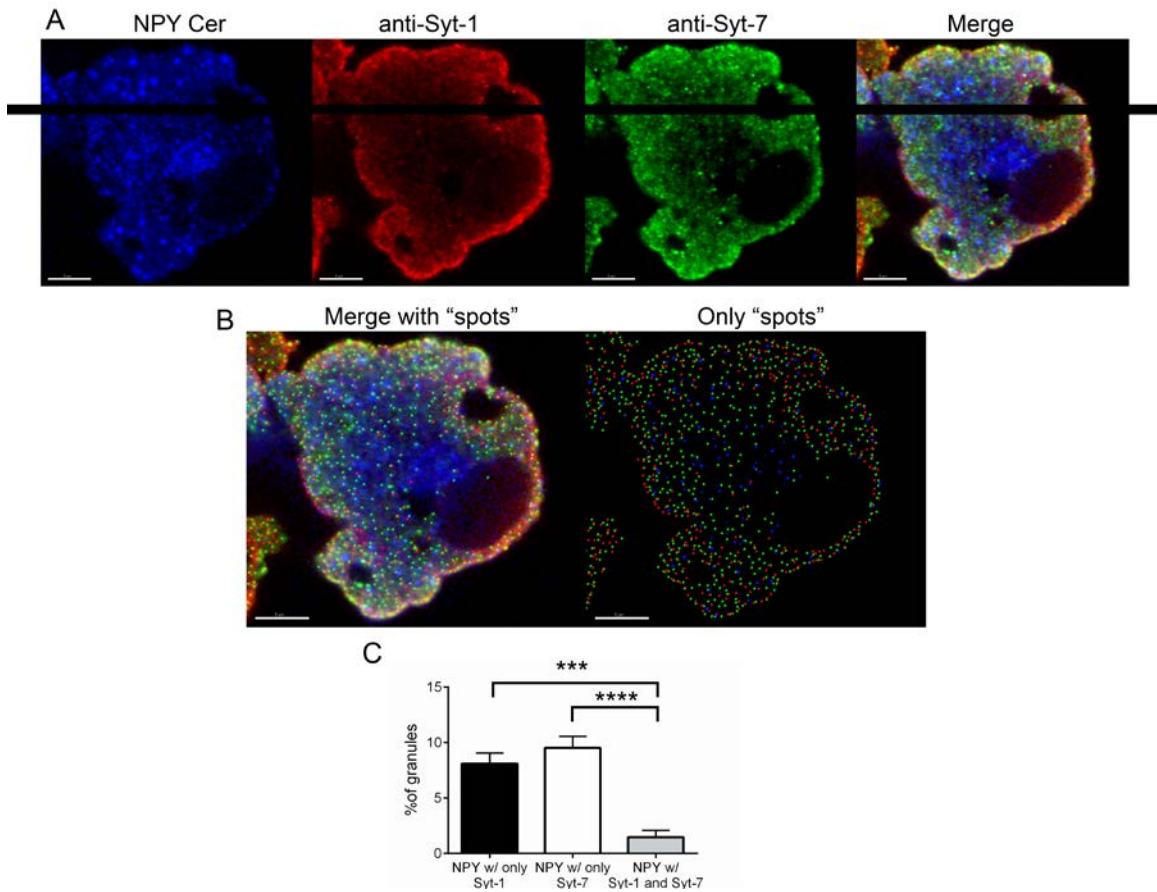


Figure S4.5. Confocal imaging of Syt isoform distribution on NPY-containing granules.

(A) Chromaffin cells transfected with NPY-Cerulean and stained for endogenous Syt-1 and Syt-7 with antibodies. Scale bar, 5 μm . (B) Syt puncta are identified by the method described in Figure S4.1. (C) Percent co-localization of NPY granules with one or both of the synaptotagmin isoforms. Differences between groups were assessed with the Student's t-test ($n = 6$ cells; *** $p < 0.001$, **** $p < 0.0001$).

The release kinetics of NPY from Syt granules was determined using cells co-transfected with NPY pHl and either Syt-1 or Syt-7 mCherry. Our prediction based on previous studies was that NPY would be more slowly released from granules harboring Syt-7 than those harboring Syt-1. We also sought to test the idea that the rate of release would depend less on the strength of depolarization than it would on the synaptotagmin isoform driving fusion.

Cells were depolarized with either a strong (56 mM KCl) or mild (25 mM KCl) stimulus and imaged using TIRF (Figure 4.8). We first looked at the decay times for NPY pHl fluorescence following fusion at ROIs without obvious Syt mCherry overlap. Ostensibly, these granules are associated with an unknown, endogenous isoform. The decay reflects the time taken for NPY pHl fluorescence to decrease back to baseline after granule fusion. We plotted these values as a cumulative frequency curve for each depolarizing KCl solution (Figure 4.8 A). Events were only included if their fluorescence decayed back to its initial intensity within the imaging period (roughly 30 s). NPY fluorescence decayed at a faster rate with stronger depolarization (56 mM KCl) in comparison to milder depolarization (25 mM KCl). Note the leftward shift in the cumulative frequency distributions as stimulation intensity increases from 25 to 56 mM KCl.

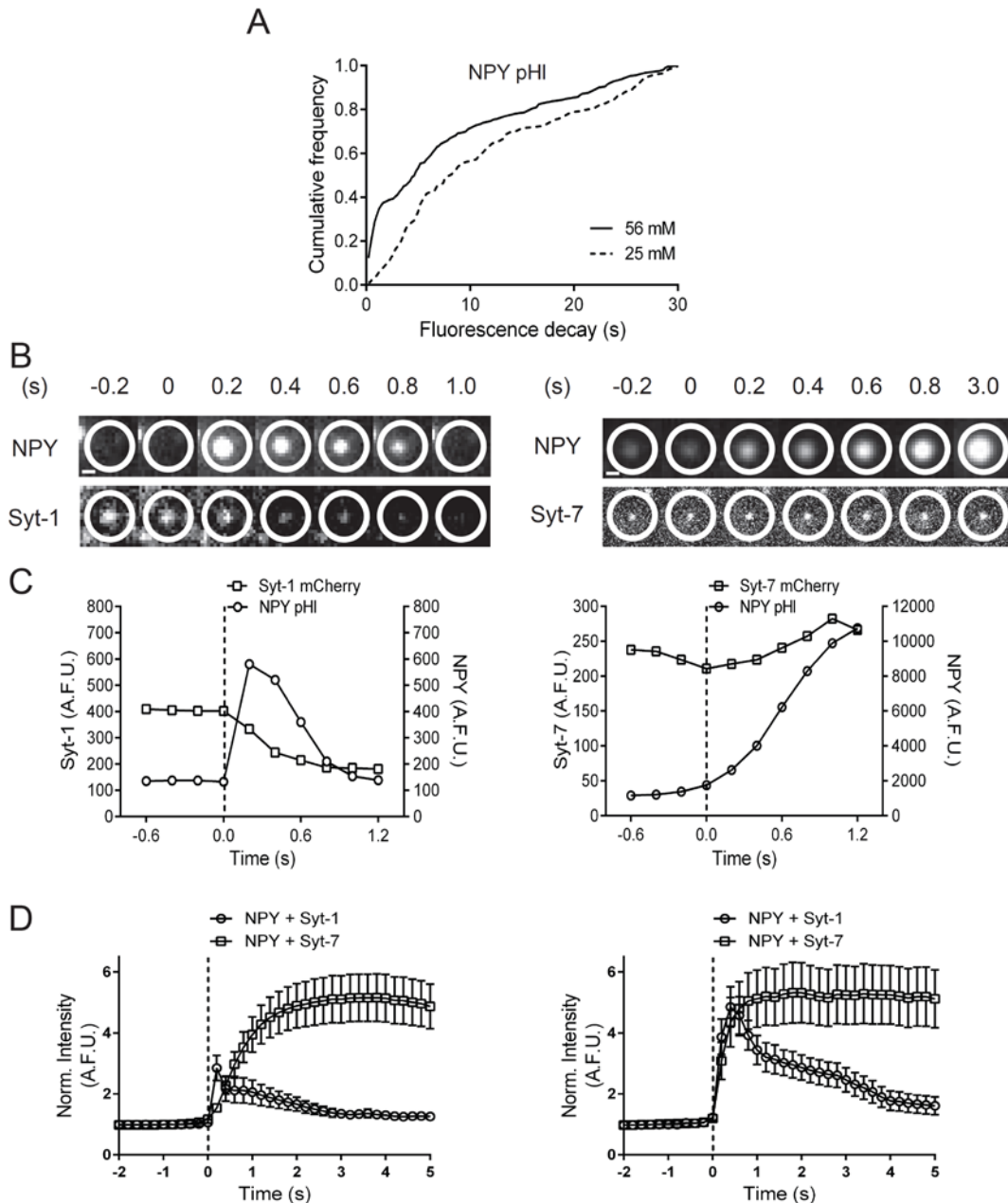


Figure 4.8. NPY pHI release kinetics from granules overexpressing Syt-1 or Syt-7 mCherry.

NPY pHI is released with faster kinetics from Syt-1 vs. Syt-7 granules. (A) The fluorescence decay time (i.e. release rates) for individual fusing NPY granules was calculated under different stimulation conditions as indicated. Release rates are significantly different between groups (Mann-Whitney non-parametric test, **** $p < 0.0001$). Number of NPY fusion events: 56 mM KCl ($n = 211$; 34 cells) and 25 mM ($n = 204$; 39 cells). (B, C) Representative fusion events for Syt mCherry granules co-packaged with NPY pHI. NPY pHI fluorescence intensity

increases (indicating fusion) at time 0.2 s. Left panel: Syt-1 and NPY quickly disperse following fusion (indicated by the dotted line). Note the loss of fluorescence within the circled region. Right panel: Syt-7 remains punctate after fusion for a longer period of time. NPY is released more slowly from these granules. Scale bar, 320 nm. (D) On average, NPY is more rapidly released from fusing Syt-1 vs. Syt-7 granules when stimulated with 56 mM KCl (left panel) or 25 mM KCl (right panel). After 1 s, averages \pm SD are significantly different (**** $p < 0.0001$) as assessed by the Student's t-test. Raw counts for fusion events and cells - 56 mM KCl: Syt-1 (n = 40; 14 cells), Syt-7 (n = 24; 20 cells); 25 mM KCl: Syt-1 (n = 39; 18 cells), Syt-7 (n = 21; 21 cells).

We next sought to address a possible reason for the shift in NPY release rates. Our previous data had shown that Syt-7 is preferentially activated with mild stimulation (25 mM KCl) and Syt-1 with strong stimulation (56 mM KCl) (Rao et al. 2014). We had also found that when Syt-1 granules fuse, their fusion pores dilate rapidly resulting in collapse or near collapse of the granule membrane into the plasma membrane. Conversely, when Syt-7 granules fuse, their pores tend to remain constricted. Based on this, we predicted that NPY would be released more slowly under milder depolarization, because fusion is largely controlled by Syt-7. Indeed, NPY pHl intensity decayed more slowly (or did not decay) following fusion of Syt-7 granules (Figure 4.8, B-D). The long decay time for NPY pHl fluorescence is consistent with its slow release through a narrow fusion pore. Conversely, NPY pHl intensity decayed rapidly following fusion of Syt-1 granules (Figure 4.8, B-D), which are preferentially activated at 56 mM KCl (Rao et al., 2014). Representative release events from Syt-1 and Syt-7 granules are shown in Figure 4.8, B and C. These data also show that irrespective of the strength of depolarization, NPY is released rapidly from Syt-1 fusion pores and slowly from Syt-7 fusion pores. This suggests that release rates are influenced as much, if

not more, by the isoform driving fusion as they are by the strength of depolarization.

The post-fusion membrane distribution of synaptotagmin isoforms is distinct

Based on the above results we wanted to visualize how the Syt proteins are arranged on the plasma membrane following fusion. We postulated that the persistence of Syt-7 and the slow release of NPY following fusion could be due to clustering or aggregation of the Syt-7 protein at the fusion pore. On the contrary, the rapid loss of Syt-1 and NPY fluorescence following fusion may indicate rapidly diffusion of Syt-1 from the site of fusion. Previous studies in our lab have supported this idea, but here we wanted to investigate this with the more robust super-resolution approach of Stochastic Optical Reconstruction Microscopy (STORM). For this, cells transfected with either Syt-1 or Syt-7 pHl were stimulated with 56 mM KCl for a period of 20 s prior to fixation. These cells were then labeled with antibodies against the pHluorin probe. Control cells were not stimulated prior to labeling in order to compare pre- and post-stimulation distribution of Syt on the membrane and determine the specificity of antibody binding. Captured single molecule images were processed using a Density Based Spatial Clustering Analysis with Noise (DBSCAN) algorithm (see methods). Control cells revealed that there is negligible Syt distribution on the membrane prior to stimulation (Figure S4.6 A). On the other hand, stimulated cells showed clustering, with Syt-7 forming substantially larger clusters in comparison to Syt-1 (Figure 4.9). Syt-1 distribution was diffuse as indicated by

the relatively smaller size of the identified clusters. Figure 4.9 B and C show the cluster analysis performed in two different ways.

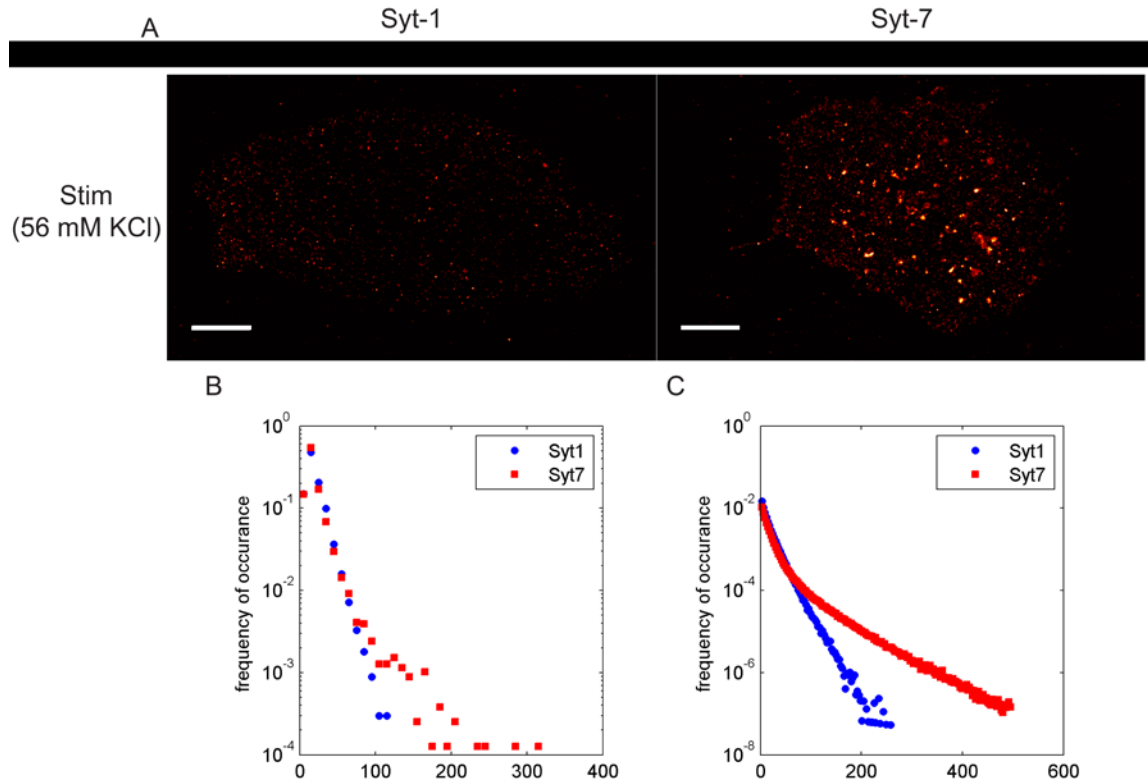


Figure 4.9. Super-resolution imaging of chromaffin cells transfected with Syt isoforms to determine membrane distribution following depolarization.

Transfected cells were stained with antibodies following depolarization for 20 s with 56 mM KCl. The images obtained were first run through a code using a DBSCAN algorithm to figure out which points are associated with clustered 'objects'. (A) Representative Syt-1 and Syt-7 images showing their distribution on the plasma membrane following depolarization. Syt-7 forms larger clusters on the membrane following depolarization in comparison to Syt-1. Scale bar, 5 μ m. (B) Plot representing cluster frequencies in relation to their size for all super-resolution images. Clusters of Syt-7 have larger radii in comparison to those of Syt-1. (C) Plot quantifying the distances between an object center and the points comprising that object. The center of each object was determined by taking the mean position of the composite points. This histogram emphasizes the larger size of Syt-7 clusters in comparison with Syt-1.

First, we plotted a frequency distribution for each isoform depicting the radii of all objects across images (Figure 4.9 B). As might be expected, both

isoforms show an abundance of objects with smaller radii, however only Syt-7 cells display larger clusters (radii $> \sim 150$ nm). Second, we plotted the distances between an object center and all points comprising that object (Figure 4.9 C). This analysis better emphasizes the presence of larger objects, as these clusters are comprised of more points than smaller ones. From this plot, it is clear that many Syt-7 clusters have larger dimensions relative to Syt-1. The clustered surface distribution of Syt-7 could reflect protein aggregating at a partially open fusion pore and thereby restricting the pore from collapsing into the plasma membrane.

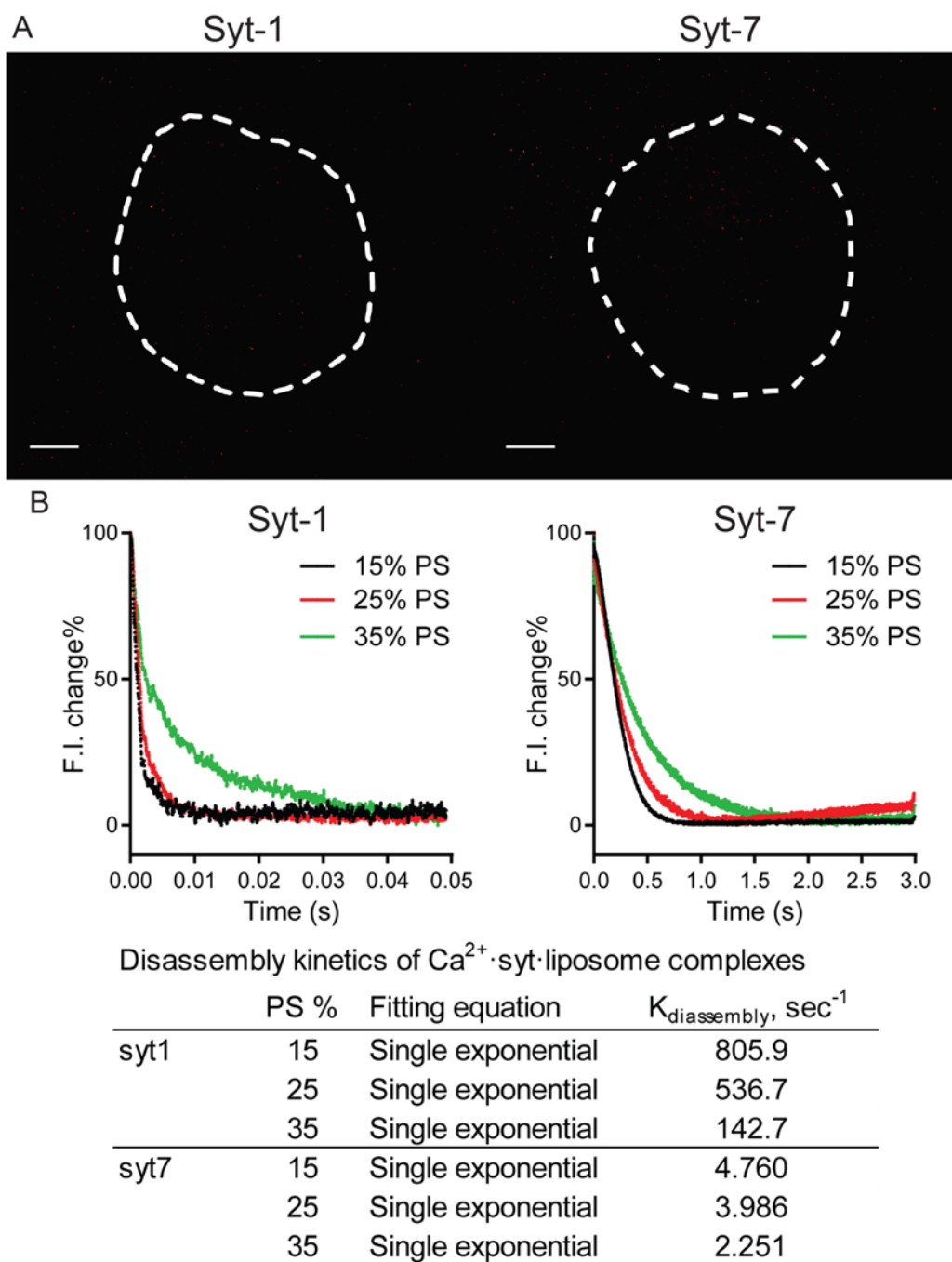


Figure S4.6. Distribution of Syt isoforms on the plasma membrane and their *in vitro* disassembly kinetics from liposomes.

(A) Representative super-resolution images showing either Syt-1 or Syt-7 distribution on the plasma membrane in unstimulated (control) cells (see Figure 4.9). In the absence of stimulation, little surface Syt fluorescence is visible. Dotted white line demarcates the cell boundary. Scale bar, 5 μm . (B) Stopped-

flow traces for Ca^{2+} -Syt-liposome disassembly reactions were monitored using FRET. Dissociation of Syt-1 or Syt-7 cytoplasmic domains (C2AB) from phosphatidylserine (PS) containing liposomes was measured following Ca^{2+} chelation with EGTA (See Hui et al., 2005). Syt-1 shows substantially faster disassembly kinetics in comparison with Syt-7 (see table). Note the different time scales on the x-axis for each of the isoforms.

DISCUSSION

In this study, we extensively characterized numerous differences in chromaffin granules using synaptotagmin as a molecular marker for heterogeneity. Specifically, we found that: (1) Syt-1 and -7 are rarely sorted to the same granule in chromaffin cells; (2) granules expressing Syt-7 tend to be located closer to the plasma membrane in steady state; (3) Syt-7 granules require only mild membrane depolarization to initiate fusion and fuse earlier following application of a stimulus; (4) Syt-1 granules travel a greater distance to their eventual fusion sites and newcomers comprise a larger proportion of all fusion events for Syt-1 versus Syt-7; (5) Syt-1 granules require less time to transition into a fusion-competent state; (6) at lower Ca^{2+} concentrations, Syt-7 granules exhibit greater fusion efficiency than Syt-1, and regardless of concentration, Syt-7 fusion occurs with less delay following Ca^{2+} application; (7) NPY is released more slowly from granules harboring Syt-7 than those with Syt-1; (8) Syt-7 persists in clusters at the site of fusion while Syt-1 diffuses rapidly.

Steady-state distribution of synaptotagmin isoforms

Our results indicating that Syt-1 and Syt-7 are sorted to different granule populations in chromaffin cells is in line with our earlier findings regarding these two isoforms (Rao et al., 2014). The current study, which uses a variety of

software-based co-localization analyses, has identified even lower co-localization values than our previous work (Figure S4.1). We used an object-based approach to minimize the confounding effects of variable background associated with pixel-by-pixel analysis methods, while providing a more informative way of representing granule distribution rather than simply fluorescence distribution *per se* (Dunn *et al.*, 2011). Our results do appear to differ from what has been observed in PC12 cells, an immortalized cell line originally derived from chromaffin cells, in which Syt-1 and Syt-7 display approximately 45% co-localization on granules (Greene and Tischler, 1976; Wang *et al.*, 2005; Zhang *et al.*, 2011). These differences may be reconciled by the fact that PC12 cells are no longer under the selection pressures imposed by maintenance of homeostasis within an organism. In addition to Syt granules being differentially distributed with respect to one another, they also differ with respect to their average distance from the plasma membrane (Figure 4.1). Syt-7 granules reside closer to the plasma membrane than Syt-1 granules, whereas granules with both isoforms are highly variable in their distribution.

Dynamic and functional behaviors of synaptotagmin granules leading to fusion

The differences in sorting of Syt isoforms, along with their previously established biochemical properties, suggested a further distinction in the functional response of each granule population. Here, we validated our previous findings using elevated K^+ to elicit exocytosis and built upon this by, 1) directly manipulating intracellular Ca^{2+} levels in live cells, and 2) determining the time

course for Syt isoform activation. Irrespective of the trigger for exocytosis (elevated K^+ or Ca^{2+} application following permeabilization), lower Ca^{2+} concentrations favor fusion of docked Syt-7 granules (Figure 4.2 A and 4.6 D). These differences become negligible at the highest Ca^{2+} concentrations. Furthermore, independent of the strength of this trigger, Syt-7 granules fuse earlier as compared to Syt-1 (Figure 4.3 and 4.6 C). Importantly, our findings are also in accordance with *in vitro* binding assays for Syt-1 and Syt-7, which identify a roughly 10-fold lower Ca^{2+} binding affinity for Syt-1 (Hui *et al.*, 2005).

One limitation of our methodology is the use of a perfusion system to apply solutions for both KCl and permeabilization experiments. Diffusion of solution from its source to the cell membrane has an inherent delay that precludes us from making direct kinetic comparisons between the rates of fusion in our experiments and those measured with electrophysiology (Augustine and Neher, 1992; Chow *et al.*, 1994; Albillos *et al.*, 1997; Fulop *et al.*, 2005; Fulop and Smith, 2007). Also, the time course for Ca^{2+} entry into permeabilized cells differs from other techniques. For example, Ca^{2+} -uncaging results in an immediate, uniform release of Ca^{2+} , while patch clamping directly activates voltage-gated channels (Heinemann *et al.*, 1994; Albillos *et al.*, 1997). Over time, permeabilization may also lead to dialysis of the cell contents, including small molecules like ATP, low molecular weight peptides, and various ionic species (Holz and Senter, 1985; Bittner and Holz, 1992). Future studies that utilize more physiological methods for stimulating fusion such as pulsed acetylcholine (the

endogenous secretagogue) or action potential equivalent wave forms – in conjunction with TIRF imaging – may be necessary to reconcile the differences. Nonetheless, these results reveal that the Ca^{2+} requirements for chromaffin cell exocytosis depend on the activation of specific Syt isoforms.

Not all granules that undergo fusion during the imaging period are docked prior to stimulation. Therefore, we sought to identify the contribution of newcomer events to each Syt granule population. Our study indicated that a larger proportion of fusing Syt-1 granules are newcomers in comparison to Syt-7 (Figure 4.2 B). In order for a newcomer granule to undergo fusion, it must first be docked to the plasma membrane. Docking has been well characterized in chromaffin cells and is believed to be mediated in part by the activity of Munc18-1. For example, using Munc18-1 knockout mice, Neher and colleagues showed that lack of Munc18-1 drastically reduced the proportion of granules docked at the plasma membrane (Voets *et al.*, 2001d). A more recent study found that overexpression of syntaxin-3 (Syn-3) in INS-1 cells resulted in increased recruitment of newcomer granules during stimulation (Zhu *et al.*, 2013). Therefore a possible explanation for our findings is that Syt-1 granules have a higher affinity for Munc18-1 and/or Syn-3 which mediate rapid recruitment of granules from within the cell.

In addition to docking, priming is also a prerequisite for making granules fusion-competent. Here we evaluated the fate of docked granules that did not fuse during an initial stimulus. Subsequent stimulation following a shorter

recovery period favored the transition of Syt-1 granules to a release-competent state, whereas increasing the recovery period allowed both Syt populations to become equally fusion-competent. This suggests that Syt-1 granules require less time to transition from a docked state to being primed and fully fusion competent. Differences in the interaction of Syt isoforms with other molecules, such as SNAP-25, Munc18-1/2, complexin, PIP2, etc., could influence this transition rate. For example, a study in PC12 cells showed that disrupting the binding of SNAP-25 and Syt-1 significantly decreased the rate of fusion (Zhang *et al.*, 2002), while other studies in chromaffin cells showed that overexpression of SNAP-25 or Munc18-2 reduced the fraction of docked non-fusing granules (Hugo *et al.*, 2013). Biochemical experiments using *in vitro* assays showed that complexin and synaptotagmin 1 stimulate rapid, synchronous fusion of docked granules in response to physiological Ca^{2+} concentrations (Malsam *et al.*, 2012). In another study, PIP2 increased the speed of response of Syt-1 and promoted plasma membrane-penetration. (Bai *et al.*, 2004a). Thus, if Syt-1 granules have a higher affinity for some or all of these proteins, it could explain the rapid transition from docking to fusion. However, these studies have only focused on Syt-1, and therefore future studies are needed to understand if Syt-7 differs in its interaction with these molecules.

Lateral movement of granules in the evanescent field prior to fusion has been previously reported (Allersma *et al.*, 2006). This led us to question if there were differences in the displacement of Syt granules from their initial position to

their eventual fusion site on the plasma membrane (Allersma *et al.*, 2006; Degtyar *et al.*, 2007). Our present findings indicate that granules destined to fuse with the plasma membrane move significantly more than their non-fusing counterparts (Figure 4.4). Of the fusing granules, those bearing Syt-1 display greater motion in the final 100 – 200 msec prior to fusion. The increased mobility may arise from differences in how granules interact with the proteins (e.g. t-SNARE complexes) and lipids (e.g. PIP2) associated with candidate fusion sites (Matos *et al.*, 2000; Holz and Axelrod, 2002; Allersma *et al.*, 2006; Lynch *et al.*, 2008; Park *et al.*, 2015). Moreover, Syt-1 granules tend to be further displaced from their eventual fusion site than Syt-7 granules (Figure 4.4 D). This displacement might reflect the movement of granules from the Ca²⁺ entry sights associated with voltage-gated channels to sites on the membrane where fusion occurs.

Numerous *in vitro* studies have shown that Syt-1 can directly bind to P/Q-, N-, and L-type Ca²⁺ channels found in chromaffin cells (Charvin *et al.*, 1997; Sheng *et al.*, 1997; Wiser *et al.*, 1999; Rosa *et al.*, 2011; Mahapatra *et al.*, 2012). Although very little is known about the relation of Syt-7 to these channels, one could speculate that Syt-1 granules reside closer to Ca²⁺ channels in order to compensate for their lower Ca²⁺ binding affinities (Hui *et al.*, 2005; Bhalla *et al.*, 2008). Conversely, Syt-7 granules may reside closer to their eventual fusion sites and still experience sufficient Ca²⁺ to initiate exocytosis. In bovine chromaffin cells, P/Q-type channels carry the largest proportion of total Ca²⁺ current (50%),

while N- and L-type carry 30% and 20% current respectively (Garcia *et al.*, 2006). We wanted to determine if differences in channel subtype dependency underlie the observed heterogeneity in Syt granule populations. Although we observed a general reduction in fusion upon application of blockers, there were noticeable differences in the extent of inhibition between Syt isoforms when blocking specific channels. Blocking L-type channels significantly reduced Syt-1 fusion while blocking N and P/Q-type channels was more effective in reducing Syt-7 fusion. In accordance with this, and our findings regarding lateral mobility, Lara *et al.*, concluded that P/Q-type channels were located closer to sites of exocytosis than L-type channels using K^+ evoked stimulation (Lara *et al.*, 1998). Other studies have found conflicting results, and this may be in part due to the differences in cell preparation and stimulation paradigms (Jimenez *et al.*, 1993; Artalejo *et al.*, 1994). For example, Neher and colleagues did not find any specific coupling between channel subtypes and exocytosis in general using depolarizing electrical pulses (Lukyanetz and Neher, 1999). Therefore, the relationship between specific Syt granules and channel subtypes should be explored in further detail to better address this question.

Differences in post-fusion behavior of Syt isoforms

We also find that synaptotagmin isoforms expressed in chromaffin cells regulate the release kinetics of granular cargos. Specifically, we observed that NPY is more rapidly released from Syt-1 granules than it is from Syt-7 granules (Figure 4.8 D). Our results lead us to conclude that the influence of the Syt

isoform is greater than that of the stimulus strength alone. When looking at NPY release from granules associated with an unknown endogenous isoform, the rate of NPY release is clearly affected by the strength of stimulus (Figure 4.8 A). However, when comparing NPY release from only Syt-7 granules, the rate is slower even with the stronger stimulus (Figure 4.8 D).

Past studies have noted that NPY is generally released quickly from chromaffin granules when compared to other cargos such as tissue plasminogen activator (tPA) (Taraska *et al.*, 2003; Perrais *et al.*, 2004; Weiss *et al.*, 2014). One way that cargo discharge rates are likely regulated in secretory cells is by controlling fusion pore expansion (Albillos *et al.*, 1997). For example, Weiss *et al.* have proposed that tPA may be able to slow its own release by binding to, and stabilizing, the membrane of the pore (Weiss *et al.*, 2014). Other studies have implicated fusion pore modulation through: 1) local recruitment of proteins from within the cytosol, 2) proteins or lipids on the plasma membrane, 3) cargo packaged within the granule or 4) proteins present on the granule membrane (Wang *et al.*, 2001; Graham *et al.*, 2002; Fulop *et al.*, 2008; Anantharam *et al.*, 2011; Zhang and Castle, 2011; Zhang *et al.*, 2011; Bao *et al.*, 2016). Our previous work had revealed divergent post-fusion outcomes for synaptotagmin granules on the plasma membrane (Rao *et al.*, 2014). In the current study, we explored this in more detail using super-resolution microscopy. Our finding that Syt-7 remains clustered on the plasma membrane following fusion, lends support to the idea that synaptotagmin acts from a position on the membrane to directly

influence the rate of pore expansion. For example, the higher membrane binding affinity of the Syt-7 C2 domains following Ca^{2+} binding may result in an extended association of the protein with the plasma membrane to stabilize the fusion pore. However, in the case of Syt-1, the rapid expansion of the fusion pore may be attributable to its higher membrane dissociation rates. As a consequence, Syt-1 does not remain clustered at the fusion site and instead rapidly diffuses. This is in accordance with our *in vitro* studies demonstrating that Syt-7 has a much lower lipid dissociation rate than Syt-1 (Figure S4.5 B). This prolonged interaction between Syt-7 and anionic phospholipids has been demonstrated in various biochemical studies (Sugita *et al.*, 2002; Tucker *et al.*, 2003; Bhalla *et al.*, 2005; Hui *et al.*, 2005). Our results do not, however, rule out the possibility of other factors controlling pore expansion and thereby cargo release rates. Therefore, it might be interesting to compare the release kinetics of other cargoes from Syt-1 and Syt-7 granules.

Overall, our findings may be relevant to the vertebrate stress response, where the release rate of hormones and neuropeptides is tightly coupled to the strength of sympathetic nervous system activation (Fulop *et al.*, 2005; Fulop and Smith, 2007). Cells may regulate this is by producing a heterogeneous population of secretory granules that respond differentially to stimuli. Our studies have identified a major molecular marker underlying this heterogeneity in chromaffin cells. Not only do synaptotagmin granules differ in their steady-state distribution within cells, but the isoform itself confers granules with distinct Ca^{2+} -

dependent pre- and post-fusion behaviors. This concept of heterogeneity may be applicable across other cell types including neurons and other neuroendocrine cells in which multiple synaptotagmin isoforms have been identified.

CHAPTER 5 - SUMMARY AND SIGNIFICANCE

Adrenomedullary chromaffin cells play a vital role in human physiology by synthesizing, storing, and secreting a complex mixture of neuropeptides and catecholamines into the systemic circulation (Fischer-Colbrie *et al.*, 1986; Egger *et al.*, 1993; Weiss *et al.*, 1996). At rest, chromaffin cells receive low-frequency sympathetic input from innervating splanchnic nerve fibers and release their contents at a basal rate (de Diego *et al.*, 2008a; de Diego *et al.*, 2008b). Stronger activation causes a surge in chromaffin cell secretion and is most commonly associated with the vertebrate stress – “fight or flight” – response. The ensuing physiological changes, including elevations in heart rate and blood glucose, bronchial dilation, and redistribution of blood flow help to maximize an organism’s chances for escape or survival. In addition to its homeostatic and protective roles, exaggerated release of adrenal contents can be quite damaging to an organism. Long-term elevation in blood pressure to ensure adequate blood flow to the brain during stress has the potential to cause heart or kidney failure (Goldstein, 2010). Similarly, chronically elevated catecholamine secretion can contribute to the progression of cardiac hypertrophy and fibrosis (Braunwald and Bristow, 2000) and increases the incidence of arrhythmias and sudden cardiac death (Kaye *et al.*, 1995). Sympathetic overstimulation of the heart may induce accelerated cell damage during myocardial ischemia and malignant arrhythmias. Higher concentrations of catecholamines observed within the myocardium, in combination with enhanced myocyte sensitivity to adrenergic stimuli together

contribute to this overstimulation of the heart (Schomig, 1990). In early myocardial infarction, plasma noradrenaline and adrenaline concentrations are enhanced, reflecting increased activity of the whole sympathetic nervous system, rather than local activity in the heart (Goldstein, 2010).

The profound physiological effects of adrenomedullary hormones in the periphery provide compelling reasons to define how stimulation of chromaffin cells, both at rest and stress, is coupled to release. Our contribution here is to elucidate the roles for the critical Ca^{2+} -sensors for exocytosis – Syt-1 and Syt-7. This contribution is significant, and can provide a molecular framework for understanding how membrane depolarization, Ca^{2+} elevation, granule fusion, pore expansion, and content release are all biochemically and functionally linked to the heterogeneity found in the population of secretory granules. If secretion of adrenomedullary hormones could be precisely controlled, they might have tremendous therapeutic value. For example, since chromaffin cells secrete large amounts of the opioid enkephalin (Enk), they have been widely used in allografts to treat chronic pain (Jain, 2008; Ambriz-Tututi *et al.*, 2012; Chen *et al.*, 2013a; Qu *et al.*, 2013). The studies in this thesis suggest stimulation paradigms that more effectively and selectively trigger the release of these peptides known to have strong peripheral effects. We have made an attempt to fill the gap in our current knowledge for the precise mechanisms that control fusion pore dilation and granule content release in chromaffin cells. Our results have led us to novel

mechanisms which can be further generalized and applied to other cell types including neurons and neuroendocrine cells.

REFERENCES

- Ahnert-Hilger, G., Wegenhorst, U., Stecher, B., Spicher, K., Rosenthal, W., and Gratzl, M. (1992). Exocytosis from permeabilized bovine adrenal chromaffin cells is differently modulated by guanosine 5'-[gamma-thio]triphosphate and guanosine 5'-[beta gamma-imido]triphosphate. Evidence for the involvement of various guanine nucleotide-binding proteins. *Biochemical Journal* 284, 321-326.
- Akerboom, J., Chen, T.W., Wardill, T.J., Tian, L., Marvin, J.S., Mutlu, S., Calderon, N.C., Esposti, F., Borghuis, B.G., Sun, X.R., Gordus, A., Orger, M.B., Portugues, R., Engert, F., Macklin, J.J., Filosa, A., Aggarwal, A., Kerr, R.A., Takagi, R., Kracun, S., Shigetomi, E., Khakh, B.S., Baier, H., Lagnado, L., Wang, S.S., Bargmann, C.I., Kimmel, B.E., Jayaraman, V., Svoboda, K., Kim, D.S., Schreiter, E.R., and Looger, L.L. (2012). Optimization of a GCaMP calcium indicator for neural activity imaging. *J Neurosci* 32, 13819-13840.
- Al-Lami, F. (1969). Light and electron microscopy of the adrenal medulla of macaca mulata monkey. *The Anatomical Record* 164, 317-332.
- al-Lami, F., and Carmichael, S.W. (1991). Microscopic anatomy of the baboon (*Papio hamadryas*) adrenal medulla. *J Anat* 178, 213-221.
- Albillos, A., Dernick, G., Horstmann, H., Almers, W., Alvarez de Toledo, G., and Lindau, M. (1997). The exocytotic event in chromaffin cells revealed by patch amperometry. *Nature* 389(6650), 509-512.

- Albright, T.D., Jessell, T.M., Kandel, E.R., and Posner, M.I. (2000). Neural Science: A Century of Progress and the Mysteries that Remain. *Neuron* 25, S1-S55.
- Ales, E., Tabares, L., Poyato, J.M., Valero, V., Lindau, M., and Alvarez, d. (1999). High calcium concentrations shift the mode of exocytosis to the kiss-and-run mechanism.[comment]. *Nature Cell Biology*. 1, 40-44.
- Allersma, M.W., Bittner, M.A., Axelrod, D., and Holz, R.W. (2006). Motion Matters: Secretory Granule Motion Adjacent to the Plasma Membrane and Exocytosis. *Molecular Biology of the Cell* 17, 2424-2438.
- Allersma, M.W., Wang, L., Axelrod, D., and Holz, R.W. (2004). Visualization of Regulated Exocytosis with a Granule-Membrane Probe using Total Internal Reflection Microscopy. *Molecular Biology of the Cell* 15, 4658-4668.
- Ambriz-Tututi, M., Monjaraz-Fuentes, F., and Drucker-Colin, R. (2012). Chromaffin cell transplants: from the lab to the clinic. *Life Sci* 91, 1243-1251.
- An, S., and Zenisek, D. (2004). Regulation of exocytosis in neurons and neuroendocrine cells. *Current opinion in neurobiology* 14, 522-530.
- Anantharam, A., Bittner, M.A., Aikman, R.L., Stuenkel, E.L., Schmid, S.L., Axelrod, D., and Holz, R.W. (2011). A new role for the dynamin GTPase in the regulation of fusion pore expansion. *Mol Biol Cell* 22, 1907-1918.

- Anantharam, A., Onoa, B., Edwards, R.H., Holz, R.W., and Axelrod, D. (2010). Localized topological changes of the plasma membrane upon exocytosis visualized by polarized TIRFM. *J Cell Biol* 188, 415-428.
- Andrews, N.W., and Chakrabarti, S. (2005). There's more to life than neurotransmission: the regulation of exocytosis by synaptotagmin VII. *Trends Cell Biol* 15, 626-631.
- Arac, D., Chen, X., Khant, H.A., Ubach, J., Ludtke, S.J., Kikkawa, M., Johnson, A.E., Chiu, W., Sudhof, T.C., and Rizo, J. (2006). Close membrane-membrane proximity induced by Ca²⁺-dependent multivalent binding of synaptotagmin-1 to phospholipids. *Nat Struct Mol Biol* 13, 209-217.
- Artalejo, C.R., Adams, M.E., and Fox, A.P. (1994). Three types of Ca²⁺ channel trigger secretion with different efficacies in chromaffin cells. *Nature* 367, 72-76.
- Ashery, U., Varoqueaux, F., Voets, T., Betz, A., Thakur, P., Koch, H., Neher, E., Brose, N., and Rettig, J. (2000). Munc13-1 acts as a priming factor for large dense-core vesicles in bovine chromaffin cells. *EMBO J* 19, 3586-3596.
- Augustine, G.J., and Neher, E. (1992). Calcium requirements for secretion in bovine chromaffin cells. *J Physiol* 450, 247-271.
- Bai, J., Tucker, W.C., and Chapman, E.R. (2004a). PIP₂ increases the speed of response of synaptotagmin and steers its membrane-penetration activity

- toward the plasma membrane. *Nature Structural & Molecular Biology*. 11, 36-44.
- Bai, J., Wang, C.T., Richards, D.A., Jackson, M.B., and Chapman, E.R. (2004b). Fusion pore dynamics are regulated by synaptotagmin**t*-SNARE interactions. *Neuron* 41, 929-942.
- Banerjee, A., Barry, V.A., DasGupta, B.R., and Martin, T.F.J. (1996). N-Ethylmaleimide-sensitive factor acts at a prefusion ATP-dependent step in Ca²⁺-activated exocytosis. *Journal of Biological Chemistry* 271, 20223-20226.
- Bao, H., Goldschen-Ohm, M., Jeggle, P., Chanda, B., Edwardson, J.M., and Chapman, E.R. (2016). Exocytotic fusion pores are composed of both lipids and proteins. *Nature structural & molecular biology* 23, 67-73.
- Bennett, M.K., Calakos, N., and Scheller, R.H. (1992). Syntaxin: a synaptic protein implicated in docking of synaptic vesicles at presynaptic active zones. *Science* 257, 255-259.
- Berberian, K., Torres, A.J., Fang, Q., Kisler, K., and Lindau, M. (2009). F-actin and myosin II accelerate catecholamine release from chromaffin granules. *J Neurosci* 29, 863-870.
- Bhalla, A., Chicka, M.C., and Chapman, E.R. (2008). Analysis of the synaptotagmin family during reconstituted membrane fusion. Uncovering a class of inhibitory isoforms. *J Biol Chem* 283, 21799-21807.

- Bhalla, A., Tucker, W.C., and Chapman, E.R. (2005). Synaptotagmin isoforms couple distinct ranges of Ca^{2+} , Ba^{2+} , and Sr^{2+} concentration to SNARE-mediated membrane fusion. *Mol Biol Cell* 16, 4755-4764.
- Bittner, M.A., Aikman, R.L., and Holz, R.W. (2013). A nibbling mechanism for clathrin-mediated retrieval of secretory granule membrane after exocytosis. *J Biol Chem* 288, 9177-9188.
- Bittner, M.A., and Holz, R.W. (1992). Kinetic analysis of secretion from permeabilized adrenal chromaffin cells reveals distinct components. *Journal of Biological Chemistry* 267, 16219-16225.
- Bittner, M.A., Holz, R.W., and Neubig, R.R. (1986). Guanine nucleotide effects on catecholamine secretion from digitonin-permeabilized adrenal chromaffin cells. *Journal of Biological Chemistry* 261, 10182-10188.
- Borisovska, M., Zhao, Y., Tsytsyura, Y., Glyvuk, N., Takamori, S., Matti, U., Rettig, J., Südhof, T., and Bruns, D. (2005). v-SNAREs control exocytosis of vesicles from priming to fusion. *The EMBO journal* 24, 2114-2126.
- Braunwald, E., and Bristow, M.R. (2000). Congestive heart failure: fifty years of progress. *Circulation* 102, IV14-23.
- Breckenridge, L.J., and Almers, W. (1987). Final steps in exocytosis observed in a cell with giant secretory granules. *Proceedings of the National Academy of Sciences of the United States of America* 84, 1945-1949.
- Brose, N., Petrenko, A.G., Südhof, T.C., and Rizo, J. (1994). A calcium sensor on the synaptic vesicle surface. *Science* 256, 1021-1025.

- Brunger, A.T. (2005). Structure and function of SNARE and SNARE-interacting proteins. *Quarterly Reviews of Biophysics* 38, 1-47.
- Burgess, T.L., and Kelly, R.B. (1987). Constitutive and regulated secretion of proteins. *Annual Review of Cell Biology* 3, 243-294.
- Burgoyne, R.D., and Handel, S.E. (1994). Activation of exocytosis by GTP analogues in adrenal chromaffin cells revealed by patch-clamp capacitance measurement. *FEBS Letters* 344, 139-142.
- Burgoyne, R.D., and Morgan, A. (2003). Secretory granule exocytosis. *Physiol Rev* 83, 581-632.
- Calakos, N., and Scheller, R.H. (1996). Synaptic vesicle biogenesis, docking, and fusion: a molecular description. *Physiological Reviews* 76, 1-29.
- Campbell, T.N., and Choy, F.Y. (2001). The effect of pH on green fluorescent protein: a brief review. *Mol. Biol. Today* 2, 1-4.
- Carmichael, S.W., Spagnoli, D.B., Frederickson, R.G., Krause, W.J., and Culberson, J.L. (1987). Opossum adrenal medulla: I. Postnatal development and normal anatomy. *Am J Anat* 179, 211-219.
- Carmichael, S.W., and Winkler, H. (1985). The Adrenal Chromaffin Cell. *Sci Am* 253, 40-+.
- Ceccarelli, B., Hurlbut, P., and Mauro, A. (1973). Turnover of transmitter and synaptic vesicles at the frog neuromuscular junction. *Journal of Cell Biology* 57, 499-524.

- Chakrabarti, S., Kobayashi, K.S., Flavell, R.A., Marks, C.B., Miyake, K., Liston, D.R., Fowler, K.T., Gorelick, F.S., and Andrews, N.W. (2003). Impaired membrane resealing and autoimmune myositis in synaptotagmin VII-deficient mice. *J Cell Biol* 162, 543-549.
- Chan, S.A., Doreian, B., and Smith, C. (2010). Dynamin and myosin regulate differential exocytosis from mouse adrenal chromaffin cells. *Cell Mol Neurobiol* 30, 1351-1357.
- Chapman, E.R. (2002). Synaptotagmin: a Ca^{2+} sensor that triggers exocytosis? *Nat Rev Mol Cell Biol* 3, 498-508.
- Chapman, E.R., An, S., Edwardson, J.M., and Jahn, R. (1996). A novel function for the second C2 domain of synaptotagmin. Ca^{2+} -triggered dimerization. *J Biol Chem* 271, 5844-5849.
- Chapman, E.R., Hanson, P.I., An, S., and Jahn, R. (1995). Ca^{2+} regulates the interaction between synaptotagmin and syntaxin 1. *Journal of Biological Chemistry* 270, 23667-23671.
- Charvin, N., L'Evêque, C., Walker, D., Berton, F., Raymond, C., Kataoka, M., Shoji-Kasai, Y., Takahashi, M., De Waard, M., and Seagar, M.J. (1997). Direct interaction of the calcium sensor protein synaptotagmin I with a cytoplasmic domain of the $\alpha 1A$ subunit of the P/Q-type calcium channel. *The EMBO Journal* 16, 4591-4596.

- Chen, L., Huang, H., Sharma, H.S., Zuo, H., and Sanberg, P.R. (2013a). Cell transplantation as a pain therapy targets both analgesia and neural repair. *Cell Transplant* 22 *Suppl 1*, S11-19.
- Chen, T.-W., Wardill, T.J., Sun, Y., Pulver, S.R., Renninger, S.L., Baohan, A., Schreiter, E.R., Kerr, R.A., Orger, M.B., Jayaraman, V., Looger, L.L., Svoboda, K., and Kim, D.S. (2013b). Ultrasensitive fluorescent proteins for imaging neuronal activity. *Nature* 499, 295-300.
- Chen, X.-K., Wang, L.-C., Zhou, Y., Cai, Q., Prakriya, M., Duan, K.-L., Sheng, Z.-H., Lingle, C., and Zhou, Z. (2005). Activation of GPCRs modulates quantal size in chromaffin cells through G $\beta\gamma$ and PKC. *Nature neuroscience* 8, 1160-1168.
- Chen, X., Tomchick, D.R., Kovrigin, E., Arac, D., Machius, M., Sudhof, T.C., and Rizo, J. (2002). Three-dimensional structure of the complexin/SNARE complex. *Neuron* 33, 397-409.
- Chen, Y.A., Scales, S.J., and Scheller, R.H. (2001). Sequential SNARE assembly underlies priming and triggering of exocytosis. *Neuron* 30, 161-170.
- Chow, R.H., Klingauf, J., Heinemann, C., Zucker, R.S., and Neher, E. (1996). Mechanisms determining the time course of secretion in neuroendocrine cells. *Neuron* 16(2), 369-376.
- Chow, R.H., Klingauf, J., and Neher, E. (1994). Time course of Ca²⁺ concentration triggering exocytosis in neuroendocrine cells. *Proceedings*

- of the National Academy of Sciences of the United States of America *91*, 12765-12769.
- Coupland, R.E. (1965a). Electron microscopic observations on the structure of the rat adrenal medulla: I. The ultrastructure and organization of chromaffin cells in the normal adrenal medulla. *Journal of Anatomy* *99*, 231-254.
- Coupland, R.E. (1965b). Electron microscopic observations on the structure of the rat adrenal medulla: II. Normal innervation. *Journal of Anatomy* *99*, 255-272.
- Coupland, R.E. (1989). The natural history of the chromaffin cell--twenty-five years on the beginning. *Arch Histol Cytol* *52 Suppl*, 331-341.
- Coupland, R.E., and Hopwood, D. (1966). The mechanism of the differential staining reaction for adrenaline-and noreadrenaline-storing granules in tissues fixed in glutaraldehyde. *Journal of Anatomy* *100*, 227-243.
- Damase-Michel, C., Tavernier, G., Giraud, P., Montastruc, J.-L., Montastruc, P., and Tran, M.-A. (1993). Effects of clonidine, dihydralazine and splanchnic nerve stimulation on the release of neuropeptide Y, MET-enkephalin and catecholamines from dog adrenal medulla. *Naunyn-Schmiedeberg's Archives of Pharmacology* *348*, 379-384.
- De Camilli, P., and Jahn, R. (1990). Pathways to regulated exocytosis in neurons. *Annu.Rev.Physiol.* *52*, 625-645.

- de Diego, A.M., Arnaiz-Cot, J.J., Hernandez-Guijo, J.M., Gandia, L., and Garcia, A.G. (2008a). Differential variations in Ca²⁺ entry, cytosolic Ca²⁺ and membrane capacitance upon steady or action potential depolarizing stimulation of bovine chromaffin cells. *Acta Physiol (Oxf)* 194, 97-109.
- de Diego, A.M., Gandia, L., and Garcia, A.G. (2008b). A physiological view of the central and peripheral mechanisms that regulate the release of catecholamines at the adrenal medulla. *Acta Physiol (Oxf)* 192, 287-301.
- Degtyar, V.E., Allersma, M.W., Axelrod, D., and Holz, R.W. (2007). Increased motion and travel, rather than stable docking, characterize the last moments before secretory granule fusion. *Proc Natl Acad Sci U S A* 104, 15929-15934.
- Díaz-Flores, L., Gutiérrez, R., Varela, H., Valladares, F., Alvarez-Argüelles, H., and Borges, R. (2008). Histogenesis and morphofunctional characteristics of chromaffin cells. *Acta Physiologica* 192, 145-163.
- Doreian, B.W., Fulop, T.G., Meklemburg, R.L., and Smith, C.B. (2009). Cortical F-actin, the exocytic mode, and neuropeptide release in mouse chromaffin cells is regulated by myristoylated alanine-rich C-kinase substrate and myosin II. *Mol Biol Cell* 20, 3142-3154.
- Doreian, B.W., Fulop, T.G., and Smith, C.B. (2008). Myosin II Activation and Actin Reorganization Regulate the Mode of Quantal Exocytosis in Mouse Adrenal Chromaffin Cells. *Journal of Neuroscience* 28, 4470-4478.

- Douglas, W.W. (1968). Stimulus-secretion coupling: the concept and clues from chromaffin and other cells. *Br J Pharmacol* 34, 451-474.
- Douglas, W.W., and Rubin, R.P. (1961). The role of calcium in the secretory response of the adrenal medulla to acetylcholine. *The Journal of Physiology* 159, 40-57.
- Duncan, R.R., Greaves, J., Wiegand, U.K., Matskevich, I., Bodammer, G., Apps, D.K., Shipston, M.J., and Chow, R.H. (2003). Functional and spatial segregation of secretory vesicle pools according to vesicle age. *Nature*. 422, 176-180.
- Dunn, K.W., Kamocka, M.M., and McDonald, J.H. (2011). A practical guide to evaluating colocalization in biological microscopy. *American Journal of Physiology - Cell Physiology* 300, C723-C742.
- Edwards, A.V., and Jones, C.T. (1993). Autonomic control of adrenal function. *Journal of Anatomy* 183, 291-307.
- Egger, C., Kirchmair, R., Hogue-Angeletti, R., Fischer-Colbrie, R., and Winkler, H. (1993). Different degrees of processing of secretogranin II in large dense core vesicles of bovine adrenal medulla and sympathetic axons correlate with their content of soluble PC1 and PC2. *Neuroscience Letters* 159, 199-201.
- Engisch, K.L., and Nowycky, M.C. (1998). Compensatory and excess retrieval: two types of endocytosis following single step depolarizations in bovine adrenal chromaffin cells. *Journal of Physiology* 506, 591-608.

- Ester, M., Kriegel, H.-P., Sander, J., and Xu, X. (1996). A density-based algorithm for discovering clusters in large spatial databases with noise. *Kdd*, 96, 226-231.
- Farquhar, M.G., and Palade, G.E. (1998). The Golgi apparatus: 100 years of progress and controversy. *Trends in Cell Biology* 8, 2-10.
- Fernandez-Chacon, R., Konigstorfer, A., Gerber, S.H., Garcia, J., Matos, M.F., Stevens, C.F., Brose, N., Rizo, J., Rosenmund, C., and Sudhof, T.C. (2001). Synaptotagmin I functions as a calcium regulator of release probability. *Nature* 410, 41-49.
- Fernandez, I., Arac, D., Ubach, J., Gerber, S.H., Shin, O., Gao, Y., Anderson, R.G., Sudhof, T.C., and Rizo, J. (2001). Three-dimensional structure of the synaptotagmin 1 C2B-domain: synaptotagmin 1 as a phospholipid binding machine. *Neuron* 32, 1057-1069.
- Fernandez, J.M., Neher, E., and Gomperts, B.D. (1984). Capacitance measurements reveal stepwise fusion events in degranulating mast cells. *Nature* 312, 453-455.
- Fischer-Colbrie, R., Diez-Guerra, J., Emson, P.C., and Winkler, H. (1986). Bovine chromaffin granules: immunological studies with antisera against neuropeptide Y, [Met]enkephalin and bombesin. *Neuroscience* 18, 167-174.
- Fujita, Y., Xu, A., Xie, L., Arunachalam, L., Chou, T.-C., Jiang, T., Chiew, S.-K., Kourtesis, J., Wang, L., Gaisano, H.Y., and Sugita, S. (2007). Ca²⁺-

- dependent Activator Protein for Secretion 1 Is Critical for Constitutive and Regulated Exocytosis but Not for Loading of Transmitters into Dense Core Vesicles. *Journal of Biological Chemistry* 282, 21392-21403.
- Fukuda, M. (2004). RNA interference-mediated silencing of synaptotagmin IX, but not synaptotagmin I, inhibits dense-core vesicle exocytosis in PC12 cells. *Biochem J* *In press*.
- Fukuda, M., Kanno, E., Satoh, M., Saegusa, C., and Yamamoto, A. (2004). Synaptotagmin VII Is Targeted to Dense-core Vesicles and Regulates Their Ca²⁺-dependent Exocytosis in PC12 Cells. *Journal of Biological Chemistry* 279, 52677-52684.
- Fukuda, M., Kowalchuk, J.A., Zhang, X., Martin, T.F., and Mikoshiba, K. (2002). Synaptotagmin IX regulates Ca²⁺-dependent secretion in PC12 cells. *J Biol Chem* 277, 4601-4604.
- Fulop, T., Doreian, B., and Smith, C. (2008). Dynamin I plays dual roles in the activity-dependent shift in exocytic mode in mouse adrenal chromaffin cells. *Archives of Biochemistry and Biophysics* 477, 146-154.
- Fulop, T., Radabaugh, S., and Smith, C. (2005). Activity-Dependent Differential Transmitter Release in Mouse Adrenal Chromaffin Cells. *Journal of Neuroscience* 25, 7324-7332.
- Fulop, T., and Smith, C. (2007). Matching native electrical stimulation by graded chemical stimulation in isolated mouse adrenal chromaffin cells. *J Neurosci Methods* 166, 195-202.

- Fung, M.M., Viveros, O.H., and O'Connor, D.T. (2008). Diseases of the adrenal medulla. *Acta physiologica (Oxford, England)* 192, 325-335.
- Garcia, A.G., Garcia-De-Diego, A.M., Gandia, L., Borges, R., and Garcia-Sancho, J. (2006). Calcium signaling and exocytosis in adrenal chromaffin cells. *Physiol Rev* 86, 1093-1131.
- Geppert, M., Goda, Y., Hammer, R.E., Li, C., Rosahl, T.W., Stevens, C.F., and Sudhof, T.C. (1994). Synaptotagmin I: a major Ca²⁺ sensor for transmitter release at a central synapse. *Cell* 79, 717-727.
- Giovannucci, D.R., and Stuenkel, E.L. (1997). Regulation of secretory granule recruitment and exocytosis at rat neurohypophysial nerve endings. *Journal of Physiology* 498, 735-751.
- Giraud, C.G., Garcia-Diaz, A., Eng, W.S., Chen, Y., Hendrickson, W.A., Melia, T.J., and Rothman, J.E. (2009). Alternative Zippering as an On-Off Switch for SNARE-Mediated Fusion. *Science* 323, 512-516.
- Giraud, C.G., Garcia-Diaz, A., Eng, W.S., Yamamoto, A., Melia, T.J., and Rothman, J.E. (2008). Distinct domains of complexins bind SNARE complexes and clamp fusion in vitro. *Journal of Biological Chemistry*, M803478200.
- Goldstein, D.S. (2010). Adrenal responses to stress. *Cell Mol Neurobiol* 30, 1433-1440.
- Gomperts, B. (1983). Involvement of guanine nucleotide-binding protein in the gating of Ca²⁺ by receptors.

- Gonzalez-Jamett, A.M., Baez-Matus, X., Hevia, M.A., Guerra, M.J., Olivares, M.J., Martinez, A.D., Neely, A., and Cardenas, A.M. (2010). The association of dynamin with synaptophysin regulates quantal size and duration of exocytotic events in chromaffin cells. *J Neurosci* 30, 10683-10691.
- Gonzalez-Jamett, A.M., Momboisse, F., Guerra, M.J., Ory, S., Baez-Matus, X., Barraza, N., Calco, V., Houy, S., Couve, E., Neely, A., Martinez, A.D., Gasman, S., and Cardenas, A.M. (2013). Dynamin-2 regulates fusion pore expansion and quantal release through a mechanism that involves actin dynamics in neuroendocrine chromaffin cells. *PLoS One* 8, e70638.
- Grabner, C.P., Price, S.D., Lysakowski, A., and Fox, A.P. (2005). Mouse Chromaffin Cells Have Two Populations of Dense Core Vesicles. *Journal of Neurophysiology* 94, 2093-2104.
- Graham, M.E., O'Callaghan, D.W., McMahon, H.T., and Burgoyne, R.D. (2002). Dynamin-dependent and dynamin-independent processes contribute to the regulation of single vesicle release kinetics and quantal size. *Proceedings of the National Academy of Sciences* 99, 7124-7129.
- Greene, L.A., and Tischler, A.S. (1976). Establishment of a noradrenergic clonal line of rat adrenal pheochromocytoma cells which respond to nerve growth factor. *Proceedings of the National Academy of Sciences of the United States of America* 73, 2424-2428.

- Grishanin, R.N., Klenchin, V.A., Loyet, K.M., Kowalchuk, J.A., Ann, K., and Martin, T.F. (2002). Membrane association domains in Ca²⁺-dependent activator protein for secretion mediate plasma membrane and dense-core vesicle binding required for Ca²⁺-dependent exocytosis. *Journal of Biological Chemistry* 277, 22025-22034.
- Grishanin, R.N., Kowalchuk, J.A., Klenchin, V.A., Ann, K., Earles, C.A., Chapman, E.R., Gerona, R.R.L., and Martin, T.F.J. (2004). CAPS Acts at a Prefusion Step in Dense-Core Vesicle Exocytosis as a PIP₂ Binding Protein. *Neuron* 43, 551-562.
- Gulyas-Kovacs, A., de Wit, H., Milosevic, I., Kochubey, O., Toonen, R., Klingauf, J., Verhage, M., and Sorensen, J.B. (2007). Munc18-1: Sequential Interactions with the Fusion Machinery Stimulate Vesicle Docking and Priming. *Journal of Neuroscience* 27, 8676-8686.
- Hafez, I., Kisler, K., Berberian, K., Dernick, G., Valero, V., Yong, M.G., Craighead, H.G., and Lindau, M. (2005). Electrochemical imaging of fusion pore openings by electrochemical detector arrays. *Proc Natl Acad Sci U S A* 102, 13879-13884.
- Hata, Y., Slaughter, C.A., and Sudhof, T.C. (1993). Synaptic vesicle fusion complex contains unc-18 homologue bound to syntaxin. *Nature* 366, 347-351.

- Hay, J.C., Fiset, P.L., Jenkins, G.H., Fukami, K., Takenawa, T., Anderson, R.A., and Martin, T.F.J. (1995). ATP-dependent inositol phosphorylation required for Ca^{2+} -activated secretion. *Nature* 374, 173-177.
- Hay, J.C., and Martin, T.F.J. (1993). Phosphatidylinositol transfer protein required for ATP-dependent priming of Ca^{2+} -activated secretion. *Nature* 366, 572-575.
- Haynes, C.L., Siff, L.N., and Wightman, R.M. (2007). Temperature-dependent differences between readily releasable and reserve pool vesicles in chromaffin cells. *Biochim Biophys Acta* 1773, 728-735.
- Heinemann, C., Chow, R.H., Neher, E., and Zucker, R.S. (1994). Kinetics of the secretory response in bovine chromaffin cells following flash photolysis of caged Ca^{2+} . *Biophysical Journal*. 67(6), 2546-2557.
- Hernández-Guijo, M.J., de Pascual, R., García, G.A., and Gandía, L. (1998). Separation of calcium channel current components in mouse chromaffin cells superfused with low- and high-barium solutions. *Pflügers Archiv* 436, 75-82.
- Hervonen, A. (1971). Development of catecholamine--storing cells in human fetal paraganglia and adrenal medulla. A histochemical and electron microscopical study. *Acta Physiol Scand Suppl* 368, 1-94.
- Heuser, J.E., and Reese, T.S. (1973). Evidence for recycling of synaptic vesicle membrane during transmitter release at the frog neuromuscular junction. *Journal of Cell Biology* 57, 315-344.

- Holz, R.W., and Axelrod, D.A.N.I. (2002). Localization of Phosphatidylinositol 4,5-P2 Important in Exocytosis and a Quantitative Analysis of Chromaffin Granule Motion Adjacent to the Plasma Membrane. *Annals of the New York Academy of Sciences* 971, 232-243.
- Holz, R.W., Bittner, M.A., Peppers, S.C., Senter, R.A., and Eberhard, D.A. (1989). MgATP-independent and MgATP-dependent exocytosis. Evidence that MgATP primes adrenal chromaffin cells to undergo exocytosis. *Journal of Biological Chemistry* 264, 5412-5419.
- Holz, R.W., and Senter, R.A. (1985). Plasma membrane and chromaffin granule characteristics in digitonin-treated chromaffin cells. *Journal of Neurochemistry* 45, 1548-1557.
- Hong, W. (2005). SNAREs and traffic. *Biochimica et Biophysica Acta (BBA) - Molecular Cell Research* 1744, 120-144.
- Horrigan, F.T., and Bookman, R.J. (1994). Releasable pools and the kinetics of exocytosis in adrenal chromaffin cells. *Neuron* 13, 1119-1129.
- Huang, F., Schwartz, S.L., Byars, J.M., and Lidke, K.A. (2011). Simultaneous multiple-emitter fitting for single molecule super-resolution imaging. *Biomed. Opt. Express* 2, 1377-1393.
- Hugo, S., Dembla, E., Halimani, M., Matti, U., Rettig, J., and Becherer, U. (2013). Deciphering dead-end docking of large dense core vesicles in bovine chromaffin cells. *J Neurosci* 33, 17123-17137.

- Hui, E., Bai, J., Wang, P., Sugimori, M., Llinas, R.R., and Chapman, E.R. (2005). Three distinct kinetic groupings of the synaptotagmin family: Candidate sensors for rapid and delayed exocytosis. *Proceedings of the National Academy of Sciences* 102, 5210-5214.
- Jahn, R., and Scheller, R.H. (2006). SNAREs [mdash] engines for membrane fusion. *Nat Rev Mol Cell Biol* 7, 631-643.
- Jahn, R., and Südhof, T.C. (1999). Membrane Fusion and Exocytosis. *Annual Review of Biochemistry* 68, 863-911.
- Jain, K.K. (2008). Cell therapy for pain. *Expert Opin Biol Ther* 8, 1847-1853.
- Jaiswal, J.K., Chakrabarti, S., Andrews, N.W., and Simon, S.M. (2004). Synaptotagmin VII Restricts Fusion Pore Expansion during Lysosomal Exocytosis. *PLoS Biology* 2, e233.
- Jaiswal, J.K., Rivera, V.M., and Simon, S.M. (2009). Exocytosis of post-Golgi vesicles is regulated by components of the endocytic machinery. *Cell* 137, 1308-1319.
- Jimenez, R.R., Lopez, M.G., Sancho, C., Maroto, R., and Garcia, A.G. (1993). A component of the catecholamine secretory response in the bovine adrenal gland is resistant to dihydropyridines and omega-conotoxin. *Biochem Biophys Res Commun* 191, 1278-1283.
- Kataoka, Y., Majane, E.A., and Yang, H.Y. (1985). Release of NPY-like immunoreactive material from primary cultures of chromaffin cells prepared from bovine adrenal medulla. *Neuropharmacology* 24, 693-695.

- Katz, B. (1971). Quantal Mechanism of Neural Transmitter Release. *Science* 173, 123-126.
- Katz, B., and Miledi, R. (1965). The Effect of Calcium on Acetylcholine Release from Motor Nerve Terminals. *Proceedings of the Royal Society of London B: Biological Sciences* 161, 496-503.
- Kaye, D.M., Lefkovits, J., Jennings, G.L., Bergin, P., Broughton, A., and Esler, M.D. (1995). Adverse consequences of high sympathetic nervous activity in the failing human heart. *J Am Coll Cardiol* 26, 1257-1263.
- Kelly, R.B. (1985). Pathways of protein secretion in eukaryotes. *Science* 230, 24-32.
- Kelly, R.B. (1993). Storage and release of neurotransmitters. *Cell* 72, 43-53.
- Klenchin, V.A., Kowalchuk, J.A., and Martin, T.F. (1998). Large dense-core vesicle exocytosis in PC12 cells. *Methods* 16, 204-208.
- Klyachko, V.A., and Jackson, M.B. (2002). Capacitance steps and fusion pores of small and large-dense-core vesicles in nerve terminals. *Nature* 418, 89-92.
- Kneen, M., Farinas, J., Li, Y., and Verkman, A.S. (1998). Green Fluorescent Protein as a Noninvasive Intracellular pH Indicator. *Biophysical Journal* 74, 1591-1599.
- Kobayashi, H., Yanagita, T., Yokoo, H., and Wada, A. (2003). Pathophysiological function of adrenomedullin and proadrenomedullin N-terminal peptides in adrenal chromaffin cells. *Hypertension Research* 26, S71-S78.

- Kuner, T., Li, Y., Gee, K.R., Bonewald, L.F., and Augustine, G.J. (2008). Photolysis of a caged peptide reveals rapid action of N-ethylmaleimide sensitive factor before neurotransmitter release. *Proc Natl Acad Sci U S A* 105, 347-352.
- Lara, B., Gandia, L., Martinez-Sierra, R., Torres, A., and Garcia, A.G. (1998). Q-type Ca^{2+} channels are located closer to secretory sites than L-type channels: functional evidence in chromaffin cells. *Pflugers Arch* 435, 472-478.
- Le Douarin, N. (1982). *The Neural Crest*. Cambridge University Press: Cambridge, UK.
- Le Douarin, N.M., Dupin, E., and Ziller, C. (1994). Genetic and epigenetic control in neural crest development. *Current opinion in genetics & development* 4, 685-695.
- Leszczyszyn, D.J., Jankowski, J.A., Viveros, O.H., Diliberto, E.J., Jr., Near, J.A., and Wightman, R.M. (1990). Nicotinic receptor-mediated catecholamine secretion from individual chromaffin cells. Chemical evidence for exocytosis. *Journal of Biological Chemistry* 265, 14736-14737.
- Lledo, P.M., Zhang, X., Sudhof, T.C., Malenka, R.C., and Nicoll, R.A. (1998). Postsynaptic membrane fusion and long-term potentiation. *Science* 279, 399-403.
- Lukyanetz, E.A., and Neher, E. (1999). Different types of calcium channels and secretion from bovine chromaffin cells. *Eur J Neurosci* 11, 2865-2873.

- Lynch, K.L., Gerona, R.R., Kielar, D.M., Martens, S., McMahon, H.T., and Martin, T.F. (2008). Synaptotagmin-1 utilizes membrane bending and SNARE binding to drive fusion pore expansion. *Mol Biol Cell* 19, 5093-5103.
- Lynch, K.L., and Martin, T.F.J. (2007). Synaptotagmins I and IX function redundantly in regulated exocytosis but not endocytosis in PC12 cells. *Journal of Cell Science* 120, 617-627.
- Mahapatra, S., Calorio, C., Vandael, D.H.F., Marcantoni, A., Carabelli, V., and Carbone, E. (2012). Calcium channel types contributing to chromaffin cell excitability, exocytosis and endocytosis. *Cell Calcium* 51, 321-330.
- Malhotra, V., Orci, L., Glick, B.S., Block, M.R., and Rothman, J.E. (1988). Role of an N-ethylmaleimide-sensitive transport component in promoting fusion of transport vesicles with cisternae of the Golgi stack. *Cell* 54, 221-227.
- Malsam, J., Parisotto, D., Bharat, T.A.M., Scheutzow, A., Krause, J.M., Briggs, J.A.G., and Söllner, T.H. (2012). Complexin arrests a pool of docked vesicles for fast Ca(2+)-dependent release. *The EMBO Journal* 31, 3270-3281.
- Maravall, M., Mainen, Z.F., Sabatini, B.L., and Svoboda, K. (2000). Estimating intracellular calcium concentrations and buffering without wavelength ratioing. *Biophys J* 78, 2655-2667.
- Martelli, A.M., Baldini, G., Tabellini, G., Koticha, D., Bareggi, R., and Baldini, G. (2000). Rab3A and Rab3D Control the Total Granule Number and the

- Fraction of Granules Docked at the Plasma Membrane in PC12 Cells. *Traffic* 1, 976-986.
- Martin, T.F.J. (2003). Tuning exocytosis for speed: fast and slow modes. *Biochimica et Biophysica Acta (BBA) - Molecular Cell Research* 1641, 157-165.
- Matos, M.F., Rizo, J., and Südhoff, T.C. (2000). The relation of protein binding to function: what is the significance of munc18 and synaptotagmin binding to syntaxin 1, and where are the corresponding binding sites? *European Journal of Cell Biology* 79, 377-382.
- Milosevic, I., Sorensen, J.B., Lang, T., Krauss, M., Nagy, G., Haucke, V., Jahn, R., and Neher, E. (2005). Plasmalemmal Phosphatidylinositol-4,5-Bisphosphate Level Regulates the Releasable Vesicle Pool Size in Chromaffin Cells. *Journal of Neuroscience* 25, 2557-2565.
- Moghadam, P.K., and Jackson, M.B. (2013). The Functional Significance of Synaptotagmin Diversity in Neuroendocrine Secretion. *Front Endocrinol (Lausanne)* 4, 124.
- Montero-Hadjadje, M., Vaingankar, S., Elias, S., Tostivint, H., Mahata, S.K., and Anouar, Y. (2008). Chromogranins A and B and secretogranin II: evolutionary and functional aspects. *Acta Physiologica* 192, 309-324.
- Morgan, A., and Burgoyne, R.D. (1997). Common mechanisms for regulated exocytosis in the chromaffin cell and the synapse. *Seminars in Cell & Developmental Biology* 8, 141-149.

- Neco, P., Fernandez-Peruchena, C., Navas, S., Lindau, M., Gutierrez, L.M., Alvarez de Toledo, G., and Ales, E. (2008). Myosin II contributes to fusion pore expansion during exocytosis. *Journal of Biological Chemistry*, M709058200.
- Neher, E. (1995). The use of fura-2 for estimating Ca buffers and Ca fluxes. *Neuropharmacology* 34, 1423-1442.
- Neher, E., and Augustine, G.J. (1992). Calcium gradients and buffers in bovine chromaffin cells. *J.Physiol.(Lond.)* 450, 273-301.
- Neher, E., Fernandez, J.M., and Lindau, M. (1987). The calcium dependence of vesicle exocytosis. *Res Publ Assoc Res Nerv Ment Dis* 65, 103-110.
- Neher, E., and Marty, A. (1982). Discrete changes of cell membrane capacitance observed under conditions of enhanced secretion in bovine adrenal chromaffin cells. *Proceedings of the National Academy of Sciences of the United States of America* 79, 6712-6716.
- Neher, E., and Sakaba, T. (2008). Multiple roles of calcium ions in the regulation of neurotransmitter release. *Neuron* 59, 861-872.
- Neher, E., and Zucker, R.S. (1993). Multiple calcium-dependent processes related to secretion in bovine chromaffin cells. *Neuron* 10, 21-30.
- O'Connor, D.T., and Frigon, R.P. (1984). Chromogranin A, the major catecholamine storage vesicle soluble protein. Multiple size forms, subcellular storage, and regional distribution in chromaffin and nervous

- tissue elucidated by radioimmunoassay. *Journal of Biological Chemistry* 259, 3237-3247.
- O'Connor, D.T., Mahata, S.K., Mahata, M., Jiang, Q., Hook, V.Y., and Taupenot, L. (2007). Primary culture of bovine chromaffin cells. *Nat Protoc* 2, 1248-1253.
- Ovesný, M., Křížek, P., Borkovec, J., Švindrych, Z., and Hagen, G.M. (2014). ThunderSTORM: a comprehensive ImageJ plug-in for PALM and STORM data analysis and super-resolution imaging. *Bioinformatics* 30, 2389-2390.
- Pabst, S., Margittai, M., Vainius, D., Langen, R., Jahn, R., and Fasshauer, D. (2002). Rapid and Selective Binding to the Synaptic SNARE Complex Suggests a Modulatory Role of Complexins in Neuroexocytosis. *J Biol Chem* 277, 7838-7848.
- Palade, G. (1975). Intracellular aspects of the process of protein synthesis. *Science* 189, 347-358.
- Park, Y., Seo, J.B., Fraind, A., Perez-Lara, A., Yavuz, H., Han, K., Jung, S.-R., Kattan, I., Walla, P.J., Choi, M., Cafiso, D.S., Koh, D.-S., and Jahn, R. (2015). Synaptotagmin-1 binds to PIP2-containing membrane but not to SNAREs at physiological ionic strength. *Nat Struct Mol Biol* 22, 815-823.
- Parmer, R.J., Mahata, M., Mahata, S., Sebald, M.T., O'Connor, D.T., and Miles, L.A. (1997). Tissue plasminogen activator (t-PA) is targeted to the regulated secretory pathway. Catecholamine storage vesicles as a reservoir for the rapid release of t-PA. *J Biol Chem* 272, 1976-1982.

- Passmore, D.R., Rao, T.C., Peleman, A.R., and Anantharam, A. (2014). Imaging plasma membrane deformations with pTIRFM. *J Vis Exp*.
- Perin, M.S., Fried, V.A., Mignery, G.A., Jahn, R., and Sudhof, T.C. (1990). Phospholipid binding by a synaptic vesicle protein homologous to the regulatory region of protein kinase C. *Nature* 345, 260-263.
- Perin, M.S., Johnston, P.A., Ozcelik, T., Jahn, R., Francke, U., and Sudhof, T.C. (1991). Structural and functional conservation of synaptotagmin (p65) in *Drosophila* and humans. *Journal of Biological Chemistry* 266, 615-622.
- Perrais, D., Kleppe, I.C., Taraska, J.W., and Almers, W. (2004). Recapture after exocytosis causes differential retention of protein in granules of bovine chromaffin cells. *The Journal of Physiology Online* 560, 413-428.
- Pevsner, J., Hsu, S.C., Braun, J.E.A., Calakos, N., Ting, A.E., Bennett, M.K., and Scheller, R.H. (1994). Specificity and regulation of a synaptic vesicle docking complex. *Neuron* 13, 353-361.
- Plattner, H., Artalejo, A.R., and Neher, E. (1997). Ultrastructural organization of bovine chromaffin cell cortex- analysis by cryofixation and morphometry of aspects pertinent to exocytosis [In Process Citation]. *Journal of Cell Biology* 139(7), 1709-1717.
- Qu, T., Shi, G., Ma, K., Yang, H.N., Duan, W.M., and Pappas, G.D. (2013). Targeted cell reprogramming produces analgesic chromaffin-like cells from human mesenchymal stem cells. *Cell Transplant* 22, 2257-2266.

- Rao, T.C., Passmore, D.R., Peleman, A.R., Das, M., Chapman, E.R., and Anantharam, A. (2014). Distinct fusion properties of synaptotagmin-1 and synaptotagmin-7 bearing dense core granules. *Mol Biol Cell* 25, 2416-2427.
- Regazzi, R., Li, G., Ullrich, S., Jaggi, C., and Wollheim, C.B. (1989). Different requirements for protein kinase C activation and Ca²⁺-independent insulin secretion in response to guanine nucleotides. Endogenously generated diacylglycerol requires elevated Ca²⁺ for kinase C insertion into membranes. *Journal of Biological Chemistry* 264, 9939-9944.
- Rizzo, M.A., Springer, G.H., Granada, B., and Piston, D.W. (2004). An improved cyan fluorescent protein variant useful for FRET. *Nature Structural Biology* 22 445-449.
- Rosa, J.M., Torregrosa-Hetland, C.J., Colmena, I., Gutiérrez, L.M., García, A.G., and Gandía, L. (2011). Calcium entry through slow-inactivating L-type calcium channels preferentially triggers endocytosis rather than exocytosis in bovine chromaffin cells. *American Journal of Physiology - Cell Physiology* 301, C86-C98.
- Rothman, J.E. (1994). Mechanisms of intracellular protein transport. *Nature* 372, 55-63.
- Rothman, J.E. (2002). The machinery and principles of vesicle transport in the cell. *Nat Med* 8, 1059-1062.

- Sabatini, D.D. (1999). George E. Palade: charting the secretory pathway. *Trends in Cell Biology* 9, 413-417.
- Schaub, J.R., Lu, X., Doneske, B., Shin, Y.K., and McNew, J.A. (2006). Hemifusion arrest by complexin is relieved by Ca²⁺-synaptotagmin I. *Nat Struct Mol Biol* 13, 748-750.
- Schekman, R. (2002). SEC mutants and the secretory apparatus. *Nat Med* 8, 1055-1058.
- Schlüter, O.M., Khvotchev, M., Jahn, R., and Südhof, T.C. (2002). Localization Versus Function of Rab3 Proteins: EVIDENCE FOR A COMMON REGULATORY ROLE IN CONTROLLING FUSION. *Journal of Biological Chemistry* 277, 40919-40929.
- Schoch, S., Castillo, P.E., Jo, T., Mukherjee, K., Geppert, M., Wang, Y., Schmitz, F., Malenka, R.C., and Südhof, T.C. (2002). Rim1à forms a protein scaffold for regulating neurotransmitter release at the active zone. *Nature* 415, 321-326.
- Schonn, J.S., Maximov, A., Lao, Y., Südhof, T.C., and Sorensen, J.B. (2008). Synaptotagmin-1 and -7 are functionally overlapping Ca²⁺ sensors for exocytosis in adrenal chromaffin cells. *Proc Natl Acad Sci U S A* 105, 3998-4003.
- Schumm, M.A., Castellanos, D.A., Frydel, B.R., and Sagen, J. (2004). Improved neural progenitor cell survival when cografted with chromaffin cells in the rat striatum. *Exp Neurol* 185, 133-142.

- Schütz, D., Zilly, F., Lang, T., Jahn, R., and Bruns, D. (2005). A dual function for Munc-18 in exocytosis of PC12 cells. *European Journal of Neuroscience* 21, 2419-2432.
- Shao, X., Li, C., Fernandez, I., Zhang, X., Südhof, T.C., and Rizo, J. (1997). Synaptotagmin α ;Syntaxin Interaction: The C₂ Domain as a Ca²⁺-Dependent Electrostatic Switch. *Neuron* 18, 133-142.
- Sheng, Z.-H., Yokoyama, C.T., and Catterall, W.A. (1997). Interaction of the synprint site of N-type Ca(2+) channels with the C2B domain of synaptotagmin I. *Proceedings of the National Academy of Sciences of the United States of America* 94, 5405-5410.
- Sollner, T., Whiteheart, S.W., Brunner, M., Erdjument-Bromage, H., Geromanos, S., Tempst, P., and Rothman, J.E. (1993). SNAP receptors implicated in vesicle targeting and fusion. *Nature* 362, 318-324.
- Sorensen, J.B., Fernandez-Chacon, R., Südhof, T.C., and Neher, E. (2003a). Examining synaptotagmin 1 function in dense core vesicle exocytosis under direct control of Ca²⁺. *J Gen Physiol* 122, 265-276.
- Sorensen, J.B., Nagy, G., Varoqueaux, F., Nehring, R.B., Brose, N., Wilson, M.C., and Neher, E. (2003b). Differential control of the releasable vesicle pools by SNAP-25 splice variants and SNAP-23. *Cell* 114, 75-86.
- Sørensen, J.B., Wiederhold, K., Müller, E.M., Milosevic, I., Nagy, G., de Groot, B.L., Grubmüller, H., and Fasshauer, D. (2006). Sequential N- to C-

- terminal SNARE complex assembly drives priming and fusion of secretory vesicles. *The EMBO Journal* 25, 955-966.
- Speidel, D., Bruederle, C.E., Enk, C., Voets, T., Varoqueaux, F., Reim, K., Becherer, U., Fornai, F., Ruggieri, S., Holighaus, Y., Weihe, E., Bruns, D., Brose, N., and Rettig, J. (2005). CAPS1 Regulates Catecholamine Loading of Large Dense-Core Vesicles. *Neuron* 46, 75-88.
- Speidel, D., Varoqueaux, F., Enk, C., Nojiri, M., Grishanin, R.N., Martin, T.F.J., Hofmann, K., Brose, N., and Reim, K. (2003). A Family of Ca²⁺-Dependent Activator Proteins for Secretion: COMPARATIVE ANALYSIS OF STRUCTURE, EXPRESSION, LOCALIZATION, AND FUNCTION. *Journal of Biological Chemistry* 278, 52802-52809.
- Stevens, D.R., Wu, Z.X., Matti, U., Junge, H.J., Schirra, C., Becherer, U., Wojcik, S.M., Brose, N., and Rettig, J. (2005). Identification of the minimal protein domain required for priming activity of Munc13-1. *Curr Biol.* 15, 2243-2248.
- Steyer, J.A., Horstman, H., and Almers, W. (1997). Transport, docking and exocytosis of single secretory granules in live chromaffin cells. *Nature* 388, 474-478.
- Südhof, T.C. (2002). Synaptotagmins: Why So Many? *Journal of Biological Chemistry* 277, 7629-7632.
- Südhof, T.C. (2004). THE SYNAPTIC VESICLE CYCLE. *Annual Review of Neuroscience* 27, 509-547.

- Südhof, T.C., and Rizo, J. (1996). Synaptotagmins: C2-Domain Proteins That Regulate Membrane Traffic. *Neuron* 17, 379-388.
- Sugita, S. (2008). Mechanisms of exocytosis. *Acta Physiologica* 192, 185-193.
- Sugita, S., Shin, O.H., Han, W., Lao, Y., and Südhof, T.C. (2002). Synaptotagmins form a hierarchy of exocytotic Ca(2+) sensors with distinct Ca(2+) affinities. *EMBO J* 21, 270-280.
- Sun, T., Wu, X.S., Xu, J., McNeil, B.D., Pang, Z.P., Yang, W., Bai, L., Qadri, S., Molkentin, J.D., Yue, D.T., and Wu, L.G. (2010). The role of calcium/calmodulin-activated calcineurin in rapid and slow endocytosis at central synapses. *J Neurosci* 30, 11838-11847.
- Sutton, R.B., Davletov, B.A., Berghuis, A.M., Südhof, T.C., and Sprang, S.R. (1995). Structure of the first C2 domain of synaptotagmin I: a novel Ca²⁺/phospholipid-binding fold. *Cell* 80, 929-938.
- Takiyuddin, M.A., Brown, M.R., Dinh, T.Q., Cervenka, J.H., Braun, S.D., Parmer, R.J., Kennedy, B., and O'Connor, D.T. (1994). Sympatho-adrenal secretion in humans: factors governing catecholamine and storage vesicle peptide co-release. *Journal of autonomic pharmacology* 14, 187-200.
- Takiyuddin, M.A., Cervenka, J.H., Sullivan, P.A., Pandian, M.R., Parmer, R.J., Barbosa, J.A., and O'Connor, D.T. (1990). Is physiologic sympathoadrenal catecholamine release exocytotic in humans? *Circulation* 81, 185-195.

- Taraska, J.W., and Almers, W. (2004). Bilayers merge even when exocytosis is transient. *Proceedings of the National Academy of Sciences of the United States of America* 101, 8780-8785.
- Taraska, J.W., Perrais, D., Ohara-Imaizumi, M., Nagamatsu, S., and Almers, W. (2003). Secretory granules are recaptured largely intact after stimulated exocytosis in cultured endocrine cells. *Proceedings of the National Academy of Sciences of the United States of America* 100, 2070-2075.
- Thomas-Reetz, A.C., and De Camilli, P. (1994). A role for synaptic vesicles in non-neuronal cells: clues from pancreatic beta cells and from chromaffin cells. *The FASEB Journal* 8, 209-216.
- Toth, I.E., and Hinson, J.P. (1995). Neuropeptides in the adrenal gland: distribution, localization of receptors, and effects on steroid hormone synthesis. *Endocr Res* 21, 39-51.
- Trifaro, J.M., Glavinovic, M., and Rose, S.D. (1997). Secretory vesicle pools and rate and kinetics of single vesicle exocytosis in neurosecretory cells. *Neurochem Res* 22, 831-841.
- Tsien, R.Y. (1998). The green fluorescent protein. *Annu.Rev.Biochem.* 67, 509-544.
- Tsuboi, T., and Fukuda, M. (2006). The Slp4-a Linker Domain Controls Exocytosis through Interaction with Munc18-1-Syntaxin-1a Complex. *Molecular Biology of the Cell* 17, 2101-2112.

- Tsuboi, T., Kanno, E., and Fukuda, M. (2007). The polybasic sequence in the C2B domain of rabphilin is required for the vesicle docking step in PC12 cells. *Journal of Neurochemistry* 100, 770-779.
- Tucker, W.C., Edwardson, J.M., Bai, J., Kim, H.J., Martin, T.F., and Chapman, E.R. (2003). Identification of synaptotagmin effectors via acute inhibition of secretion from cracked PC12 cells. *J Cell Biol* 162, 199-209.
- Tucker, W.C., Weber, T., and Chapman, E.R. (2004). Reconstitution of Ca²⁺-Regulated Membrane Fusion by Synaptotagmin and SNAREs. *Science* 304, 435-438.
- Turner, R.C., Hattersley, A.T., Shaw, J.T., and Levy, J.C. (1995). Type II Diabetes: Clinical Aspects of Molecular Biological Studies. *Diabetes* 44, 1-10.
- Ubach, J., Zhang, X., Shao, X., Sudhof, T.C., and Rizo, J. (1998). Ca²⁺ binding to synaptotagmin: how many Ca²⁺ ions bind to the tip of a C2-domain? *EMBO Journal* 17, 3921-3930.
- Vitale, M.L., Seward, E.P., and Trifaro, J.M. (1995). Chromaffin cell cortical actin network dynamics control the size of the release-ready vesicle pool and the initial rate of exocytosis. *Neuron* 14, 353-363.
- Viveros, O.H., Arqueros, L., and Kirshner, N. (1969). Quantal secretion from adrenal medulla: all-or-none release of storage vesicle content. *Science* 165, 911-913.

- Voets, T., Moser, T., Lund, P.E., Chow, R.H., Geppert, M., Sudhof, T.C., and Neher, E. (2001a). Intracellular calcium dependence of large dense-core vesicle exocytosis in the absence of synaptotagmin I. *Proceedings of the National Academy of Sciences* 98, 11680-11685.
- Voets, T., Moser, T., Lund, P.E., Chow, R.H., Geppert, M., Sudhof, T.C., and Neher, E. (2001b). Intracellular calcium dependence of large dense-core vesicle exocytosis in the absence of synaptotagmin I. *Proceedings of the National Academy of Sciences of the United States of America* 98, 11680-11685.
- Voets, T., Neher, E., and Moser, T. (1999a). Mechanisms underlying phasic and sustained secretion in chromaffin cells from mouse adrenal slices. *Neuron* 23, 607-615.
- Voets, T., Neher, E., and Moser, T. (1999b). Mechanisms underlying phasic and sustained secretion in chromaffin cells from mouse adrenal slices. *Neuron* 23, 607-615.
- Voets, T., Toonen, R.F., Brian, E.C., de W., Moser, T., Rettig, J., Sudhof, T.C., Neher, E., and Verhage, M. (2001c). Munc18-1 promotes large dense-core vesicle docking. *Neuron* 31, 581-591.
- Voets, T., Toonen, R.F., Brian, E.C., de Wit, H., Moser, T., Rettig, J., Sudhof, T.C., Neher, E., and Verhage, M. (2001d). Munc18-1 promotes large dense-core vesicle docking. *Neuron* 31, 581-591.

- Wang, C.T., Bai, J., Chang, P.Y., Chapman, E.R., and Jackson, M.B. (2006). Synaptotagmin-Ca²⁺ triggers two sequential steps in regulated exocytosis in rat PC12 cells: fusion pore opening and fusion pore dilation. *J Physiol* 570, 295-307.
- Wang, C.T., Grishanin, R., Earles, C.A., Chang, P.Y., Martin, T.F., Chapman, E.R., and Jackson, M.B. (2001). Synaptotagmin modulation of fusion pore kinetics in regulated exocytosis of dense-core vesicles. *Science* 294, 1111-1115.
- Wang, C.T., Lu, J.C., Bai, J., Chang, P.Y., Martin, T.F., Chapman, E.R., and Jackson, M.B. (2003a). Different domains of synaptotagmin control the choice between kiss-and-run and full fusion. *Nature* 424, 943-947.
- Wang, P., Chicka, M.C., Bhalla, A., Richards, D.A., and Chapman, E.R. (2005). Synaptotagmin VII is targeted to secretory organelles in PC12 cells, where it functions as a high-affinity calcium sensor. *Mol Cell Biol* 25, 8693-8702.
- Wang, P., Wang, C.T., Bai, J., Jackson, M.B., and Chapman, E.R. (2003b). Mutations in the effector binding loops in the C2A and C2B domains of synaptotagmin I disrupt exocytosis in a nonadditive manner. *J Biol Chem* 278, 47030-47037.
- Watkinson, A., O'Sullivan, A.J., Burgoyne, R.D., and Dockray, G.J. (1990). Differential accumulation of catecholamines, proenkephalin- and chromogranin A-derived peptides in the medium after chronic nicotine

- stimulation of cultured bovine adrenal chromaffin cells. *Peptides* 11, 435-441.
- Weber, T., Parlati, F., McNew, J.A., Johnston, R.J., Westermann, B., Söllner, T.H., and Rothman, J.E. (2000). Snarepins Are Functionally Resistant to Disruption by Nsf and α SNAP. *The Journal of Cell Biology* 149, 1063-1072.
- Weiss, A.N., Anantharam, A., Bittner, M.A., Axelrod, D., and Holz, R.W. (2014). Luminal Protein within Secretory Granules Affects Fusion Pore Expansion. *Biophys J* 107, 26-33.
- Weiss, C., Cahill, A.L., Laslop, A., Fischer-Colbrie, R., Perlman, R.L., and Winkler, H. (1996). Differences in the composition of chromaffin granules in adrenaline and noradrenaline containing cells of bovine adrenal medulla. *Neurosci Lett* 211, 29-32.
- Wick, P.W., Senter, R.A., Parsels, L.A., and Holz, R.W. (1993). Transient transfection studies of secretion in bovine chromaffin cells and PC12 cells: generation of kainate-sensitive chromaffin cells. *Journal of Biological Chemistry* 268, 10983-10989.
- Wilburn, L.A., and Jaffe, R.B. (1988). Quantitative assessment of the ontogeny of met-enkephalin, norepinephrine and epinephrine in the human fetal adrenal medulla. *Acta endocrinologica* 118, 453-459.

- Winkler, H. (1993). The adrenal chromaffin granule: a model for large dense core vesicles of endocrine and nervous tissue. *Journal of Anatomy* 183, 237-252.
- Winkler, H., and Fischer-Colbrie, R. (1998). Regulation of the Biosynthesis of Large Dense-Core Vesicles in Chromaffin Cells and Neurons. *Cellular and Molecular Neurobiology* 18, 193-209.
- Winkler, H., and Fischer-Colbrie, R. (1992). The chromogranins A and B: the first 25 years and future perspectives. *Neuroscience* 49, 497-528.
- Winkler, H., and Westhead, E. (1980). The molecular organization of adrenal chromaffin granules. *Neuroscience* 5, 1803-1823.
- Wiser, O., Trus, M., Hernández, A., Renström, E., Barg, S., Rorsman, P., and Atlas, D. (1999). The voltage sensitive Lc-type Ca(2+) channel is functionally coupled to the exocytotic machinery. *Proceedings of the National Academy of Sciences of the United States of America* 96, 248-253.
- Wit, H.d., Cornelisse, L.N., Toonen, R.F.G., and Verhage, M. (2006). Docking of Secretory Vesicles Is Syntaxin Dependent. *PLoS ONE* 1, e126.
- Xu, Z., Sato, K., and Wickner, W. (1998). LMA1 binds to vacuoles at Sec18p (NSF), transfers upon ATP hydrolysis to a t-SNARE (Vam3p) complex, and is released during fusion. *Cell* 93, 1125-1134.

- Yoo, S.H., You, S.H., and Huh, Y.H. (2005). Presence of syntaxin 1A in secretory granules of chromaffin cells and interaction with chromogranins A and B. *FEBS Lett* 579, 222-228.
- Zanin, M.P., Mackenzie, K.D., Peiris, H., Pritchard, M.A., and Keating, D.J. (2013). RCAN1 regulates vesicle recycling and quantal release kinetics via effects on calcineurin activity. *J Neurochem* 124, 290-299.
- Zhang, J., and Castle, D. (2011). Regulation of Fusion Pore Closure and Compound Exocytosis in Neuroendocrine PC12 Cells by SCAMP1. *Traffic (Copenhagen, Denmark)* 12, 600-614.
- Zhang, X., Kim-Miller, M.J., Fukuda, M., Kowalchuk, J.A., and Martin, T.F. (2002). Ca²⁺-dependent synaptotagmin binding to SNAP-25 is essential for Ca²⁺-triggered exocytosis. *Neuron*. 34, 599-611.
- Zhang, X., Rizo, J., and Sudhof, T.C. (1998). Mechanism of phospholipid binding by the C2A-domain of synaptotagmin I. *Biochemistry* 37, 12395-12403.
- Zhang, Z., Wu, Y., Wang, Z., Dunning, F.M., Rehfuss, J., Ramanan, D., Chapman, E.R., and Jackson, M.B. (2011). Release mode of large and small dense-core vesicles specified by different synaptotagmin isoforms in PC12 cells. *Mol Biol Cell* 22, 2324-2336.
- Zhou, Z., Mislner, S., and Chow, R.H. (1996). Rapid fluctuations in transmitter release from single vesicles in bovine adrenal chromaffin cells. *Biophysical Journal* 70, 1543-1552.

Zhu, D., Koo, E., Kwan, E., Kang, Y., Park, S., Xie, H., Sugita, S., and Gaisano, H.Y. (2013). Syntaxin-3 regulates newcomer insulin granule exocytosis and compound fusion in pancreatic beta cells. *Diabetologia* 56, 359-369.

ABSTRACT**ROLE OF SECRETORY GRANULE HETEROGENEITY IN
CALCIUM-TRIGGERED EXOCYTOSIS**

by

TEJESHWAR RAO**August 2016****Advisor:** Dr. Arun Anantharam**Major:** Biological Sciences**Degree:** Doctor of Philosophy

The sympathetic nervous system is activated by a variety of threats to organismal homeostasis. The adrenomedullary chromaffin cell is the core effector of sympathetic activity in the peripheral nervous system. By design, the chromaffin cell secretory response is mutable so that release can be rapidly tuned to drive context-dependent changes in physiological function. However, the mechanisms by which this tuning is achieved with such high temporal fidelity and context specificity remain unclear. This represents a major gap in our understanding of the sympatho-adrenal system since it is known to modify the function of nearly every organ system in the body.

In chromaffin cells, the trigger for stimulus-evoked exocytosis is a rise in intracellular Ca^{2+} . The level of intracellular Ca^{2+} accumulation varies with the stimulus intensity and secretagogue. Ca^{2+} regulates release by acting on the Ca^{2+} -binding synaptotagmin (Syt) protein family, driving their penetration into membranes that harbor anionic lipids, and possibly bending those membranes.

Chromaffin cells only express two of the 17 known Syt isoforms: Syt-1 and Syt-7. Previous studies had identified that Syt-1 and Syt-7 possess distinct affinities for Ca^{2+} in the presence of phospholipid membranes and, once bound release membranes differentially. An underlying assumption in previous studies of chromaffin cell secretion was that granules are homogeneous, with the same biochemical constituents and the potential for similar rates of content discharge. This idea is challenged by the work in this dissertation. We discovered that granules harbor functionally different isoforms of Syt, and therefore reasoned that these isoforms (Syt-1 and Syt-7) may confer different Ca^{2+} sensitivities to the granules *in situ*. This would thereby enable them to respond differentially to depolarizing stimuli. In order to study this, we first focused our attention on developing an imaging tool (pTIRFM) that could combine nanoscale measurements of membrane curvature changes with single-molecule imaging. This tool would allow us to study the interaction of synaptotagmin with the plasma membrane in unprecedented kinetic and topological detail, and would be necessary to resolve how specific structural differences in Syt isoforms relate to their distinct functional properties.

Using pTIRFM we first observed that topological changes associated with Syt-1 granules are more short-lived than those of Syt-7 granules. This finding led credence to the idea that fused Syt-7 granules maintain a narrow fusion pore and more often undergo the “kiss-and-run” mode of exocytosis. Conversely, Syt-1 granules collapse onto the plasma membrane following fusion with rapid dilation

of the fusion pore (“full-collapse” mode of exocytosis). Also, luminal and membrane proteins are released more slowly from Syt-7 than from Syt-1 granules. The above findings led us to propose the hypothesis that chromaffin granules are not in fact homogenous but instead may exploit the molecular and functional heterogeneity conferred by Syt to regulate release in an activity-dependent manner.

To explore this, we decided to focus our attention on identifying novel differences between the spatial and functional properties of granules expressing the two Syt isoforms. These isoforms are not only sorted to separate granule populations, but Syt-1 granules are also distributed further away from the plasma membrane in comparison to Syt-7 granules. Lower stimulation conditions are more effective in activating Syt-7 granules, and on average they begin fusing with the membrane earlier following depolarization. On the contrary, more Ca^{2+} is needed for Syt-1 activation, and these granules require less time to transition into a fusion-competent state. Thus, the behavior of Syt isoforms is strongly Ca^{2+} and stimulus-dependent. Therefore these experiments demonstrate that heterogeneity of Syt granules is utilized by the chromaffin cell to modulate the release of cargo in a physiologically relevant context.

The performed studies have led to a paradigm shift in our current understanding of the basic molecular organization of secretory systems. They have provided insight into how heterogeneity of individual secretory granules may affect the properties of regulated exocytosis in other cell types. This is a

major conceptual advance, as intrinsic functional differences among granules have not been considered as a factor in the regulation of fusion modalities.

AUTOBIOGRAPHICAL STATEMENT

TEJESHWAR RAO

Educational Qualification:

2011-2016: Doctor of Philosophy, Wayne State University, Detroit, MI, USA

2008-2010: Master of Science (Biotechnology): Institute of Science, University of Mumbai, Mumbai, Maharashtra, India

2005-2008: Bachelor of Science (Biotechnology): University of Mumbai, Mumbai, Maharashtra, India

Honors and Awards:

2015-16: Thomas C. Rumble Graduate Research Fellowship, Wayne State University

2015: Graduate Student Professional Travel Award, Wayne State University

2015: Education Committee Travel Award, Biophysical Society

2014: Graduate Teaching Assistant Recognition Award, Wayne State University

2014: Richard Barber Interdisciplinary Graduate Research Program Fellowship

Publications:

1. In preparation for submission: Rao T. C., Schmidtke M.W., Bourg J., Bai H., Veatch S.L., Chapman E. R., Giovannucci, D.R., Anantharam A. 2016. Chromaffin cell synaptotagmin isoforms form functionally and spatially separable granule pools
2. Rao T. C., Passmore D. R., Peleman A. R., Das M., Chapman E. R., Anantharam A. 2014. Distinct fusion properties of synaptotagmin-1 and synaptotagmin-7 bearing dense core granules. *Molecular Biology of the Cell* 25(16): 2416-27.
3. Passmore D. R., Rao T. C., Peleman A. R., Anantharam A. 2014. Imaging Plasma Membrane Deformations with pTIRFM. *J. Vis. Exp.* (86), e51334, doi: 10.3791/51334.
4. Passmore D. R., Rao T. C., Anantharam A. 2014. "Real Time Investigation of Plasma Membrane Deformation and Fusion Pore Expansion Using Polarized TIRFM," *Methods in Molecular Biology*.